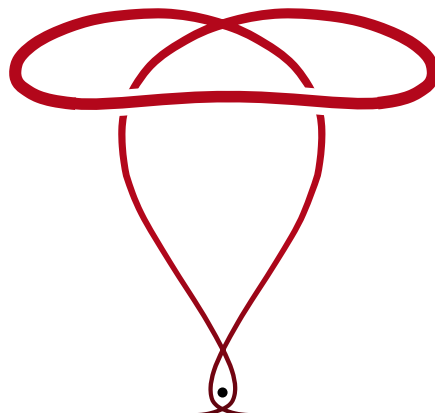# Parking orbits in the three-body problem for a low Δv Earth-Mars cycler

candidate **Giovanni Bezze**

supervisor **prof. Enrico Lorenzini**

co-supervisor **prof. Giacomo Colombatti**

I

per la nonna Romana

Abstract

In this thesis a concept for a cycler that transfers between Earth and Mars during the currently used low v_∞ launch windows and stays "parked" at the planets is explored. The parking orbits are designed to exploit the flexible dynamics of the circular restricted three-body problem so that they have a high energy, prescribed parking time and conveniently positioned injection and escape burns, in order to have a low Δv required. Methods for the computation of these parking orbits are formulated starting from the dynamical structure of the Lagrangian points and using Lambert's theorem suitable transfer dates are chosen, after that an optimization process is carried out to find the parameters that for each planetary stay phase give the parking orbit with the lowest Δv.

Sommario

In questa tesi è esplorata la possibilità di un cycler che viaggia tra Terra e Marte durante le finestre di lancio a bassa v_∞ usate correntemente e che rimane "parcheggiato" nelle vicinanze del pianeta. Le orbite di parcheggio sono progettate per sfruttare le flessibili caratteristiche dinamiche del problema dei tre corpi ristretto in modo che abbiano alta energia, tempo di parcheggio prestabilito e manovre di immissione e uscita convenientemente posizionate in modo da avere un basso requisito di Δv. I metodi per il calcolo di queste orbite di parcheggio sono formulati partendo dalla struttura dinamica dei punti Lagrangiani e le date di trasferimento interplanetario sono scelte utilizzando il teorema di Lambert, dopodiché è presentato un processo di ottimizzazione volto a trovare i parametri che per ogni periodo di stazionamento attorno a un pianeta forniscono l'orbita di parcheggio con il più basso Δv.

Contents

Chapter 1

Introduction

1.1 Cycler trajectories

The human exploration of Mars will face many challenges: one of them is the long duration of missions imposed by the scales and velocities of interplanetary travel. During their trip to and from Mars the astronauts will therefore need comfortable living spaces, much more comparable to the International Space Station in dimensions than the Apollo or Artemis capsules used for manned Lunar missions. These large spacecrafts would need very big amounts of propellant to accelerate so expedients to lower their Δv over the mission can hugely lower the mass needed to be launched from Earth.

A solution that has been investigated since the 1970s is the use of *cycler trajectories*. These are a particular kind of orbits that intercept some planets periodically, in this case Earth and Mars, where the large transfer spacecrafts can be left and used repeatedly with low to near zero Δv. The acceleration/deceleration phases near the planets can be made by smaller "taxi" spacecrafts, with a possible reduction in total mass needed for the mission. The simpler and most famous of these trajectories is the Aldrin Cycler [1] (named after its proposer Buzz Aldrin) where two transfer spacecrafts, an "ascent" and "descent" vehicle, are in elliptical heliocentric orbits. The sequence of this mission would consist in the following sequence, illustrated in figure 1.1:

1. The crew "taxies" from Earth orbit to rendez-vous with the ascent vehicle

2. The ascent vehicle arrives at Mars, where the crew taxies to its orbit (or surface). The ascent vehicle continues along its cycler trajectories.

3. The descent vehicle passes by Mars, where it rendez-vous with the taxi.

4. The descent vehicle passes by Earth and the crew lands back home after approximately 2.14 years.

5. The ascent vehicle arrives at Earth, where it conducts a gravity assist to rotate the argument of perigee of its heliocentric orbit in such a way that the relative configuration between Mars and Earth is the same as point 1 (an analogous step is made by the now uncrewed descent vehicle later). This point coincides with the arrival of a new crew, thereby completing the cycle.

The downside of this cycler is that the v_∞ of the various encounters are very high with respect to the ones "a la Hohmann" that are currently used for example in robotic exploration missions. This implies that the taxi would need much bigger amounts of fuel
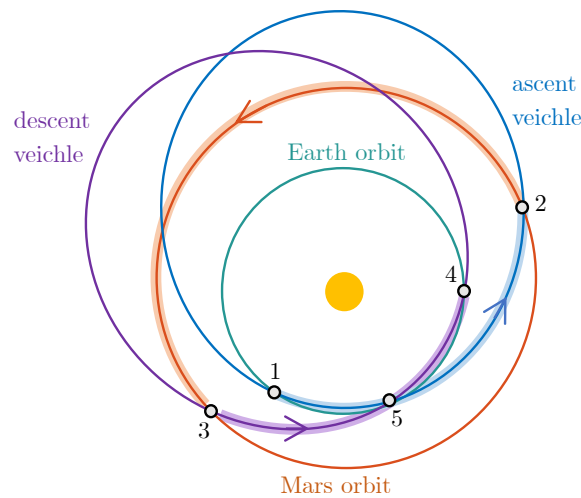
Figure 1.1: One cycle of the Aldrin cycler.

to rendez-vous with the ascent and descent vehicles than the ones that would be needed for an optimal transfer arc, diminishing the advantage that the cycler architecture brings.

Another well-investigated concept is the Versatile International Station for Interplanetary Transport (VISIT) cyclers [2]. These trajectories do not use gravity assists and exploit the fact that their period is commensurate both to Mars and Earth. For example, the VISIT-1 trajectory shown in figure 1.2 has a commensurability of 4:5 to Earth (for every four cycler orbits Earth makes five) and 3:2 with Mars. The v_∞ for these trajectories is much lower than in the Aldrin cycler as the perihelion and aphelion are very similar to the semiaxis of Earth and Mars orbits. This cycler has the big downside of irregular and possibly very long Mars stay duration, from 1.6 to 5.9 years. This can be mitigated by introducing many cycler vehicles but this reduces the mass advantage of this solution.

Figure 1.2: The VISIT-1 cycler trajectory.

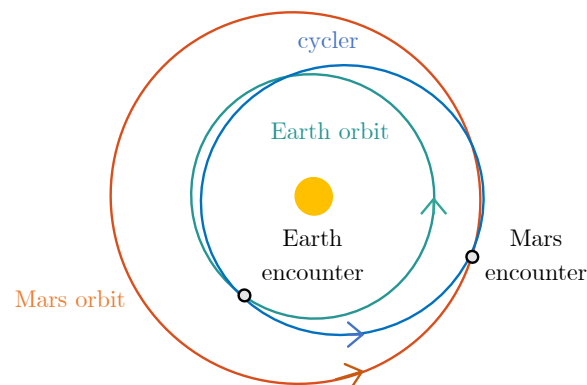## 1.2 The Three Body Problem and Lagrangian points

The kinematics of two masses under gravitational mutual interaction was known since the early 1608, when Johannes Kepler published his three laws, with the dynamical reasons of their motion being understood by Isaac Newton in 1687. The case for three masses eluded analytical solutions until in 1767 Leonhard Euler, who was studying a simplified problem in which one of the masses in negligible and the other two are in a circular orbit, discovered the *collinear libration points* and shortly after in 1772 Lagrange found out about the existence of two other *triangular libration points*. These are equilibrium points in which a spacecraft could remain stationary with respect to the geometric configuration of the two massive bodies, and are commonly referred to as the *Lagrangian points*, despite the first discovery by Euler.

Study of the so-called *circular restricted three-body problem* continued and in 1836 Jacobi discovered an integral of motion now named after him, the *Jacobi integral*. Later, in 1899 Henri Poincaré demonstrated the existence of various families of periodic orbits around the libration points, these orbits however don't have analytical forms and until the advent of computers their practical use was limited.

Since the 1960s the theoretical study of trajectories in the circular restricted three body problem flourished, both for the increasing feasibility of solving numerically the differential equations of motion and for the interest for space missions that exploited their dynamics. The first space mission to use one of such trajectories was the International Sun/Earth Explorer 3 (ISEE-3), first placed in 1978 an orbit around the Earth-Sun L_1 point to study Earth magnetic field's interaction with the solar wind. The spacecraft was re-purposed in 1982 to intercept comet Giacobini-Zinner, maneuvering into the intercept trajectory with a very low Δv.
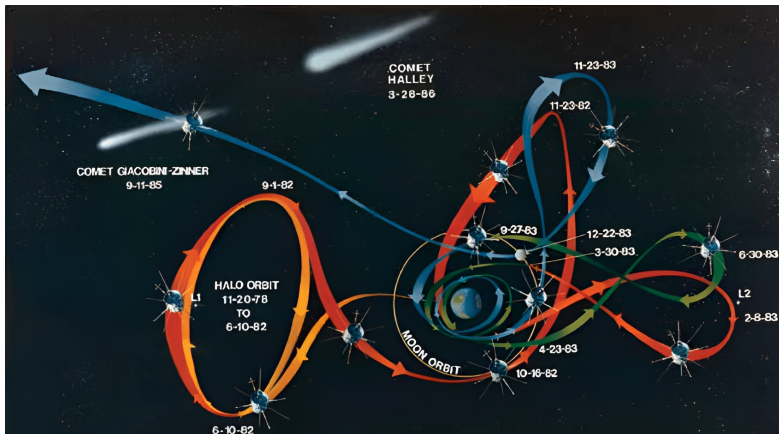
Figure 1.3: Artistic depiction of the ISEE-3 trajectory. (Painting in ISEE-3/ICE Control Center at NASA Goddard).

To this day many missions have been launched into orbits around Sun-Earth libration points, both for space weather monitoring (SOHO, ACE, WIND) and space-based astronomy (GAIA, Planck, the James Webb telescope) and the coming years the Artemis program will make wide use of the Earth-Moon three body problem for the transfers to and from the Gateway station. A relatively recent development is the exploitation of both the Sun-Earth and the Earth-Moon three-body dynamics to have low Δv transfers to the Moon, such as in the Hiten mission or SMART-1.

1.3 Thesis concept and outline

Today, missions to Mars are launched in periods when the v_∞ requirements are low due to the alignment of Earth and Mars called *launch windows*. The idea investigated in this thesis is to construct cycler trajectories that transfer to and from Mars during these launch windows, staying in high energy parking orbits during the stay at Mars and Earth. This concept, illustrated in figure 1.5, allows for the coverage of all possible launch windows with two cycler vehicles and has the minimum v_∞ requirement for the taxi, since it "follows" the launch windows.
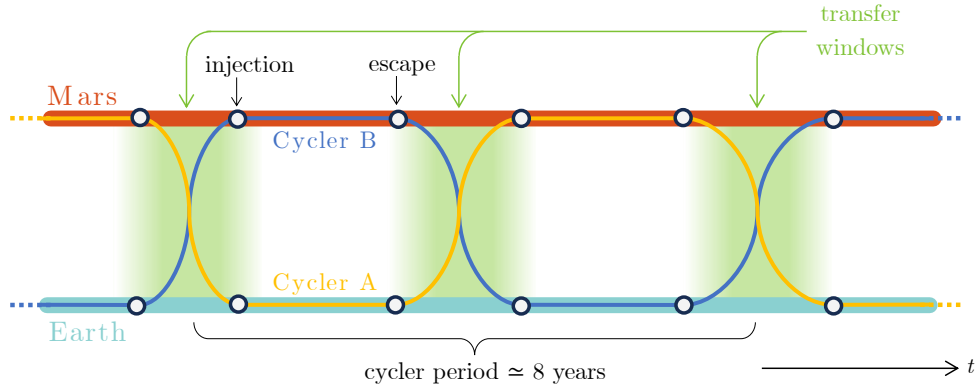
Figure 1.4: The cycler concept investigated in this thesis.

Such a cycler would need to make maneuvers to inject into and escape from planetary orbit but the Δv can potentially be low if three criteria are met:

- The parking orbit has an energy very close to zero (thus to escape).

- The injection and escape maneuvers are done at a low altitude, in such a way that the Δv is much lower than the change in v_∞ (this effect is described in detail in section 3.5).

- The parking orbit is oriented in such a way that the maneuvers do not need to rotate the velocity vector by a large amount.

Theoretical considerations (made in section 5.1) show that if these conditions are met perfectly $\Delta v \simeq 1.8$ km/s for a Mars stay and $\Delta v \simeq 9$ km/s for an Earth stay.

Trajectories that pass near the libration points could satisfy these requirements, as they have high energy and are highly flexible both in terms of geometry near the planet and periapsis-to-periapsis travel duration. A feasible parking strategy could thus be similar to the one shown in figure 1.5: the spacecrafts does the injection maneuver near the planet, follows its ballistic path towards the libration points near which it resides until the next launch windows arrives, passes again near the planet where it performs the escape maneuver and proceeds to transfer to the next planet. The taxi travels with the cycler vehicle for the interplanetary transfer and separates before the injection burn; after landing it injects into an Earth transfer orbit and meets with the cycler vehicle during the escape hyperbola, or alternatively the rendezvous can be done when the cycler vehicle is still in orbit around the planet.
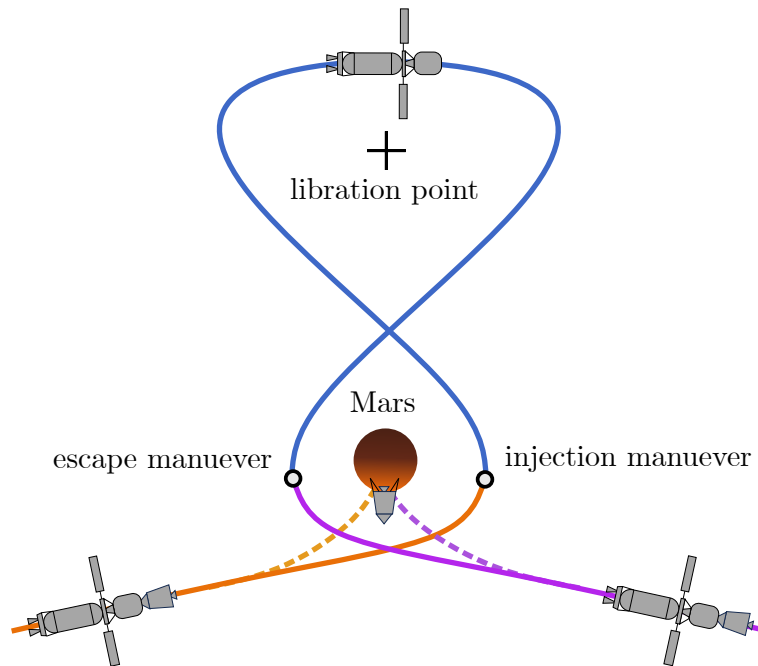
Figure 1.5: Parking trajectory concept.

Beside this introduction, this thesis is composed of the following chapters:

Chapter 2 The Circular Restricted Three Body Problem is introduced and its dynamics are derived, with particular focus on the periodic orbits around collinear points, their stability and the possible trajectories in their vicinity.

Chapter 3 Interplanetary transfers in the patched conics approach are introduced. Launch windows are visualized with the *porkchop diagram* and a lower limit to the theoretical Δv of the cycler is formulated.

Chapter 4 The method to generate the parking orbits is formulated thanks to the concepts introduced in chapter 2. The Keplerian orbit framework is used to calculate the Δv associated to a specific parking orbit.

Chapter 5 Techniques to optimize the cycler trajectory, both the interplanetary and the parking phases, are discussed and carried out.

Chapter 2

Circular Restricted Three Body Problem

The Circular Restricted Three Body Problem (CR3BP) is a dynamical model that describes the motion of a spacecraft under the gravitational influence of two massive bodies. In this thesis it is used to compute parking orbits in the Sun-Earth and Sun-Mars system. This chapter is based on *Dynamical Systems, the Three-Body Problem and Space Mission Design* by Koon, Lo, Mardsen and Ross [3], but differs in some expression due to the fact that different reference frames have been used.

The CR3BP assumes the following two hypotheses:

- The mass of the spacecraft is negligible compared to the ones of the two massive bodies m_1 and m_2. The motion of m_1 and m_2 is thus unaffected by the position of the spacecraft.

- The two massive bodies move in a circular Keplerian orbit around each other, characterized by a radius $R_\star$ and a constant angular velocity Ω

The subscripts are chosen such that $m_1 > m_2$, in this way the *mass parameter* ν of the system is defined as following:

$$\nu = \frac{m_2}{m_2 + m_1} \in (0\,,0.5] \tag{2.1}$$

Its values for the Sun-Earth ($\oplus$) and Sun-Mars ($\male$) systems are:

$$\nu_\oplus = 3.00349 \cdot 10^{-6} \qquad\qquad \nu_\male = 3.22574 \cdot 10^{-7}$$

2.1 Reference frames

The problem is formulated using two reference frames, shown in figure 2.2

- **Inertial frame** $\{X, Y, Z, t\}$ with the origin in the center of mass and the Z axis perpendicular to the massive bodies' orbital plane. In this frame m_1 and m_2 move in circles around the origin.

- **Synodic (rotating) frame** $\{x, y, z, t\}$. While the origin of this system is traditionally placed in the center of mass, for this thesis it is convenient to center the

6

coordinates in m_2: x axis is opposite to m_1, y axis is oriented towards the velocity of m_2 in the inertial frame and z is aligned with Z. In this frame apparent forces act on the spacecraft but it is still useful because m_1 and m_2 have fixed positions.
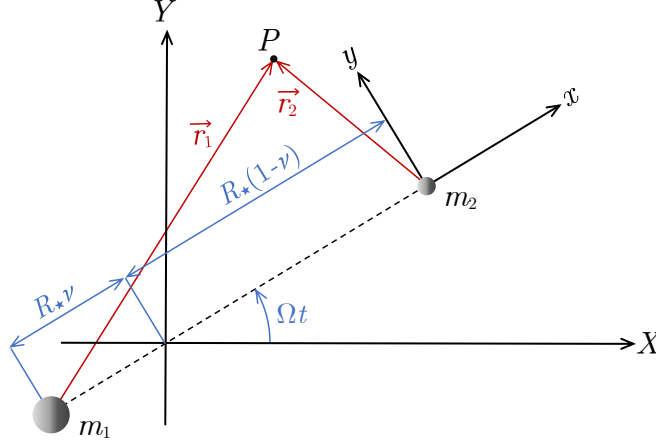
Figure 2.1: Planar projection of inertial and synodic reference frames.

The two frames are linked by the following transformations:

$$X = (x + 1 - \nu)\cos(\Omega t) - y\sin(\Omega t) \tag{2.2a}$$
$$Y = (x + 1 - \nu)\sin(\Omega t) + y\cos(\Omega t) \tag{2.2b}$$
$$Z = z \tag{2.2c}$$

As anticipated, in the fixed frame the massive bodies move in circular orbits with angular velocity Ω:

$$X_1 = -R_\star \nu \cos(\Omega t) \qquad Y_1 = -R_\star \nu \sin(\Omega t) \qquad Z_2 = 0$$
$$X_2 = R_\star (1 - \nu) \cos(\Omega t) \qquad Y_2 = R_\star (1 - \nu) \sin(\Omega t) \qquad Z_2 = 0$$

Meanwhile in the synodic frame of reference their position are fixed at:

$$x_1 = 0 \qquad y_1 = 0 \qquad z_1 = 0$$
$$x_2 = -R_\star \qquad y_2 = 0 \qquad z_2 = 0$$

The vectors that connect m_1, m_2 to the point mass P are named respectively $\vec{r}_1$ and $\vec{r}_2$, their magnitude being equal to:

$$r_1 = \sqrt{(x + R_\star)^2 + y^2 + z^2} \tag{2.3a}$$
$$r_2 = \sqrt{x^2 + y^2 + z^2} \tag{2.3b}$$

Since the synodic frame is centered on m_2, the spacecraft position $\vec{r}$ in it coincides with $\vec{r}_2$. Both names will be used on depending on context, however their numerical values are equal.

2.2 Equations of motion

Equations of motion can be derived in the synodical frame with the Euler-Lagrange equation:

$$\frac{\mathrm{d}}{\mathrm{d}t}\left(\frac{\partial \mathcal{L}}{\partial \dot{q}_j}\right) = \frac{\partial \mathcal{L}}{\partial q_j} \tag{2.4}$$

Where q_j is the j-th coordinate of the system and $\mathcal{L}$ is the difference between kinetic $\mathcal{K}$ and potential $\mathcal{U}$ energy:

$$\mathcal{L}\left(q, \dot{q}, t\right) = \mathcal{K} - \mathcal{U} \tag{2.5}$$

The (specific) kinetic energy $\mathcal{K}$ in the inertial frame is:

$$\mathcal{K} = \frac{1}{2}\left(\dot{X}^2 + \dot{Y}^2 + \dot{Z}^2\right)$$

which by using the transformations in equations 2.2 can be expressed as:

$$\mathcal{K} = \frac{1}{2}\left((\dot{x} - \Omega y)^2 + (\dot{y} + \Omega(x + R_\star(1 - \nu)))^2 + \dot{z}^2\right)$$

The potential energy $\mathcal{U}$ is given by the gravitational potential of the two bodies:

$$\mathcal{U} = -\frac{\mu_1}{r_1} - \frac{\mu_2}{r_2}$$

where $\mu_1 = Gm_1$ and $\mu_2 = Gm_2$ are the gravitational parameters of the two bodies. Since r_1 and r_2 are the magnitudes of two vectors, their value is independent of the reference frame, thus this expression is valid in both systems. By defining the characteristic gravitational parameter $\mu_\star = G(m_1 + m_2)$ the expression for $\mathcal{U}$ becomes

$$\mathcal{U} = -\frac{(1 - \nu)\mu_\star}{r_1} - \frac{\nu\mu_\star}{r_2}$$

In conclusion, the lagrangian $\mathcal{L}$ becomes:

$$\mathcal{L} = \frac{1}{2}\left((\dot{x} - \Omega y)^2 + (\dot{y} + \Omega(x + R_\star(1 - \nu)))^2 + \dot{z}^2\right) + \frac{(1 - \nu)\mu_\star}{r_1} + \frac{\nu\mu_\star}{r_2} \tag{2.6}$$

This expression can be simplified by choosing an adimensional set of coordinates $\{x', y', z', t'\}$, defined as follows:

$$x' = \frac{x}{R_\star} \qquad y' = \frac{y}{R_\star} \qquad z' = \frac{z}{R_\star} \qquad t' = \frac{t}{T_\star}$$

where the time unit $T_\star$ is defined as the reciprocal of the angular velocity Ω:

$$T_\star = \frac{1}{\Omega} = \sqrt{\frac{R_\star^3}{\mu_\star}} \tag{2.7}$$

By applying these transformations, the lagrangian becomes:

$$\mathcal{L} = \frac{1}{2}\left((\dot{x}' - y')^2 + (\dot{y}' + (x' + 1 - \nu))^2 + \dot{z}'^2\right)\frac{R_\star^2}{T_\star^2} + \left(\frac{1 - \nu}{r_1'} + \frac{\nu}{r_2'}\right)\frac{\mu_\star}{R_\star}$$

From equation 2.7 it can be seen that $\mu_\star/R_\star = R_\star^2/T_\star^2$, thus both terms can be divided by this quantity obtaining the adimensional lagrangian $\mathcal{L}'$. The $'$ superscript will be omitted

and for the rest of the chapter the coordinates will be adimensional (unless specified otherwise):

$$\mathcal{L} = \frac{1}{2}\left((\dot{x}-y)^2 + (\dot{y}+(x+1-\nu))^2 + \dot{z}^2\right) + \frac{1-\nu}{r_1} + \frac{\nu}{r_2}$$

where $r_1 = \sqrt{(x+1)^2 + y^2 + z^2}$ and $r_2 = \sqrt{x^2+y^2+z^2}$. The expression can then be rewritten in the following form:

$$\mathcal{L} = \frac{1}{2}\left(\dot{x}^2 + \dot{y}^2 + \dot{z}^2\right) - \dot{x}y + (x+1-\nu)\dot{y} + \frac{1}{2}\left((x+1-\nu)^2 + y^2\right) + \frac{1-\nu}{r_1} + \frac{\nu}{r_2}$$

Then, all terms depending only on the position can be grouped in a single term constituting an *effective potential U*:

$$U(x,y,z) = \frac{1}{2}\left((x+1-\nu)^2 + y^2\right) + \frac{1-\nu}{r_1} + \frac{\nu}{r_2} \tag{2.8}$$

The final form of the lagrangian is thus:

$$\mathcal{L} = \frac{1}{2}\left(\dot{x}^2 + \dot{y}^2 + \dot{z}^2\right) - \dot{x}y + (x+1-\nu)\dot{y} + U(x,y,z) \tag{2.9}$$

Using this lagrangian in the Euler-Lagrange equations 2.4, yields the following equations:

$$\begin{cases} \ddot{x} = \dfrac{\partial U}{\partial x} + 2\dot{y} & \text{(2.10a)} \\[2mm] \ddot{y} = \dfrac{\partial U}{\partial x} - 2\dot{x} & \text{(2.10b)} \\[2mm] \ddot{z} = \dfrac{\partial U}{\partial z} & \text{(2.10c)} \end{cases}$$

The derivatives of U are reported in appendix A at page 62.

System 2.10 is composed by second-order differential equations, but they can be transformed into first-order by considering $\dot{x}, \dot{y}, \dot{z}$ not as derivatives but as separate variables v_x, v_y, v_z, linked to x, y and z by being their derivatives. This lets us write a 6-dimensional *state vector* $\boldsymbol{x}$, comprised of the position $\vec{r}$ and the velocity $\vec{v}$ of the spacecraft in the synodic frame of reference:

$$\boldsymbol{x} = \begin{bmatrix} \vec{r} \\ \vec{v} \end{bmatrix} = \begin{bmatrix} x \\ y \\ z \\ v_x \\ v_y \\ v_z \end{bmatrix} \tag{2.11}$$

The time derivative $\dot{\boldsymbol{x}}$ of the state vector is given by equations 2.10 and $\frac{\mathrm{d}}{\mathrm{d}t}\vec{r} = \vec{v}$, it is therefore a function $\boldsymbol{f}(\boldsymbol{x})$ of the state vector only. Denoting partial derivatives with a subscript under ∂ as in $\frac{\partial}{\partial q_j} = \partial_{q_j}$, the equation of motion becomes:

$$\frac{\mathrm{d}}{\mathrm{d}t}\begin{bmatrix} x \\ y \\ z \\ v_x \\ v_y \\ v_z \end{bmatrix} = \begin{bmatrix} v_x \\ v_y \\ v_z \\ \partial_x U + 2v_y \\ \partial_y U - 2v_x \\ \partial_z U \end{bmatrix} \qquad \text{or shortly} \qquad \dot{\boldsymbol{x}} = \boldsymbol{f}(\boldsymbol{x}) \tag{2.12}$$

The CR3BP admits one integral of motion J called *Jacobi integral* or *Jacobi energy*. By multiplying equations 2.10 respectively by $\dot{x}$, $\dot{y}$ and $\dot{z}$ and adding them together, the following equation can be obtained:

$$\ddot{x}\dot{x} + \ddot{y}\dot{y} + \ddot{z}\dot{z} = \partial_x U \dot{x} + \partial_y U \dot{y} + \partial_z U \dot{z}$$

then the following two identities can be verified:

$$\frac{\mathrm{d}U(x,y,z)}{\mathrm{d}t} = \frac{\partial U}{\partial x}\frac{\mathrm{d}x}{\mathrm{d}t} + \frac{\partial U}{\partial y}\frac{\mathrm{d}y}{\mathrm{d}t} + \frac{\partial U}{\partial z}\frac{\mathrm{d}z}{\mathrm{d}t} = \partial_x U \dot{x} + \partial_y U \dot{y} + \partial_z U \dot{z}$$

$$\frac{1}{2}\frac{\mathrm{d}}{\mathrm{d}t}\left(\dot{x}^2 + \dot{y}^2 + \dot{z}^2\right) = \ddot{x}\dot{x} + \ddot{y}\dot{y} + \ddot{z}\dot{z}$$

Substituting these identities in the first equation gives:

$$\frac{\mathrm{d}U(x,y,z)}{\mathrm{d}t} = \frac{1}{2}\frac{\mathrm{d}}{\mathrm{d}t}\left(\dot{x}^2 + \dot{y}^2 + \dot{z}^2\right)$$

which can show explicitly a time invariant quantity (the Jacobi integral) by bringing the second term to the left of the equal sign:

$$\frac{\mathrm{d}J}{\mathrm{d}t} = 0 \tag{2.13}$$

$$J(\boldsymbol{x}) = \frac{1}{2}\left(\dot{x}^2 + \dot{y}^2 + \dot{z}^2\right) - U(x,y,z) \tag{2.14}$$

2.3   Equilibrium Points

The spacecraft is in equilibrium when $\dot{\boldsymbol{x}} = 0$, which directly implies $\vec{v} = 0$. It's easy to see from equation 2.12 that requiring $\vec{v} = 0$ and $\dot{\boldsymbol{x}} = 0$ reduces to $\partial_x U = \partial_y U = \partial_z U = 0$. So equilibrium points are found by solving:

$$\begin{cases} (x+1-\nu) - \dfrac{1-\nu}{r_1^3}(x+1) - \dfrac{\nu}{r_2^3}x = 0 & (2.15) \\[4mm] y - \left(\dfrac{1-\nu}{r_1^3} + \dfrac{\nu}{r_2^3}\right)y = 0 & (2.16) \\[4mm] -\left(\dfrac{1-\nu}{r_1^3} + \dfrac{\nu}{r_2^3}\right)z = 0 & (2.17) \end{cases}$$

Equation 2.17 reduces to $z = 0$: equilibrium points must lie in the $x - y$ plane.
The remaining equations can be solved in two different ways, generating two families of equilibrium points:

- It's easy to verify that 2.15 and 2.16 are solved when $r_1 = r_2 = 1$. These solution correspond to two equilibrium points placed on the vertexes of two equilateral triangles with a common side whose vertexes are m_1 and m_2, for this reason they are referred to as *triangular points*. They are usually labeled L_4 and L_5.

- The other equilibrium points are found by imposing $y = 0$, this identically satisfies 2.16 and leaves only 2.15. These solutions correspond to equilibrium points lying on

the x axis and are referred to as *collinear points*. Since $y = z = 0$ the radii r_1 and r_2 become functions of x only:

$$r_1 \rightarrow |x - 1| \qquad\qquad\qquad r_2 \rightarrow |x|$$

By doing this substitution in 2.15 the following equation is obtained:

$$(x + 1 - \nu) - \frac{(1 - \nu)(x + 1)}{|x + 1|^3} - \frac{\nu x}{|x|^3} = 0 \qquad\qquad (2.18)$$

This equation does not have closed form solutions but can be solved numerically for a given value of ν. It has three solutions: one equilibrium point between m_1 and m_2 called L_1, two beyond them called L_2 (beyond m_2) and L_3 (beyond m_1).

These equilibrium points are often referred to as *Lagrangian Points*.
When ν is small, like in the case of the Sun-Earth and Sun-Mars systems, L_1 and L_2 are much closer to m_2 than the other points, thus their dynamics is useful in designing parking orbits that stay relatively close to the planetary body. Their dimensional x coordinates are listed in table 2.1.

	x_{L_1} [km]	x_{L_2} [km]
$\oplus$	-108 228.86	108 566.48
♂	-149 139.13	150 136.99

Table 2.1: x coordinates of L_1 and $L2$ in the Sun-Earth ($\oplus$) and Sun-Mars (♂) systems
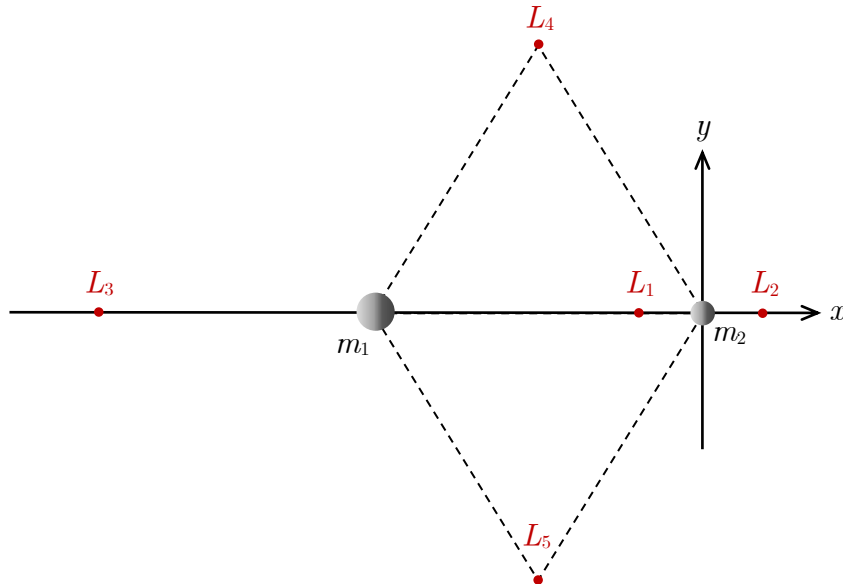

Figure 2.2: Positions of equilibrium points and naming convention.

2.4   Linearized dynamics and stability of collinear points

To investigate the stability of L_1 and L_2, system 2.12 needs to be linearized around the equilibrium points. It will be later shown in section 2.8 that the qualitative geometry of the solutions to the linearized equations will be the same of the full non-linear system. First, a new $\tilde{x}$ axis is defined, parallel to x but centered in the equilibrium point:

$$\tilde{x} = x - \gamma \qquad \text{where} \qquad \begin{cases} \gamma = x_{L_1} \text{ at } L_1 \\ \gamma = x_{L_2} \text{ at } L_2 \end{cases}$$

The new $\{\tilde{x}, y, z\}$ frame is centered in the equilibrium point and since $\dot{\tilde{x}} = \dot{x}$, equation 2.12 can be used after substituting $\tilde{x}$ to x. Assuming small deviations from equilibrium, the derivatives of the potential can be expanded in a Taylor series to first order:

$$\partial_x U = \partial_{xx} U_\gamma \tilde{x} + \partial_{xy} U_\gamma y + \partial_{xz} U_\gamma z + ...$$
$$\partial_y U = \partial_{yx} U_\gamma \tilde{x} + \partial_{yy} U_\gamma y + \partial_{yz} U_\gamma z + ...$$
$$\partial_z U = \partial_{xx} U_\gamma \tilde{x} + \partial_{zy} U_\gamma y + \partial_{zz} U_\gamma z + ...$$

where the subscript γ indicates evaluation at the equilibrium point. First order derivatives $\partial_{q_j} U_\gamma$ are not present since partial derivatives of the potential are zero at equilibrium points. The previous Taylor expansions can be used in equation 2.12, which can now be turned into matrix form:

$$\frac{\mathrm{d}}{\mathrm{d}t} \begin{bmatrix} \tilde{x} \\ y \\ z \\ v_x \\ v_y \\ v_z \end{bmatrix} = \begin{bmatrix} 0 & 0 & 0 & 1 & 0 & 0 \\ 0 & 0 & 0 & 0 & 1 & 0 \\ 0 & 0 & 0 & 0 & 0 & 1 \\ \partial_{xx} U_\gamma & \partial_{xy} U_\gamma & \partial_{xz} U_\gamma & 0 & 2 & 0 \\ \partial_{xy} U_\gamma & \partial_{yy} U_\gamma & \partial_{yz} U_\gamma & -2 & 0 & 0 \\ \partial_{xz} U_\gamma & \partial_{yz} U_\gamma & \partial_{zz} U_\gamma & 0 & 0 & 0 \end{bmatrix} \begin{bmatrix} \tilde{x} \\ y \\ z \\ v_x \\ v_y \\ v_z \end{bmatrix}$$

which can be written in more compact form as:

$$\dot{\tilde{\boldsymbol{x}}} = \mathbf{A}_\gamma \tilde{\boldsymbol{x}} \tag{2.19}$$

Matrix $\mathbf{A}_\gamma$ is constant. The second derivatives of the potential are found by plugging $x = \gamma$, $y = 0$ and $z = 0$ in the expressions listed in appendix A:

- Since $y = z = 0$ it is trivial to see that $\partial_{xy} U_\gamma = \partial_{xz} U_\gamma = \partial_{yz} U_\gamma = 0$

- Remaining nonzero derivatives are made simpler by substituting $r_1 = 1 + \gamma$ (valid for L_1 and L_2), $r_2 = |\gamma|$ and removing terms multiplied by y or z:

$$\partial_{xx} U_\gamma = 1 + 2 \left(\frac{1-\nu}{(1+\gamma)^3} + \frac{\nu}{|\gamma|^3} \right) \tag{2.20}$$

$$\partial_{yy} U_\gamma = 1 - \left(\frac{1-\nu}{(1+\gamma)^3} + \frac{\nu}{|\gamma|^3} \right) \tag{2.21}$$

$$\partial_{zz} U_\gamma = - \left(\frac{1-\nu}{(1+\gamma)^3} + \frac{\nu}{|\gamma|^3} \right) \tag{2.22}$$

Their expression can be further simplified by defining a new quantity ξ as the term inside the parenthesis, which is strictly positive:

$$\xi = \frac{1-\nu}{(1+\gamma)^3} + \frac{\nu}{|\gamma|^3} > 0 \tag{2.23}$$

thus, the derivatives' expressions become

$$\partial_{xx}U_\gamma = 1 + 2\xi \qquad\qquad \partial_{yy}U_\gamma = 1 - \xi \qquad\qquad \partial_{zz}U_\gamma = -\xi$$

Substituting these results in $\mathbf{A}_\gamma$, the final form of the linearized dynamical system becomes:

$$\frac{\mathrm{d}}{\mathrm{d}t}\begin{bmatrix} \tilde{x} \\ y \\ z \\ v_x \\ v_y \\ v_z \end{bmatrix} = \begin{bmatrix} 0 & 0 & 0 & 1 & 0 & 0 \\ 0 & 0 & 0 & 0 & 1 & 0 \\ 0 & 0 & 0 & 0 & 0 & 1 \\ 1+2\xi & 0 & 0 & 0 & 2 & 0 \\ 0 & 1-\xi & 0 & -2 & 0 & 0 \\ 0 & 0 & -\xi & 0 & 0 & 0 \end{bmatrix}\begin{bmatrix} \tilde{x} \\ y \\ z \\ v_x \\ v_y \\ v_z \end{bmatrix}$$

Since the third and sixth row of $\mathbf{A}_\gamma$ contains only one element, the motion in z can be decoupled from the one in the $x - y$ plane, reducing the system to:

$$\ddot{z} = -\xi z \tag{2.24}$$

$$\frac{\mathrm{d}}{\mathrm{d}t}\begin{bmatrix} \tilde{x} \\ y \\ v_x \\ v_y \end{bmatrix} = \begin{bmatrix} 0 & 0 & 1 & 0 \\ 0 & 0 & 0 & 1 \\ 1+2\xi & 0 & 0 & 2 \\ 0 & 1-\xi & -2 & 0 \end{bmatrix}\begin{bmatrix} \tilde{x} \\ y \\ v_x \\ v_y \end{bmatrix} \tag{2.25}$$

The two motions can thus be solved separately:

Vertical motion.   Since $\xi > 0$, equation 2.24 describes an harmonic oscillation with pulsation:

$$\omega_z = \sqrt{\xi} \tag{2.26}$$

Thus, linearized motion along the z axis around the collinear points is always stable, and can be expressed as:

$$z(t) = A_z \sin(\omega_z t + \psi_z) \tag{2.27}$$

where A_z is the semiamplitude of the oscillation and ψ_z the initial phase.

Planar motion.   The matrix and state vector from equation 2.25 will still be referred to as $\mathbf{A}_\gamma$ and $\tilde{\boldsymbol{x}}$ for brevity, but they will not include the z and v_z components. Since $\mathbf{A}_\gamma$ is invertible, its eigenvalues λ_j can be calculated by solving:

$$\det(\mathbf{A}_\gamma - \lambda \mathbf{I}_4) = 0$$

where $\mathbf{I}$ is the 4×4 identity matrix. The determinant yields the following characteristic polynomial equation:

$$\lambda^4 - \lambda^2(\xi + 2) + (1 + \xi - 2\xi^2) = 0 \tag{2.28}$$

Roots can be found by solving it as a second degree equation of λ^2. They are:

$$\lambda_{1,2} = \pm\sqrt{\frac{\xi - 2 + \sqrt{\xi(9\xi - 8)}}{2}}$$

$$\lambda_{3,4} = \pm\sqrt{\frac{\xi - 2 - \sqrt{\xi(9\xi - 8)}}{2}}$$

The zero degree term of 2.28 can be traced back to:

$$1 + \xi - 2\xi^2 = (1 - 2\xi)(1 + \xi) = \partial_{xx}U_\gamma \ \partial_{yy}U_\gamma$$

It is trivial to see from equation 2.20 that $\partial_{xx}U_\gamma$ is positive, the sign of $\partial_{xx}U_\gamma$ is not trivial to determine but it can be proven to be negative (a demonstration is shown in appendix B). This means that the zero-degree term of 2.28 is negative, thus one of the λ^2 roots is positive and one negative: looking at their expressions it can be concluded that $\lambda_{1,2}^2 > 0$ and $\lambda_{3,4}^2 < 0$, so $\lambda_{1,2}$ must be real and $\lambda_{3,4}$ imaginary. Following these considerations, λ_j can be written in the form:

$$\lambda_1 = + \sigma \tag{2.29a}$$
$$\lambda_2 = - \sigma \tag{2.29b}$$
$$\lambda_3 = + i\omega_p \tag{2.29c}$$
$$\lambda_4 = - i\omega_p \tag{2.29d}$$

where i is the imaginary unit, σ and ω_p are positive real numbers defined as:

$$\sigma = \sqrt{\frac{\xi - 2 + \sqrt{\xi(9\xi - 8)}}{2}} > 0 \tag{2.30}$$

$$\omega_p = \sqrt{\frac{\sqrt{\xi(9\xi - 8)} + 2 - \xi}{2}} > 0 \tag{2.31}$$

Each eigenvalue λ_j of $\mathbf{A}_\gamma$ is associated to an eigenvector $\boldsymbol{w}_j$ satisfying:

$$\mathbf{A}_\gamma \boldsymbol{w}_j = \lambda_j \boldsymbol{w}_j \tag{2.32}$$

The state vector $\tilde{\boldsymbol{x}}$ can be written as a linear combination of the eigenvectors $\boldsymbol{w}_j$:

$$\tilde{\boldsymbol{x}}(t) = \sum_j a_j(t)\boldsymbol{w}_j \tag{2.33}$$

Using this expression of $\tilde{\boldsymbol{x}}$ the dynamical system 2.25 becomes:

$$\frac{\mathrm{d}}{\mathrm{d}t} \sum_j a_j(t)\boldsymbol{w}_j = \mathbf{A}_\gamma \sum_j a_j(t)\boldsymbol{w}_j$$

the derivative and matrix multiplication can be moved inside the j-summation due to their linearity, then by virtue of 2.32 the equation becomes:

$$\sum_j \frac{\mathrm{d}a_j}{\mathrm{d}t}\boldsymbol{w}_j = \sum_j \lambda_j a_j(t)\boldsymbol{w}_j$$

Since each a_j except an arbitrarily chosen one can be set to zero, this relation must hold for every j. The equation can thus be reduced, removing the summation and simplifying $\boldsymbol{w}_j$ from both members:

$$\frac{\mathrm{d}a_j}{\mathrm{d}t} = \lambda_j a_j(t)$$

which is solved by an exponential evolution of a_j from an initial condition $a_{j,0}$:

$$a_j(t) = a_{j,0}e^{\lambda_j t}$$

By using this result in combination with 2.33 and the expressions in 2.29, a general solution of the dynamical system 2.25 can be written in the form:

$$
\begin{bmatrix}
\tilde{x}(t) \\
y(t) \\
v_x(t) \\
v_y(t)
\end{bmatrix}
= a_{1,0}e^{\sigma t}\boldsymbol{w}_1 + a_{2,0}e^{-\sigma t}\boldsymbol{w}_2 + a_{3,0}e^{i\omega_p t}\boldsymbol{w}_3 + a_{4,0}e^{-i\omega_p t}\boldsymbol{w}_4 \tag{2.34}
$$

This formulation highlights the dynamical structure of the equilibrium points, we can in fact see that the motion is characterized by three behaviors:

- **Unstable behavior** associated to $a_{1,0}e^{\sigma t}\boldsymbol{w}_1$. Since $\sigma > 0$ any nonzero initial perturbation $a_{1,0}$ grows exponentially with time.

- **Stable behavior** associated to $a_{2,0}e^{-\sigma t}\boldsymbol{w}_2$. Since $-\sigma < 0$ any nonzero $a_{2,0}$ decreases exponentially with time.

- **Periodic behavior** associated to $a_{3,0}e^{i\omega_p t}\boldsymbol{w}_3 + a_{4,0}e^{-i\omega_p t}\boldsymbol{w}_4$. The exponents have no real part so $a_3(t)$ and $a_4(t)$ oscillate in time with pulsation ω_p.

The values of $\boldsymbol{w} = [w_x, w_y, w_{\dot{x}}, w_{\dot{y}}]^{\mathrm{T}}$ can be determined by solving equation 2.32. Executing the matrix multiplication and moving $\lambda\boldsymbol{w}$ to the first term gives the system:

$$
\begin{cases}
\lambda w_x - w_{\dot{x}} = 0 \\
\lambda w_y - w_{\dot{y}} = 0 \\
(1 + 2\xi)w_x - \lambda w_{\dot{x}} + 2w_{\dot{y}} = 0 \\
(1 - \xi)w_y - 2w_{\dot{x}} - \lambda w_{\dot{y}} = 0
\end{cases}
$$

Since eigenvectors' magnitude is arbitrary it can be chosen so that $w_x = 1$ (it could not be zero otherwise every component would be). Substituting it in the system gives the solution:

$$
\boldsymbol{w} =
\begin{bmatrix}
1 \\
\kappa \\
\lambda \\
\lambda\kappa
\end{bmatrix}
\qquad \text{where} \qquad \kappa = \frac{\lambda^2 - 1 - 2\xi}{2\lambda} \tag{2.35}
$$

This solution can be particularized for every j, giving:

$$
\boldsymbol{w}_1 =
\begin{bmatrix}
1 \\
\kappa' \\
\sigma \\
\sigma\kappa'
\end{bmatrix}
\qquad
\boldsymbol{w}_2 =
\begin{bmatrix}
1 \\
-\kappa' \\
-\sigma \\
\sigma\kappa'
\end{bmatrix}
\qquad
\boldsymbol{w}_3 =
\begin{bmatrix}
1 \\
i\kappa'' \\
i\omega_p \\
-\omega_p\kappa''
\end{bmatrix}
\qquad
\boldsymbol{w}_4 =
\begin{bmatrix}
1 \\
-i\kappa'' \\
-i\omega_p \\
-\omega_p\kappa''
\end{bmatrix} \tag{2.36}
$$

where two new parameters, κ' and κ'' have been introduced for compactness:

$$
\kappa' = \frac{\sigma^2 - 1 - 2\xi}{2\sigma} \tag{2.37}
$$

$$
\kappa'' = -\frac{\omega_p^2 + 1 + 2\xi}{2\omega_p} \tag{2.38}
$$

Focusing just on the x and y components of 2.34 and inserting the values of w_x and w_y found in 2.29 gives:

$$\begin{cases} \tilde{x}(t) = a_{1,0}e^{\sigma t} + a_{2,0}e^{-\sigma t} + a_{3,0}e^{i\omega_p t} + a_{4,0}e^{-i\omega_p t} \\ y(t) = a_{1,0}\kappa'e^{\sigma t} - a_{2,0}\kappa'e^{-\sigma t} + a_{3,0}i\kappa''e^{i\omega_p t} - a_{4,0}i\kappa''e^{-i\omega_p t} \end{cases}$$

Explicit $\sin(\omega_p t)$ and $\cos(\omega_p t)$ dependencies can be shown in the periodic terms by using the Euler identity $e^{ix} = \cos x + i\sin x$ in the exponentials:

$$\begin{aligned} a_{3,0}e^{i\omega_p t} + a_{4,0}e^{-i\omega_p t} &= a_{3,0}(\cos(\omega_p t) + i\sin(\omega_p t)) + a_{4,0}(\cos(\omega_p t) - i\sin(\omega_p t)) = \\ &= (a_{3,0} + a_{4,0})\cos(\omega_p t) + i(a_{3,0} - a_{4,0})\sin(\omega_p t) \\ &= b_1\cos(\omega_p t) + b_2\sin(\omega_p t) \end{aligned}$$

$$\begin{aligned} a_{3,0}i\kappa''e^{i\omega_p t} - a_{4,0}i\kappa''e^{-i\omega_p t} &= a_{3,0}i\kappa''(\cos(\omega_p) + i\sin(\omega_p)) - a_{4,0}i\kappa''(\cos(\omega_p) - i\sin(\omega_p)) = \\ &= i\kappa''(a_{3,0} - a_{4,0})\cos(\omega_p t) - \kappa''(a_{3,0} + a_{4,0})\sin(\omega_p t) \\ &= b_2\kappa''\cos(\omega_p t) - b_1\kappa''\sin(\omega_p t) \end{aligned}$$

where the quantities $b_1 = a_{3,0} + a_{4,0}$ and $b_2 = i(a_{3,0} - a_{4,0})$ have been introduced. It can be noted that to have real (thus physical) solutions, $a_{3,0}$ and $a_{4,0}$ must be complex conjugates, in such a way that both b_1 and b_2 are real. The expressions can be further simplified by defining:

$$A_x = \sqrt{b_1^2 + b_2^2}$$

$$\psi_p = \tan^{-1}\left(\frac{b_2}{b_1}\right)$$

that transform the periodic terms into

$$a_{3,0}e^{i\omega_p t} + a_{4,0}e^{-i\omega_p t} = A_x\cos(\omega_p t + \psi_p)$$

$$a_{3,0}i\kappa''e^{i\omega_p t} - a_{4,0}i\kappa''e^{-i\omega_p t} = \kappa''A_x\sin(\omega_p t + \psi_p)$$

With these relations, including the motion in z from equation 2.27, the general solution to the linearized equation of motion around L_1 and L_2 becomes

$$\begin{cases} \tilde{x}(t) = A_x\cos(\omega_p t + \psi_p) + a_u e^{\sigma t} + a_s e^{-\sigma t} & \text{(2.39a)} \\ y(t) = \kappa''A_x\sin(\omega_p t + \psi_p) + a_u\kappa'e^{\sigma t} - a_s\kappa'e^{-\sigma t} & \text{(2.39b)} \\ z(t) = A_z\sin(\omega_z t + \psi_z) & \text{(2.39c)} \end{cases}$$

Where $a_u = a_{1,0}$ and $a_s = a_{2,0}$ have been renamed with subscript u for "unstable" and s for "stable", given the behavior of those terms.

2.5 Trajectories in the linearized dynamics

The trajectories described by system 2.39 can be categorized depending on their dynamic behavior, and the various possibilities are visualized by setting to zero coefficients of the system.

Libration orbits These trajectory contain only the periodic terms ($a_u = a_s = 0$), thus the spacecraft position is bounded. The simplest type is the planar case in which $A_z = 0$ and $A_x \neq 0$: the trajectory is an elliptical retrograde orbit (since $\kappa'' < 0$) centered in the equilibrium point. These trajectories are called *Lyapunov Orbits* and have a period equal to $2\pi/\omega_p$ which is close to half of the orbital period of the massive bodies. When $A_x = 0$ and $A_z \neq 0$ a *vertical Lyapunov orbit* is generated, which in the linearized dynamics corresponds to a simple oscillation in the z axis around the equilibrium point with period $2\pi/\omega_z$. If both A_x and A_z are nonzero *Lissajous orbits* are described by the spacecraft. From equations 2.26 and 2.26 we can see that $\omega_p \neq \omega_v$ and their ratio is not a rational number, these trajectories in fact are not strictly periodic (in the sense that they are not closed on themselves). Lyapunov and Lissajous orbits are depicted in figure 2.3.

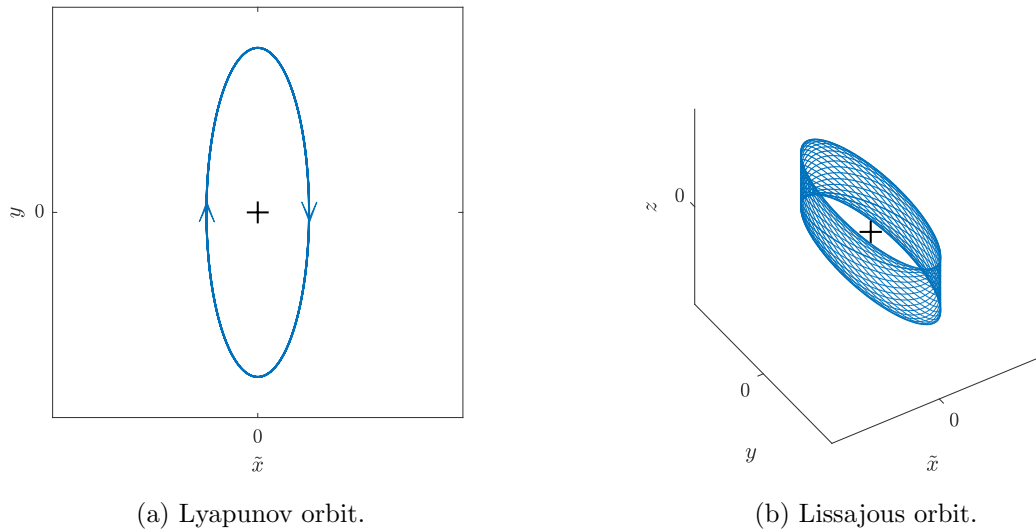(a) Lyapunov orbit.   (b) Lissajous orbit.

Figure 2.3: Libration orbits around collinear points in the with linearized dynamics. The trajectory is shown in blue, while the libration point is depicted as a cross.

With full non-linear dynamics ω_p and ω_z are not constant but vary with A_x and A_z and for a sufficiently large A_x is possible to find an A_z that satisfies $\omega_p = \omega_z$. These trajectories are truly periodic and are referred to as *Halo orbits* but due to their inherent non-linearity are not obtainable from the dynamics described by system 2.39.

Asymptotic trajectories If, in addition to the periodic terms, a_u or a_s are non-zero the trajectories approach asymptotically libration orbits at $t \to \infty$ or $t \to -\infty$: these trajectories will be referred respectively to *stable* and *unstable*. Examples of such trajectories are depicted in figure 2.4, where the z component of motion has been omitted since it is always an oscillation around $z = 0$. These trajectories can extend to negative or positive $\tilde{x}$ corresponding to a negative or positive a_s and a_u.
Given a libration orbit, the following sets can be defined:

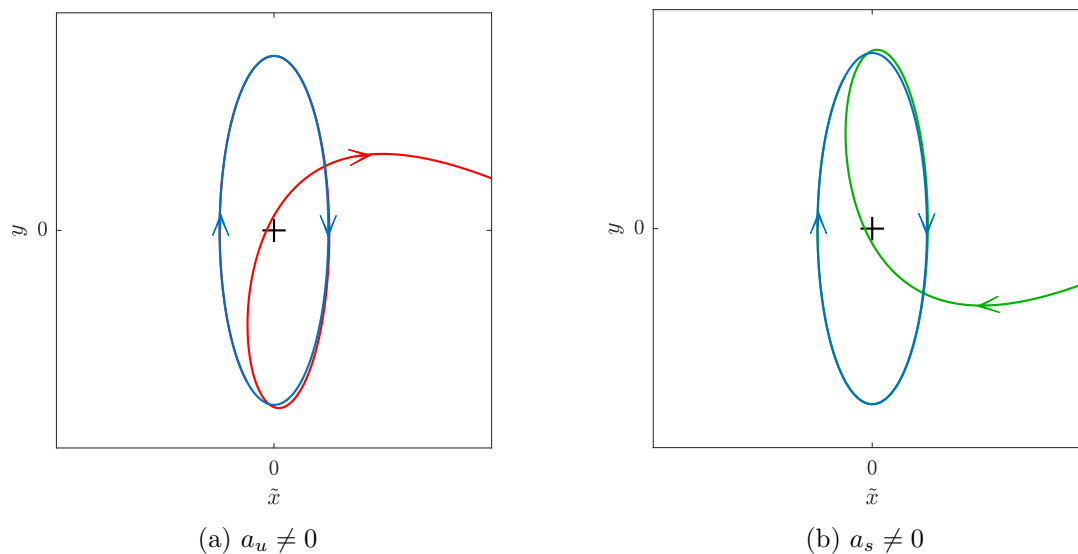(a) $a_u \neq 0$ (b) $a_s \neq 0$

Figure 2.4: Stable and unstable trajectories with linearized dynamics. The corresponding libration orbit is shown in blue, the libration point is depicted as a cross, the unstable trajectory in red while the the stable one in green.

- *Stable manifold* as the set of all the states belonging to a stable trajectory that converges to the libration orbit.

- *Unstable manifold* as the set of all the states belonging to an unstable trajectory that diverges from the libration orbit.
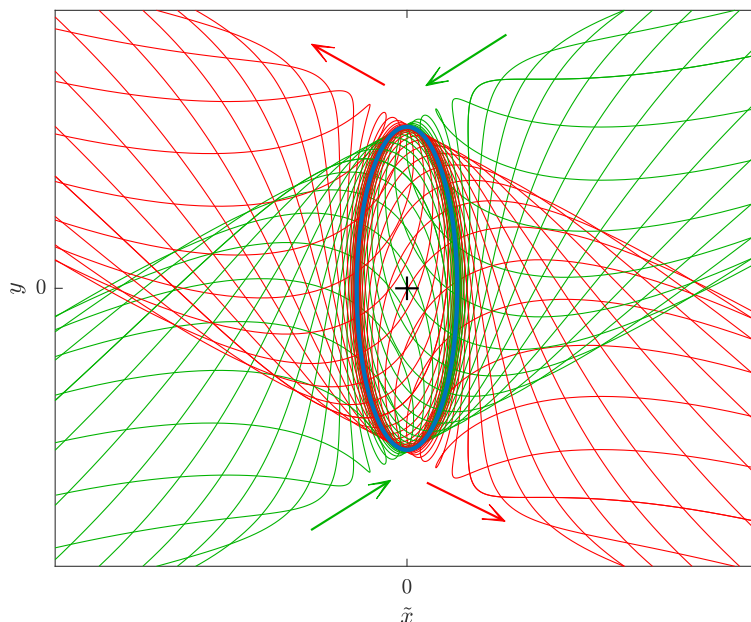

Figure 2.5: Some trajectories belonging to the stable manifold (in green) and the unstable manifold (in red) associated to a Lyapunov orbit (in blue). with linearized dynamics.

These sets (shown in figure 2.5) are collectively known as *invariant manifolds* and each of

them presents a positive branch and a negative one, relative to positive and negatives a_u and a_s.

Transit and non-transit trajectories   When both a_s and a_u are nonzero both stable and unstable behaviors are present, and are classified based on their sign:

- *Transit trajectories* have $a_u a_s < 0$. The opposing signs makes the trajectory pass from the positive to the negative $\tilde{x}$ side or vice versa.

- *Non-transit trajectories* have $a_u a_s > 0$, meaning that the spacecraft leaves the equilibrium region from the same $\tilde{x}$ side from which it came from.

These trajectories are visualized easily by setting $A_x = A_z = 0$, as shown in figure 2.6: it can be seen that trajectories in this regime describe hyperbolae and the transit and non-transit trajectories are separated by the asymptotic trajectories (that in this case collapse to a line). Non-transit trajectories are exploited in this thesis to generate parking
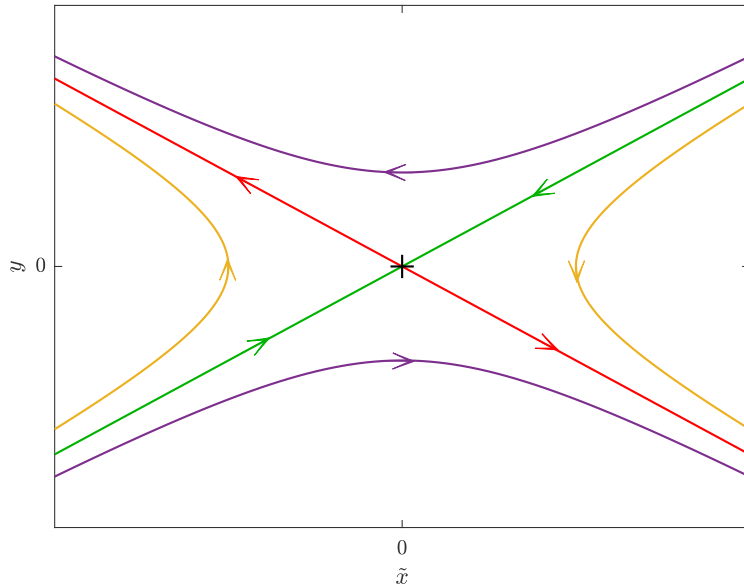

Figure 2.6: Transit (in violet) and non-transit (in yellow) trajectories, with $A_x = A_z = 0$ Stable and unstable manifold are shown respectively in green and red.

orbits with a specific time of flight, thanks to the fact that as the trajectory gets closer to equilibrium the greater the time of flight becomes, making it easy to fine tune it to fit the period of time between two launch windows. The system 2.39 can be particularized for these trajectories, by assuming $a_u = a_s$ and defining:

$$\epsilon = a_u + a_s = 2a_u = 2a_s \tag{2.40}$$

Thanks to this and the hyperbolic trigonometric functions $\cosh x = \frac{1}{2}(e^{-x} + e^x)$ and $\sinh x = \frac{1}{2}(e^x - e^{-x})$, 2.39 becomes:

$$
\begin{cases}
\tilde{x}(t) = A_x \cos(\omega_p t + \psi_p) + \epsilon \cosh(\sigma t) & \text{(2.41a)} \\
y(t) = \kappa'' A_x \sin(\omega_p t + \psi_p) + \kappa' \epsilon \sinh(\sigma t) & \text{(2.41b)} \\
z(t) = A_z \sin(\omega_z t + \psi_z) & \text{(2.41c)}
\end{cases}
$$

From this form it becomes apparent that the closest approach to equilibrium happens at $t = 0$, where $\cosh(\sigma_t) = 1$ and $\sinh(\sigma t) = 0$. A non transit trajectory with $A_x \neq 0$ is shown in figure 2.7.
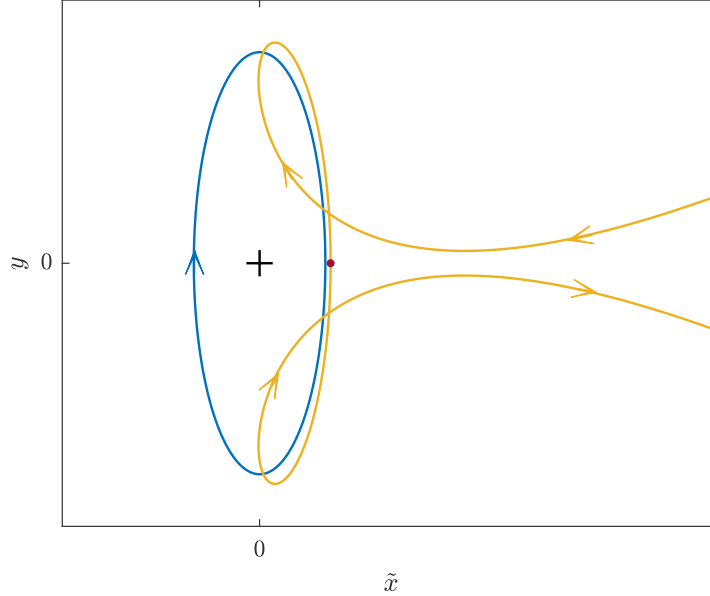

Figure 2.7: Non-transit trajectory (in yellow) and its corresponding Lyapunov orbit (in blue). The closest approach to equilibrium is shown with a red dot.

2.6 Flow and state transition matrix

Linearized dynamics are unsuitable for the design of real world trajectories, mathematical tools to deal with the full non-linear equations of motion are introduced in this section. Given a dynamical system $\dot{\boldsymbol{x}} = \boldsymbol{f}(\boldsymbol{x})$, the *flow* $\boldsymbol{\varphi}$ is a function that maps an initial position $\boldsymbol{x}_0$ at time t_0 to the position $\boldsymbol{x}(t)$ at time t:

$$\boldsymbol{\varphi}(\boldsymbol{x}_0, t) = \int_{t_0, \boldsymbol{x}_0}^{t} \boldsymbol{f}(\boldsymbol{x}(\tau)) \mathrm{d}\tau \qquad \boldsymbol{\varphi}(\boldsymbol{x}_0, t) : \ \boldsymbol{x_0} \mapsto \boldsymbol{x}(t) \qquad (2.42)$$

From this definition, it can be seen that the time derivative of the flow is $\boldsymbol{f}$:

$$\frac{\mathrm{d}\boldsymbol{\varphi}(\boldsymbol{x}_0, t)}{\mathrm{d}t} = \boldsymbol{f}(\boldsymbol{\varphi}(\boldsymbol{x}_0, t)) = \boldsymbol{f}(\boldsymbol{x}(t)) \qquad (2.43)$$

Given a reference trajectory $\bar{\boldsymbol{x}}(t) = \boldsymbol{\varphi}(\bar{\boldsymbol{x}}_0, t)$, a small perturbation in the initial state $\delta\boldsymbol{x}_0$ will evolve over time as:

$$\delta\boldsymbol{x}(t) = \boldsymbol{\varphi}(\bar{\boldsymbol{x}}_0 + \delta\boldsymbol{x}_0, t) - \bar{\boldsymbol{x}}(t)$$

which can be expanded in a Taylor series[1] to first order as
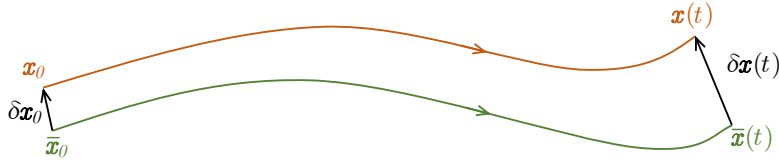
Figure 2.8: reference trajectory $\bar{\boldsymbol{x}}(t)$ and perturbed trajectory $\boldsymbol{x}(t)$

$$\delta\boldsymbol{x}(t) = \frac{\partial\boldsymbol{\varphi}(\boldsymbol{x}_0,t)}{\partial\boldsymbol{x}_0}\delta\bar{\boldsymbol{x}}_0 + ...$$

In this case, the differentiation matrix is referred to as the *state transition matrix* $\boldsymbol{\Phi}$:

$$\boldsymbol{\Phi}(\boldsymbol{x}_0,t_0,t) = \frac{\partial\boldsymbol{\varphi}(\boldsymbol{x}_0,t)}{\partial\boldsymbol{x}_0} = \frac{\partial\boldsymbol{x}(t)}{\partial\boldsymbol{x}_0} \tag{2.44}$$

where dependence on the initial condition $\boldsymbol{x_0}$ is usually omitted. With this definition, the displacement at time t_1, $\delta\boldsymbol{x}_1$, becomes to first order:

$$\delta\boldsymbol{x}_1 = \boldsymbol{\Phi}(t_0,t_1)\delta\boldsymbol{x}_0 \tag{2.45}$$

The state transition matrix has also the following properties, easily verifiable remembering that it is the derivative of the flow:

$$\boldsymbol{\Phi}(t_0,t_0) = \mathbf{I}_6 \tag{2.46}$$
$$\boldsymbol{\Phi}(t_0,t_2) = \boldsymbol{\Phi}(t_0,t_1)\boldsymbol{\Phi}(t_1,t_2) \tag{2.47}$$
$$\boldsymbol{\Phi}(t_1,t_0) = \boldsymbol{\Phi}(t_1,t_0)^{-1} \tag{2.48}$$

The $\boldsymbol{x}_0$-derivation of equation 2.43 can be manipulated to get:

$$\frac{\partial}{\partial\boldsymbol{x}_0}\left(\frac{\mathrm{d}\boldsymbol{\varphi}(\boldsymbol{x}_0,t)}{\mathrm{d}t}\right) = \frac{\partial\boldsymbol{f}(\boldsymbol{\varphi}(\boldsymbol{x}_0,t))}{\partial\boldsymbol{x}_0}$$
$$\frac{\mathrm{d}}{\mathrm{d}t}\left(\frac{\partial\boldsymbol{\varphi}(\boldsymbol{x}_0,t)}{\partial\boldsymbol{x}_0}\right) = \left.\frac{\partial\boldsymbol{f}}{\partial\boldsymbol{x}}\right|_{\boldsymbol{x}(t)}\frac{\partial\boldsymbol{\varphi}(\boldsymbol{x}_0,t)}{\partial\boldsymbol{x_0}}$$

which, recognizing $\boldsymbol{\Phi}$ from equation 2.44 becomes:

$$\dot{\boldsymbol{\Phi}} = \mathbf{A}(t)\boldsymbol{\Phi} \tag{2.49}$$

where matrix $\mathbf{A}$ contains the $\boldsymbol{x}$-derivatives of $\boldsymbol{f}$:

$$\mathbf{A}(t) = \left.\frac{\partial\boldsymbol{f}}{\partial\boldsymbol{x}}\right|_{\boldsymbol{x}(t)} = \begin{bmatrix} 0 & 0 & 0 & 1 & 0 & 0 \\ 0 & 0 & 0 & 0 & 1 & 0 \\ 0 & 0 & 0 & 0 & 0 & 1 \\ \partial_{xx}U & \partial_{xy}U & \partial_{xz}U & 0 & 2 & 0 \\ \partial_{xy}U & \partial_{yy}U & \partial_{yz}U & -2 & 0 & 0 \\ \partial_{xz}U & \partial_{yz}U & \partial_{zz}U & 0 & 0 & 0 \end{bmatrix} \tag{2.50}$$

Equation 2.49 can be used to propagate $\boldsymbol{\Phi}$ from an initial state $\boldsymbol{\Phi}_0 = \mathbf{I}_6$.

---

[1]The partial differentiation between two vectors $\frac{\partial\boldsymbol{a}}{\partial\boldsymbol{b}}$ gives a matrix $\mathbf{D}$ whose elements D_{jk} are:

$$\mathbf{D} = \frac{\partial\boldsymbol{a}}{\partial\boldsymbol{b}} \qquad\qquad\qquad D_{jk} = \frac{\partial a_j}{\partial b_k}$$

2.7   Non-linear Lyapunov orbits

Lyapunov orbits do not have a closed form in the non-linear dynamics thus a technique to approximate them numerically is needed.

By observing system 2.12 and assuming $t_0 = 0$ it can be easily verified that the equations are invariant under the substitution:

$$\boldsymbol{x} = \begin{bmatrix} x \\ y \\ z \\ v_x \\ v_y \\ v_z \end{bmatrix} \rightarrow \boldsymbol{x}^{\mathrm{M}} = \begin{bmatrix} x \\ -y \\ z \\ -v_x \\ v_y \\ -v_z \end{bmatrix} \qquad \text{and} \qquad t \rightarrow -t \qquad (2.51)$$

where $\boldsymbol{x}^{\mathrm{M}}$ will be referred to as the *mirror configuration* of $\boldsymbol{x}$. This symmetry implies that if $\boldsymbol{x}(t_0 + t)$ is a solution of 2.12, then $\boldsymbol{x}^{\mathrm{M}}(t_0 - t)$ also is:

$$\boldsymbol{\varphi}(\boldsymbol{x}_0, t_1) = \boldsymbol{x}_1 \implies \boldsymbol{\varphi}(\boldsymbol{x}_0^{\mathrm{M}}, -t_1) = \boldsymbol{x}_1^{\mathrm{M}}$$

and since $\boldsymbol{x}_1 = (\boldsymbol{x}_1^{\mathrm{M}})^{\mathrm{M}}$, it follows that:

$$\boldsymbol{\varphi}(\boldsymbol{x}_0, t_1) = \boldsymbol{\varphi}(\boldsymbol{x}_0^{\mathrm{M}}, -t_1)^{\mathrm{M}} \qquad (2.52)$$

Any periodic orbit repeats after a period T_L, thus it has the following property:

$$\boldsymbol{\varphi}(\boldsymbol{x}_0, t) = \boldsymbol{\varphi}(\boldsymbol{x}_0, t + T_L) \qquad (2.53)$$

A trajectory that satisfies this relation can be obtained by "sticking together" two mirror trajectories by requiring $\boldsymbol{x}^{\mathrm{M}} = \boldsymbol{x}$ at $t = 0$ and $T_L/2$ (as shown in figure 2.9):

$$\begin{cases} \boldsymbol{x}_0 = \boldsymbol{x}_0^{\mathrm{M}} \\ \boldsymbol{\varphi}(\boldsymbol{x}_0, T_L/2) = \boldsymbol{\varphi}(\boldsymbol{x}_0, T_L/2)^{\mathrm{M}} \end{cases} \qquad (2.54)$$

This is because, using equation 2.52 and these ansatz gives:

$$\boldsymbol{\varphi}(\boldsymbol{x}_0, T_L/2) = \boldsymbol{\varphi}(\boldsymbol{x}_0, T_L/2)^{\mathrm{M}} = (\boldsymbol{\varphi}(\boldsymbol{x}_0^{\mathrm{M}}, -T_L/2)^{\mathrm{M}})^{\mathrm{M}} = \boldsymbol{\varphi}(\boldsymbol{x}_0, -T_L/2)$$

$$\implies \boldsymbol{\varphi}(\boldsymbol{x}_0, -T_L/2) = \boldsymbol{\varphi}(\boldsymbol{x}_0, -T_L/2 + T_L)$$

ensuring the periodicity of the trajectory. The initial state $\boldsymbol{x}_0$ of the periodic orbit can be further determined by looking at $\boldsymbol{x}_0 = \boldsymbol{x}_0^{\mathrm{M}}$ component-wise:

$$\begin{bmatrix} x_0 \\ y_0 \\ z_0 \\ v_{x0} \\ v_{y0} \\ v_{z0} \end{bmatrix} = \begin{bmatrix} x_0 \\ -y_0 \\ z_0 \\ -v_{x0} \\ v_{y0} \\ -v_{z0} \end{bmatrix} \implies \boldsymbol{x}_0 = \begin{bmatrix} x_0 \\ 0 \\ z_0 \\ 0 \\ v_{y0} \\ 0 \end{bmatrix}$$

after which, the z_0 component can then be set to zero, since $z(t) = 0$ is a valid solution of equation 2.10 and linear Lyapunov orbit are planar. For this reason the z and v_z
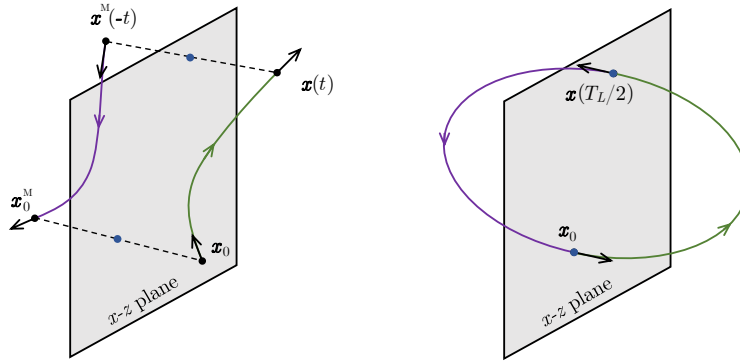
Figure 2.9: On the left, two mirror trajectories are shown with $\boldsymbol{x}(t) = \boldsymbol{\varphi}(\boldsymbol{x}_0, t)$ and $\boldsymbol{x}^{\mathrm{M}}(-t) = \boldsymbol{\varphi}(\boldsymbol{x}_0^{\mathrm{M}}, -t)$. On the right the terminal states of the mirror trajectories coincide, forming a periodic orbit. State vectors are represented by a black dot (position) and a black arrow (velocity).

component will be omitted for the rest of this section. The initial state of a Lyapunov orbit can be thus be written in the form:

$$
\boldsymbol{x}_0 = \begin{bmatrix} x_0 \\ 0 \\ 0 \\ v_{y0} \end{bmatrix}
\tag{2.55}
$$

To find a relation between x_0 and v_{y0} an iterative procedure called *differential correction* is used. First, a variation of the flow function is defined, not integrating until a certain time is reached, but until $\boldsymbol{x}(t)$ crosses the $x - z$ plane:

$$
\boldsymbol{\varphi}_{xz}(\boldsymbol{x}_0) = \int\limits_{t_0, \boldsymbol{x}_0}^{y(t)=0} \boldsymbol{f}(\boldsymbol{x}(t)) \mathrm{d}t
\tag{2.56}
$$

Supposing to know a close but inexact guess of initial state $\boldsymbol{x}_0$, its integration until the $x - z$ plane is crossed gives:

$$
\boldsymbol{x}_1 = \boldsymbol{\varphi}_{xz}(\boldsymbol{x}_0) = \begin{bmatrix} x_1 \\ 0 \\ v_{x1} \\ v_{y1} \end{bmatrix}
$$

where v_{x1} is not zero and $y_1 = 0$ from the definition of $\boldsymbol{\varphi}_{xz}$. Supposing now that a correction $\delta\boldsymbol{x}_0$ is applied to $\boldsymbol{x}_0$ causing the integration to proceed for an extra δt; the displacement $\delta\boldsymbol{x}_1$ from $\boldsymbol{x}_1$ at the final state can be approximated to first order as:

$$
\delta\boldsymbol{x}_1 = \boldsymbol{\Phi}(t_0, t_1)\delta\boldsymbol{x}_0 + \boldsymbol{f}(\boldsymbol{x}_1)\delta t
\tag{2.57}
$$

To have a Lyapunov orbit it should be true that $\boldsymbol{x}_1 = \boldsymbol{x}_1^{\mathrm{M}}$ (from ansatz 2.54), which would imply that y_1 and v_{x1} should be zero. Thus, the displacement $\delta\boldsymbol{x}_1$ should have:

$$
\delta y_1 = 0 \qquad\qquad\qquad\qquad \delta v_{x1} = -v_{x1}
$$

23

Assuming that the correction only acts on the y-velocity of the initial state, it will be in the form:

$$\delta\boldsymbol{x}_0 = \begin{bmatrix} 0 \\ 0 \\ \delta v_{y0} \\ 0 \end{bmatrix}$$

Substituting this expression in 2.57 and taking in account only the components for winch $\delta\boldsymbol{x}_1$ is known yields the system:

$$\begin{cases} \delta y_1 = 0 = \Phi_{y\dot{y}}\delta v_{y0} + v_{y1}\delta t \\ \delta v_{x1} = -v_{x1} = \Phi_{\dot{x}\dot{y}}\delta v_{y0} + \dot{v}_{x1}\delta t \end{cases}$$

where $\Phi_{y\dot{y}}$ and $\Phi_{\dot{x}\dot{y}}$ are the components of $\boldsymbol{\Phi}(t_0, t_1)$. The system can be solved for δv_{y0}:

$$\delta v_{y0} = -v_{x1}\left(\Phi_{\dot{x}\dot{y}} - \frac{\dot{v}_{x1}}{v_{y1}}\Phi_{y\dot{y}}\right)^{-1} \tag{2.58}$$

The correction $\delta\boldsymbol{x}_0$ can thus be calculated from a guess of the initial state, and applied iteratively to get arbitrarily precise results:

$$\boldsymbol{x}_0^{(j+1)} = \boldsymbol{x}_0^{(j)} + \delta\boldsymbol{x}_0^{(j)} \tag{2.59}$$

A suitable initial guess can be given by the linearized equations 2.39 and their t-derivatives:

$$\boldsymbol{x}_0^{(0)} = \begin{bmatrix} A_x + \gamma \\ 0 \\ 0 \\ \kappa''\omega_p A_x \end{bmatrix} \tag{2.60}$$

where ω_p and κ'' are defined respectively in equations 2.29 and 2.38. This guess converges rapidly for small A_x which are close to linearity, but is not suitable for large Lyapunov orbits. To deal with this issue a set of small orbits can be computed first, then a new first guess of $v_{y0,k}^{(0)}$ can be extrapolated linearly from the two nearest converged initial states $v_{y0,k-1}$ and $v_{y0,k-2}$, with:

$$v_{y0,k}^{(0)} = v_{y0,k-1} + \frac{A_{x,k} - A_{x,k-1}}{A_{x,k-1} - A_{x,k-2}}(v_{y0,k-2} - v_{y0,k-1}) \tag{2.61}$$

These procedures allow the rapid computation of families of Lyapunov orbits, which can map a wide range of A_x-v_{y0} pairs to be later interpolated obtaining initial guesses for arbitrary A_x; Lyapunov orbits calculated with this method for the Sun-Mars system are shown in figure 2.10.
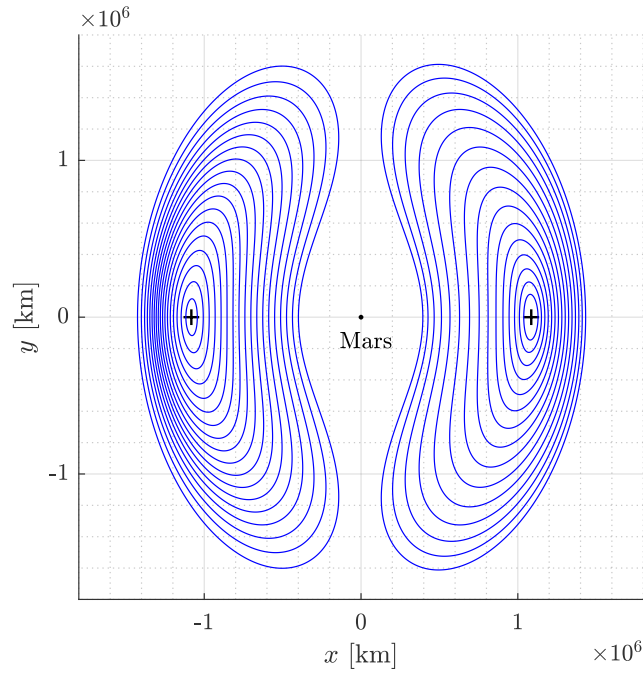
Figure 2.10: L_1 and L_2 Lyapunov orbit families in the Mars-Sun system. L_1 (negative x) and L_2 (positive x) are shown as crosses.

The orbits are very close to ellipses for small values of A_x but their shape changes significantly for bigger values, warping the upper and lower parts of the ellipse towards m_2. The period of the Lyapunov orbits increase with A_x, becoming larger than half the m_2 revolution period $(\pi T_\star)$ around m_1 at $A_x \simeq 0.26|\gamma|$.
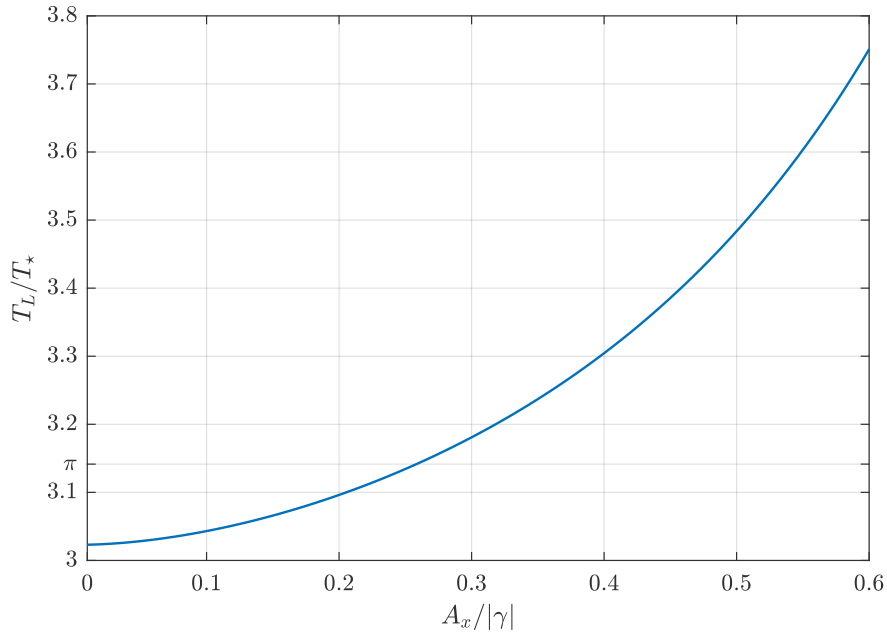

Figure 2.11: Adymensional Lyapunov orbit period versus semiamplitude for the Sun-Mars system.

2.8 Monodromy matrix and stability of Lyapunov orbits

An important tool for the study of periodic orbits is the *monodromy matrix* $\mathbf{M}$, defined as the state transition matrix evaluated over one period T_L:

$$\mathbf{M}(\boldsymbol{x}_0) = \boldsymbol{\Phi}(\boldsymbol{x}_0, t_0, t_0 + T_L) \qquad \text{where} \;\; \boldsymbol{x}_0 \;:\; \boldsymbol{\varphi}(\boldsymbol{x}_0, t_0, t_0 + T_L) = \boldsymbol{x}_0 \qquad (2.62)$$

The monodromy matrix gives information about how displacements in initial conditions $\delta\boldsymbol{x}_0$ evolve after a period:

$$\delta\boldsymbol{x}_1 = \mathbf{M}(\boldsymbol{x}_0)\delta\boldsymbol{x}_0 \qquad (2.63)$$

This equation is very similar to 2.25, the main difference being this is a relation between two states rather than a differential equation describing the evolution of a state. This makes possible to study the stability of a Lyapunov orbit in a similar fashion to how stability of equilibrium points was investigated. First, eigenvalues α and eigenvectors $\boldsymbol{u}$ of $\mathbf{M}$ are computed:

$$\mathbf{M}\boldsymbol{u} = \alpha\boldsymbol{u} \qquad (2.64)$$

Then, $\delta\boldsymbol{x}_0$ is expressed as a linear combination of eigenvectors $\boldsymbol{u}$:

$$\delta\boldsymbol{x}_0 = \sum_j c_j \boldsymbol{u}_j \qquad (2.65)$$

Thus, $\delta\boldsymbol{x}_1$ is given by:

$$\delta\boldsymbol{x}_1 = \sum_j c_j \alpha_j \boldsymbol{u}_j \qquad (2.66)$$

Thus, stability along the direction $\boldsymbol{x}$ is given by the magnitude of α_j. For Lyapunov orbits the eigenvalues take the form:

$$\alpha_1 = \Lambda > 1 \qquad \alpha_2 = \frac{1}{\Lambda} \qquad \alpha_3 = \alpha_4 = 1 \qquad \alpha_5 = \frac{1}{\alpha_6} \qquad (2.67)$$

which are indication of the following behaviors:

- *Unstable* and *stable* behavior associated to α_1 and α_2, similarly to λ_1 and λ_2 in the linearized dynamics. Stable and unstable trajectories can be approximated numerically by choosing a small but nonzero c_1 or c_2 to generate initial conditions $\boldsymbol{x}_0 = \delta\boldsymbol{x} + \boldsymbol{x}_L$ ($\boldsymbol{x}_L$ being a state in the Lyapunov orbit) and integration equations of motion. Invariant manifolds can be computed by integrating from initial conditions with small but nonzero c_1 or c_2 for various phases ψ along a Lyapunov: an example of them is shown in figure 2.12.

- *Cyclic* behavior is associated to α_3 and α_4. The first eigenvector is aligned to velocity of x_0, since the periodicity ensures that displacements along the orbit remain unchanged after one period. The second unitary eigenvalues is related to an "adjacent" periodic orbit at a different Jacobi integral J and it can be proved taking the $\boldsymbol{x}_0$-derivative of $J(\boldsymbol{\varphi}(\boldsymbol{x_0}, T_L)) = J(\boldsymbol{x}_0)$ and applying the chain rule:

$$\frac{\partial J(\boldsymbol{\varphi}(\boldsymbol{x_0}, T_L))}{\partial \boldsymbol{x_0}} = \frac{\partial J(\boldsymbol{\varphi}(\boldsymbol{x_0}, T_L))}{\partial \boldsymbol{\varphi}(\boldsymbol{x_0}, T_L)} \frac{\boldsymbol{\varphi}(\boldsymbol{x_0}, T_L)}{\partial \boldsymbol{x_0}}$$

$$\implies \frac{\partial J(\boldsymbol{x_0})}{\partial \boldsymbol{x_0}} = \frac{\partial J(\boldsymbol{x_0})}{\partial \boldsymbol{x_0}} \mathbf{M}(\boldsymbol{x_0})$$

Thus the row vector $\frac{\partial J(\boldsymbol{x_0})}{\partial \boldsymbol{x_0}}$ is a left eigenvector of $\mathbf{M}$ with eigenvalue $+1$.
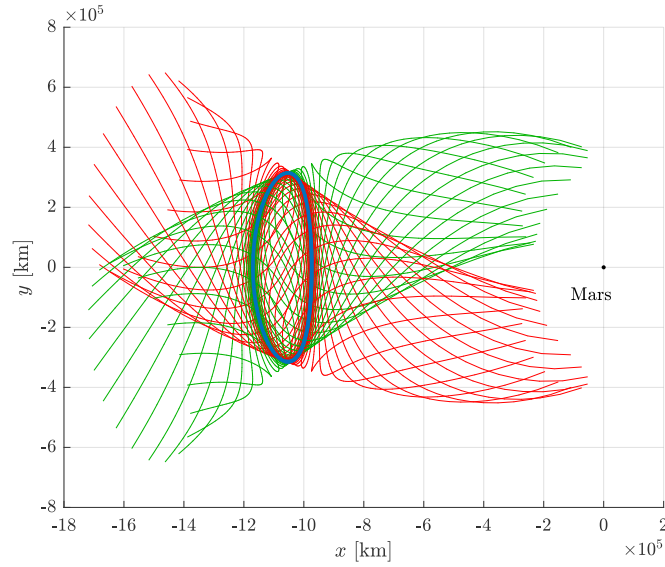
Figure 2.12: Stable (green) and unstable (red) manifolds of a Lyapunov orbit (blue) around L_1 in the Sun-Mars system

- The non planar behavior is associated to α_1 and α_2, which for small amplitudes are two complex conjugates with magnitude $|\alpha_5| = |\alpha_6| = 1$.

Analogously to the linearized dynamics, non-transit trajectories can be generated by setting, for example $c_1 = c_2$ (assuming the x component of the eigenvectors have the same sign) and defining $\epsilon = c_1 + c_2$ and $\boldsymbol{n} = \boldsymbol{u}_1 + \boldsymbol{u}_2$ by integrating from the initial conditions:

$$\boldsymbol{x}_0 = \boldsymbol{x}_L(A_x, \psi) + \epsilon \boldsymbol{n} + c_5 \boldsymbol{u}_5 + c_6 \boldsymbol{u}_6 \tag{2.68}$$

Since eigenvectors' magnitude is arbitrary vector $\boldsymbol{n}$ can be chosen such that its spatial part is pointing towards m_2, in this way non transit trajectory will approach and arrive from m_2. Like eigenvectors, $\boldsymbol{n}$ is a function of $\boldsymbol{x}_0$, thus of A_x and ψ.
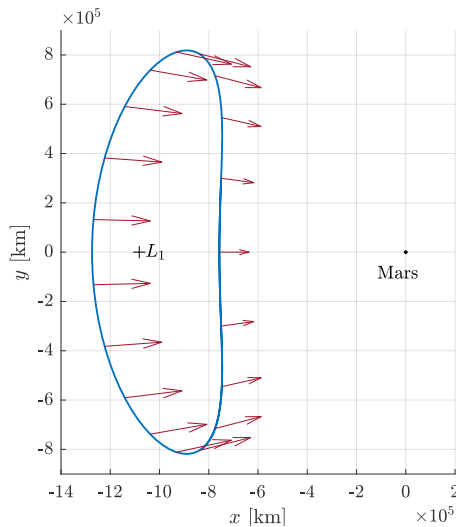
Figure 2.13: Spatial part of $\boldsymbol{n}$ (in dark red) for various phases ψ along a Lyapunov orbit

Chapter 3

Interplanetary transfers

Interplanetary transfers are modeled in a "traditional" way, using the two body problem framework and patched conics to determine the trajectories from one planetary body to another.

3.1 Keplerian orbits

Keplerian orbits are the well-known solution for the motion of a spacecraft under the influence of a single spherical massive body. The second-order equation of motion is given by the equation:

$$\frac{\mathrm{d}^2}{\mathrm{d}t^2}\vec{r} = -\frac{\mu}{r^3}\vec{r} \tag{3.1}$$

Where $\vec{r}$ is the position vector of the spacecraft relative to the massive body and μ is its *gravitational parameter*. The values of μ for Earth ($\oplus$), Mars (σ) and Sun ($\odot$) are:

$$\mu_\oplus = 3.986 \cdot 10^5 \text{ km}^3/\text{s}^2 \qquad \mu_{\sigma} = 4.283 \cdot 10^4 \text{ km}^3/\text{s}^2 \qquad \mu_\odot = 1.327 \cdot 10^{11} \text{ km}^3/\text{s}^2$$

Since the acceleration is always parallel to the radius, the trajcetory is confined to a plane, and it can be expressed in polar coordinates $\{r, \theta\}$ with the relation:

$$r(\theta) = \frac{a(1 - e^2)}{1 + e\cos\theta} \tag{3.2}$$

where a is the *semi-major axis*, e is the *eccentricity* and θ is the *true anomaly* (as shown in figure 3.1). An integral of motion called *orbital energy* or (*keplerian energy*) exists, whith expression:

$$\varepsilon = \frac{v^2}{2} - \frac{\mu}{r} = -\frac{\mu}{2a} \qquad\qquad \dot{\varepsilon} = 0 \tag{3.3}$$

where v is the velocity of the spacecraft ($\vec{v} = \dot{\vec{r}}$). Keplerian orbits can be classified in three different classes:

- **Elliptical orbits** are periodic orbits characterized by:

$$0 < e < 1 \qquad\qquad \varepsilon < 0 \qquad\qquad a > 0$$

  The shape of the trajectory is an ellipse, with a focus centered on the massive body.

- **Hyperbolic orbits** are non-closed orbits, whose parameters lie in the ranges:

$$e > 1 \qquad\qquad \varepsilon > 0 \qquad\qquad a < 0$$

Their shape is a branch of hyperbola, thus the radius r approaches infinity for some values of θ. In fact, the trajectory has two asymptotes, one for $t \to \infty$ and one for $t \to -\infty$. The asymptotic velocities $\vec{v}_\infty$ are referred to *hyperbolic excess velocities*, and since $r \to \infty$ at $t \to \pm\infty$, the keplerian energy of an hyperbolic orbit can be also written as:

$$\varepsilon = \frac{v_\infty^2}{2} \tag{3.4}$$

- **Parabolic orbits** are the boundary case between elliptical and hyperbolic, characterized by $\varepsilon = 0$ and $e = 1$. Since energy is zero, every point along the trajectory has velocity equal to the *escape velocty* v_e:

$$v_e = \sqrt{\frac{2\mu}{r}} \tag{3.5}$$
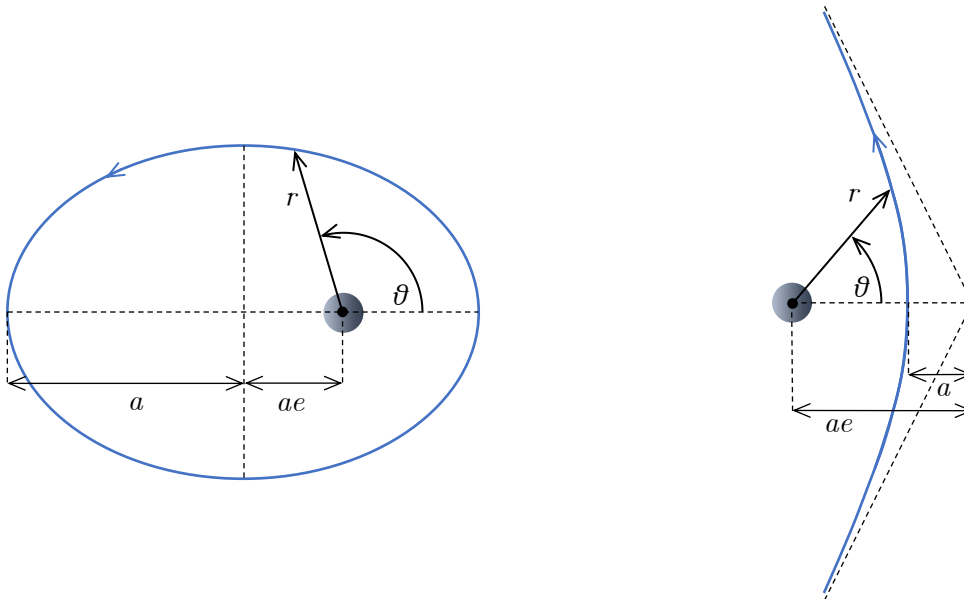
Figure 3.1: Elliptical (left) and hyperbolic (right) orbits.

3.2   Lambert's problem

Knowing the positions of a spacecraft $\vec{r}_1$, $\vec{r}_2$ at two different times separated by a known time interval Δt is sufficient, in the two body problem, to determine a keplerian trajectory between them. In fact, the Lambert theorem [4] states:

> *The transfer time Δt between two positions $\vec{r}_1$ and $\vec{r}_2$ depends only on the sum of the radii $r_1 + r_2$, the major semiaxis a of the orbit and the chord between the positions $|\vec{r}_1 - \vec{r}_2|$.*

An equivalent formulation more useful in this context, being the orbit determined by a single couple of corresponding position $\vec{r}$ and velocity $\vec{v}$ is:

> *Given two position $\vec{r}_1$, $\vec{r}_2$ along a Keplerian orbit and the time of flight Δt between them, the velocities $\vec{v}_1$ and $\vec{v}_2$ can be determined.*
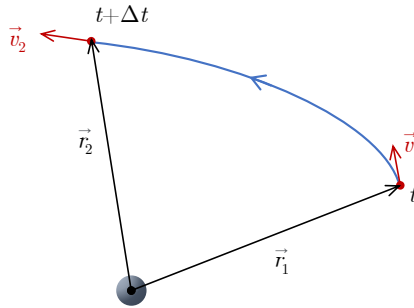
Figure 3.2: Illustration of Lambert's problem.

The analytical procedure to find $\vec{v}_1$ and $\vec{v}_2$, described in detail in chapter 5.3 of *Orbital Mechanics for Engineering Students* of Curtis [5], is the following:

1. The difference in true anomaly $\Delta\theta$ is simply the angle between $\vec{r}_1$ and $\vec{r}_2$:

$$\Delta\theta = \cos^{-1}\left(\frac{\vec{r}_1 \cdot \vec{r}_2}{r_1 r_2}\right)$$

2. The parameter A is calculated as following:

$$A = \sin(\Delta\theta)\sqrt{\frac{r_1 r_2}{1 - \cos(\Delta\theta)}}$$

3. Parameter ζ is found by solving numerically the equation

$$\left(\frac{\Gamma(\zeta)}{\mathcal{C}(\zeta)}\right)^{\frac{3}{2}} \mathcal{S}(\zeta) + A\sqrt{\zeta} - \sqrt{\mu}\Delta t = 0$$

where $\mathcal{S}(x)$ and $\mathcal{C}(x)$ are the *Stumpff' functions*, defined as following:

$$\mathcal{S}(x) = \begin{cases} x^{-2/3}(\sqrt{x} - \sin\sqrt{x}) & \text{if } x > 0 \\ 1/6 & \text{if } x = 0 \\ (-x)^{-2/3}(\sqrt{-x} - \sinh\sqrt{-x}) & \text{if } x < 0 \end{cases} \qquad \mathcal{C}(x) = \begin{cases} x^{-1}(1 - \cos\sqrt{x}) & \text{if } x > 0 \\ 1/2 & \text{if } x = 0 \\ -x^{-1}(\cosh\sqrt{-x} - 1) & \text{if } x < 0 \end{cases}$$

and $\Gamma(x)$ is a function of $\mathcal{S}(x)$ and $\mathcal{C}(x)$, defined as:

$$\Gamma(x) = r_1 + r_2 + A + \frac{x\mathcal{S}(x) - 1}{\sqrt{\mathcal{C}(x)}}$$

4. A set of parameters called *Lagrangian Coefficients* are calculated:

$$f = 1 - \frac{\Gamma(\zeta)}{r_1} \qquad g = A\sqrt{\frac{\Gamma(\zeta)}{\mu}} \qquad \dot{g} = 1 - \frac{\Gamma(\zeta)}{r_2}$$

5. Finally, velocities are found using the following formulae:

$$\vec{v}_= \frac{1}{g}\vec{r}_2 - \frac{f}{g}\vec{r}_1 \qquad\qquad \vec{v}_2 = \frac{\dot{g}}{g}\vec{r}_2 - \frac{1}{g}\vec{r}_1$$

This procedure will be indicated as the function $\mathscr{L}$:

$$(\vec{v}_1, \vec{v}_2) = \mathscr{L}(\vec{r}_1, \vec{r}_2, \Delta t) \tag{3.6}$$

3.3 Patched Conics

A common assumption for the design of interplanetary trajectories is the *patched conics approximation.* It is an approximation of the three body problem in which the spacecraft is considered to be affected only by the gravity of a single body at a time, that body being the one where the gravitational influence is the most significant. The *sphere of influence* (SOI) is defined as:

$$R_{SOI} = \left(\frac{m_1}{m_2}\right)^{2/5} R_\star \tag{3.7}$$

Where m_1 and m_2 are the masses of the two bodies ($m_1 > m_2$) and $R_\star$ is the distance between them. For example, in the case of an Earth to Mars trasnsfer the trajectory is separated into three parts:

- **Departure hyperbola**: the spacecraft starts in an hyperbolic trajectory characterized by a certain $\vec{v}_{\infty 1}$ and is considered to move along it until it exits Earth' sphere of influence.

- **Transfer ellipse**: when it exits Earth SOI, the spacecraft is considered to move in an elliptical orbit around the Sun, starting at the position the Earth is at departure, with velocity $\vec{v}_1 = \vec{v}_E + \vec{v}_{\infty 1}$ (where v_E is the velocity of Earth in the Sun-fixed frame). The trajectory continues along the elliptic arc until the spacecraft reaches Mars SOI with a velocity v_2 (in the Sun-fixed frame)

- **Arrival hyperbola**: the spacecraft moves in an hyperbolic orbit around Mars, characterized by an arrival hyperbolic excess velocity $\vec{v}_{\infty 2} = \vec{v}_2 - \vec{v}_M$.
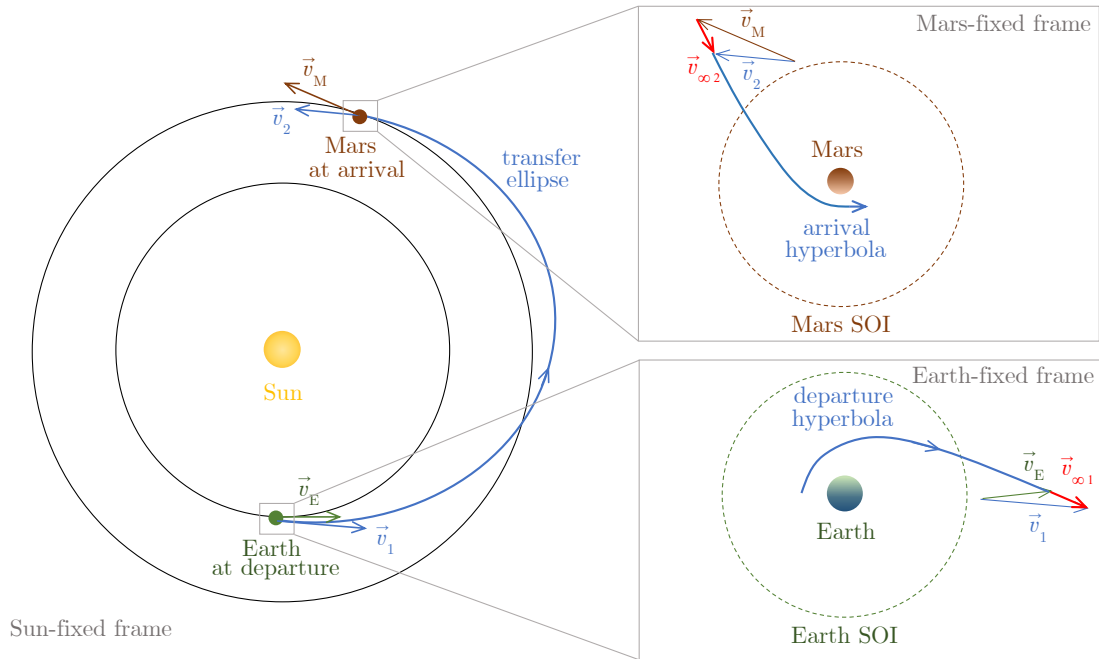
This example is shown in figure 3.3.

Figure 3.3: Illustrative example of an Earth-Mars transfer trajectory with patched conics (distances and radii are not to scale).

3.4   Porkchop plots and transfer windows

From the procedure described in section 3.2, given the Earth and Mars postions $\vec{r}_{\oplus}(t)$, $\vec{r}_{\sigma}(t)$ in the Sun-fixed frame, the velocities $\vec{v}_1$ and $\vec{v}_2$ of a transfer arc starting at Earth at t_1 and arriving at mars at t_2 can be determined univocally:

$$(\vec{v}_1, \vec{v}_2) = \mathscr{L}\left(\vec{r}_{\oplus}(t_1), \vec{r}_{\sigma}(t_2), t_2 - t_1\right) \tag{3.8}$$

Also, by knowing the velocities of Earth and Mars at departure and arrival the hyperbolic excess velocities can be computed by:

$$\vec{v}_{\infty 1} = \vec{v}_1 - \vec{v}_{\oplus} \qquad\qquad \vec{v}_{\infty 2} = \vec{v}_2 - \vec{v}_{\sigma} \tag{3.9}$$

The same applies to a Mars-Earth transfer.

Position of Earth and Mars (commonly referred to as *ephemeris*) can be found online, for example, from JPL's *Horizons System* [6]. The ephemeris can then be used to draw a so called *porkchop plot*, showing v_{∞} at arrival and departure as a function of the departure time and transfer duration. Porkchop plots for Earth and Mars are shown in the following pages, for departures dates ranging from 2020 to 2030 (if $v_{\infty} > 7$ km/s it is not plotted). It can be seen that v_{∞} has various minima, corresponding to transfers when the relative phase of Earth and Mars are such that a transfer arc arrives at Mars near apoapsis and at Earth near periapsis. These minima are called *transfer windows* and repeat roughly every synodic period T_{syn}:

$$T_{syn} \simeq 780 \text{ days} \tag{3.10}$$

Earth → Mars transfer windows

Mars → Earth transfer windows
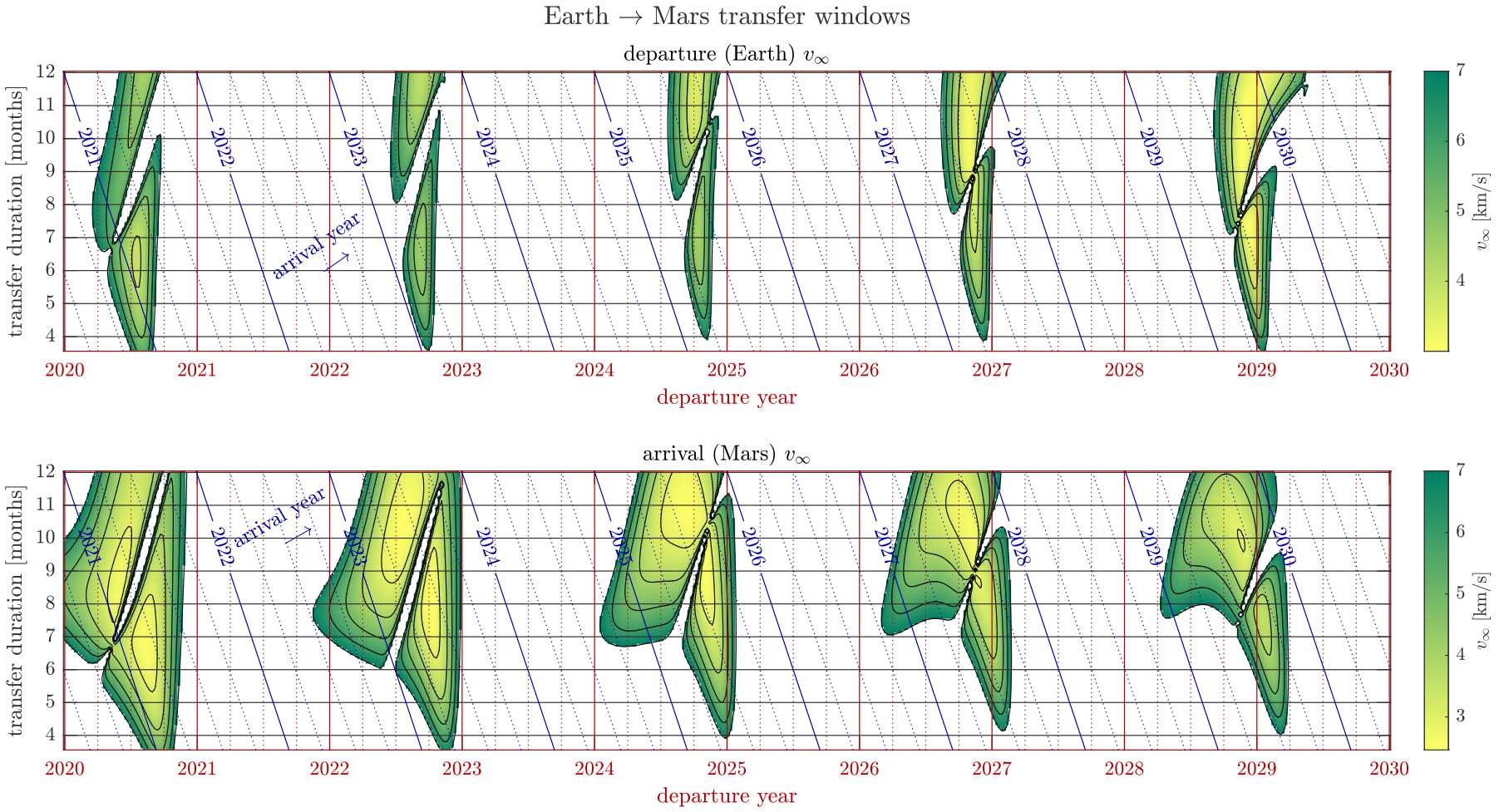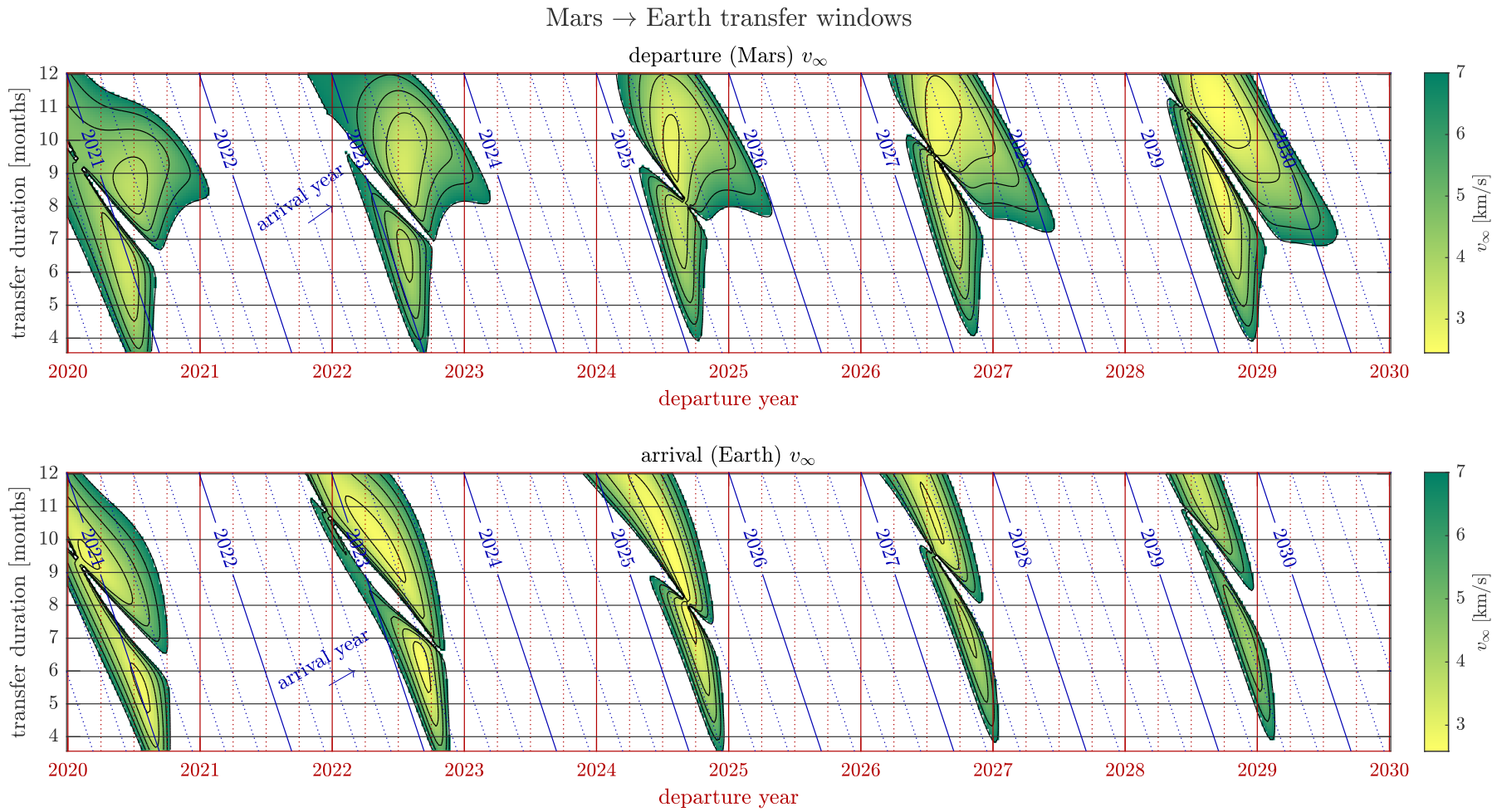
3.5   Ideal capture/departure Δv

The ideal capture/departure Δv can be defined as the Δv necessary to get to escape velocity v_e from the periapsis r_p of an hyperbolic orbit with an excess velocity v_∞ (or vice versa). The velocity at periapsis of the hyperbolic orbit can be found from equation 3.3 and 3.4 to be:

$$v_p = \sqrt{v_\infty^2 + \frac{2\mu}{r_p}}$$

Expressing the escape velocity as in equation 3.5 lets $\Delta v_i = v_p - v_e$ be written as a function of r_p and v_∞ (for a given gravitational parameter μ):

$$\Delta v_i = \sqrt{v_\infty^2 + \frac{2\mu}{r_p}} - \sqrt{\frac{2\mu}{r_p}} \tag{3.11}$$

This relation is shown in figure 3.4, from which two aspects can be seen:

- Δv_i decreases significantly with low periapsis.

- Δv_i is higher for Mars than for Earth.

This is due to the so-called *Oberth effect* [7]: changes in orbital energy are bigger for a given Δv when the manuever is done at high velocity (thus lower in the gravitational potential near the planet). The Δv_i for Earth is generally smaller than for Mars because of the greater mass of Earth, however Earth has a bigger radius so it doesn't allow periapsis low as much as at Mars.
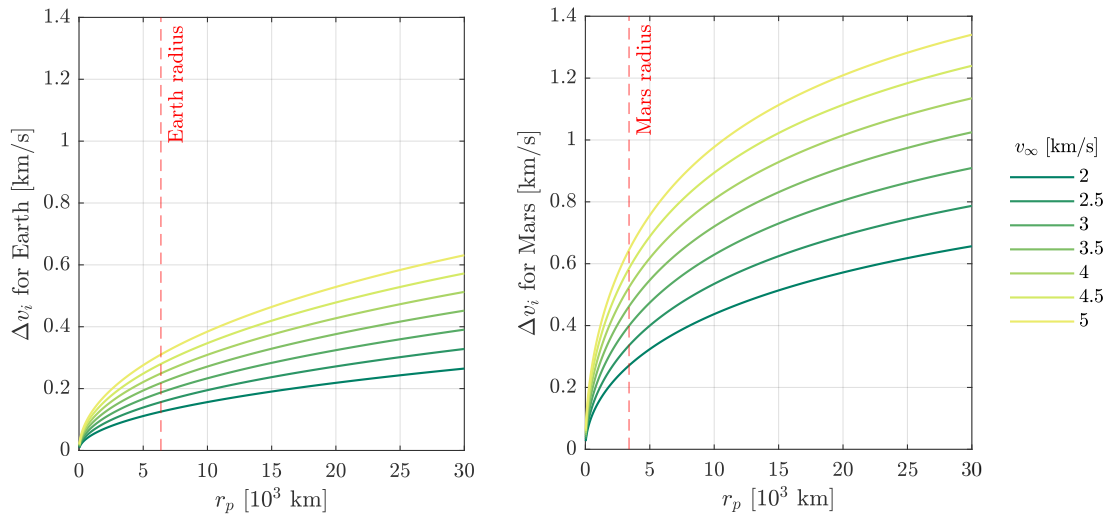
Figure 3.4: Δv_i for Earth (left) and Mars (right) as a function of periapsis radius r_p for various values of v_∞.

Chapter 4

Computation of parking orbits

The following chapter illustrates a technique to find parking orbits calcluate the Δv for capture and departure. It will be assumed that the hyperbolic excess velocities at arrival $\vec{v}_{\infty a}$ and departure $\vec{v}_{\infty d}$ are known, as well as the parking duration $t_p = t_d - t_a$ (t_a and t_d being the arrival and departure epoch). In section 5.1 the method for obtaining these quantities is discussed.

4.1   Symmetric 2D parking orbits

Two assumptions can be made in a first approximation to the parking orbit:

- **Symmetry:** The trajectory is composed by two halves, each one the mirrored version of the other, each one having a duration of $t_p/2$.

- **Planarity:** The trajectory lies in the same plane the planet orbits the Sun.

The initial state $\boldsymbol{x}_0$ can be chosen to be the halfpoint of the trajectory, and for the previous assumptions the only nonzero components will be x and v_y. Furthermore, in order to respect symmetry the state must either be in a Lyapunov orbit or in one that has both stable and unstable motion in "equal amounts".

Lyapunov orbits can be computed in the manner discussed in section 2.7, so the state $\boldsymbol{x}_L$ in a Lyapunov orbit can be expressed as a function of the x-semiamplitude A_x and the phase along the orbit ψ:

$$\boldsymbol{x}_L = \boldsymbol{x}_L(A_x, \psi)$$

The initial condition of a non-transit parking orbit can be found by adding stable $c_s \boldsymbol{u}_s$ and unstable $c_u \boldsymbol{u}_u$ eigenvectors to x_L. Symmetry requires that $c_u = c_s$ and $\psi = \{0; \pi\}$, so defining $\boldsymbol{n} = \boldsymbol{u}_u + \boldsymbol{u}_s$ and $\epsilon = c_u = c_s$ the initial state of the 2D symmetric orbit can be written as.

$$\boldsymbol{x}_0(A_x, \epsilon) = \boldsymbol{x}_L(A_x, \{0; \pi\}) + \epsilon \boldsymbol{n}(A_x) \tag{4.1}$$

Since the parking duration is known, the two branches of the parking orbit can be integrated, also obtaining the initial $\boldsymbol{x}_i$ and final $\boldsymbol{x}_f$ state

$$\boldsymbol{x}_i = \boldsymbol{\varphi}(\boldsymbol{x_0}, t_0 - t_p/2) \tag{4.2}$$

$$\boldsymbol{x}_f = \boldsymbol{\varphi}(\boldsymbol{x_0}, t_0 + t_p/2) \tag{4.3}$$

It can be seen that in this way a family of parking orbits can be generated by the variation of two continuous parameters: A_x and ε. There are actually four trajectories for every $A_x - \varepsilon$ couple, due to ψ being 0 or π and the Lyapunov state being around L_1 or L_2. An example of 2D symmetric parking orbits is shown in figure 4.1
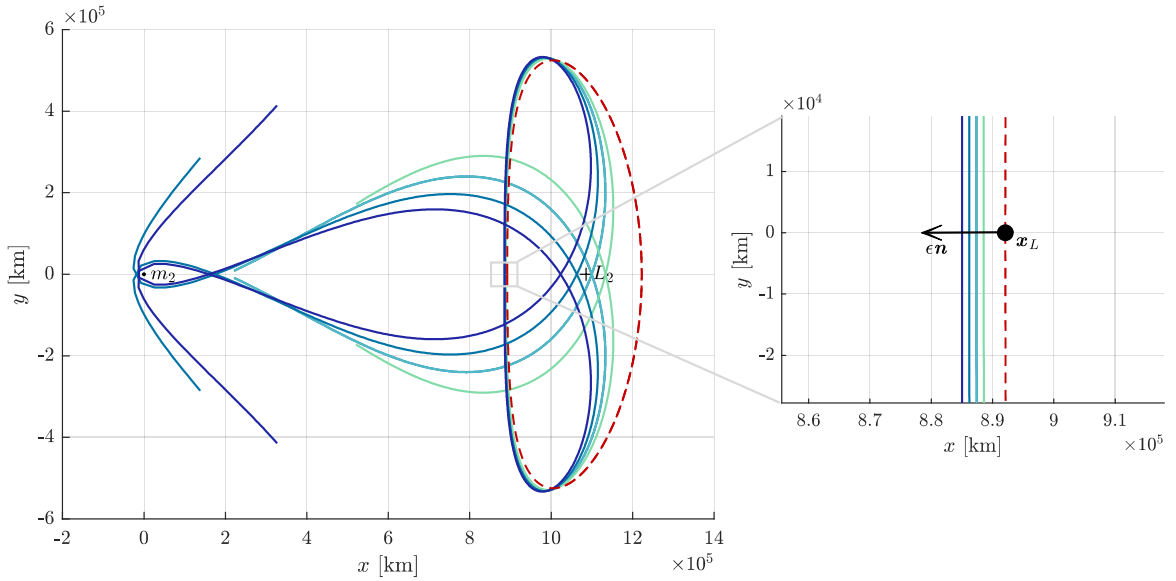
Figure 4.1: 2D symmetric parking orbits relative to a Lyapunov orbit (red dotted line) for various values of ϵ. On the right is shown a detailed zoom of the vicinity of $\boldsymbol{x}_L$.

4.2 Generic 3D parking orbits

The 2D symmetric problem is very useful for finding initial estimates of the optimal trajectory but the two assumptions are not completely realistic. This is due to two reasons:

- The magnitude of $\vec{v}_{\infty a}$ can be different to the one of $\vec{v}_{\infty d}$, this is due to the fact that every transfer window is slightly different form each other. This also means that the halfway point does not necessarily divide the parking orbit into two mirror trajectories

- In general $\vec{v}_\infty$ has nonzero z component, due to the different inclination of the orbits of Earth and Mars around the sun. For this reason injection and escape from a planar parking orbit would use some Δv to rotate the velocity vector rather than increase or decrease energy.

To allow for non-symmetric orbits it is sufficient to let ψ vary freely and keep c_u and c_s as separate parameters. To have a 3D orbit and use the same philosophy of the 2D symmetric case one would need to first compute a state in a nonlinear Lissajous trajectory and then add the unstable and stable components. However the calculations are much more complex than the Lyapunov orbit ones and since Lissajous orbits are characterized by x amplitude, z amplitude and planar-vertical phase difference any survey of a given resolution would require the cube of the computation time needed to survey the Lyapunov initial parameters space. A very useful approximation that is sufficient to compute parking orbits is to assume that a Lissajous initial state can be found by adding a z and v_z component to a Lyapunov initial state. This is not the case in the nonlinear regime and the orbit would diverge from equilibrium if propagated, however the stable and unstable components that are added with nonzero c_s and c_u diverge more rapidly than the errors introduced in the approximation.

Taking these points into consideration, the initial state for a generic parking orbit can be written as:

$$\boldsymbol{x}_0(A_x, \psi, c_s, c_u, z_0, v_{z0}) = \boldsymbol{x}_L(A_x, \psi) + c_s \boldsymbol{u}_s + c_u \boldsymbol{u}_u + [0 \ 0 \ z_0 \ 0 \ 0 \ v_{z0}]^{\mathrm{T}} \qquad (4.4)$$

The initial conditions depend on 6 variables so they are not suitable for large-scale surveys of the phase space but the extra degrees of freedom are useful for finding optimal trajectories.

It can also be seen that a relatively minor change in z_0 and v_{z0} enables to reach a wide range of periapsis inclinations. This is convenient as the injection/escape maneuvers can fully exploit the Oberth effect near the planet without "wasting" Δv for orbital plane changes. This is shown in figure 4.2.
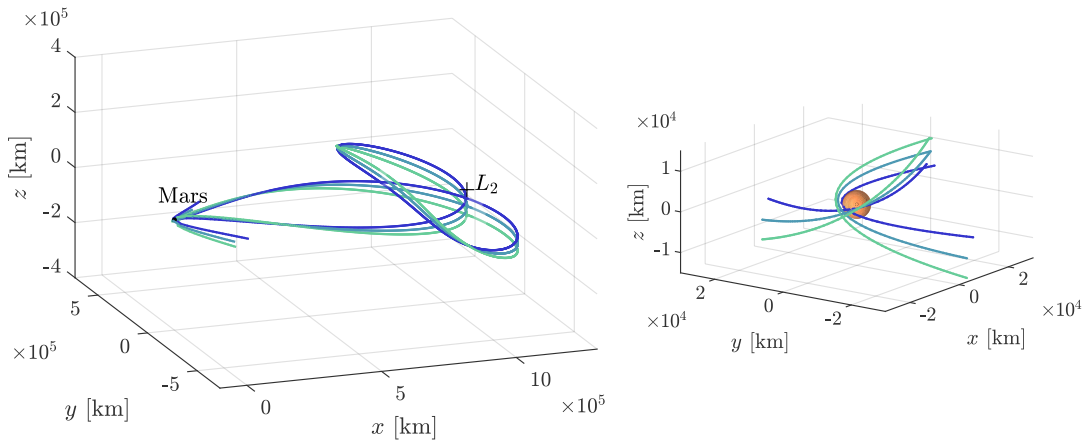
Figure 4.2: Three parking trajectories with different z_0. On the left the whole parking orbit is shown while on the right the part of the trajectory near the planet (in this case Mars) is highlighted.

4.3 Calculation of Δv

The Δv can then be found as the magnitude of the difference of velocity vectors before and after the manuever: the final and initial velocities and positions of the parking orbit can be easily retrieved by the initial and final states, thus the velocity vector at the same positions but in the hyperbolic trajectories needs to be calculated to find the Δv.

The patched conics approximation determines both $\vec{v}_\infty$ for a given transfer arc but does not fully constrain the departure/arrival hyperbolae. This is because Keplerian orbital states in three dimensions have 6 degrees of freedom (including the true anomaly or time to periapsis) and fixing $\vec{v}_\infty$ leaves three of them free. The trajectory however can be fully constrained by imposing that it passes trough a certain position $\vec{r}$, which can be the initial/final position of the parking orbit. When the orbital elements are found, the velocity in the hyperbolic trajectory can be calculated analytically.

First, knowing $\vec{r}$ and $\vec{v}_\infty$ constrains the orbital plane so the problem can be carried out with the two-dimensional equations. To treat the departure and arrival scenario with the same mathematical tools, the unit vector $\hat{u}$ is defined as:

$$\hat{u} = \begin{cases} +\hat{v}_\infty & \text{at departure} \\ -\hat{v}_\infty & \text{at arrival} \end{cases} \qquad (4.5)$$

Then the angle ϕ can be defined as the angle between $\hat{u}$ and $\vec{r}$, found with:

$$\phi = \cos^{-1}\left(\frac{\vec{r} \cdot \hat{u}}{r}\right) \tag{4.6}$$

Before proceeding it is useful to draw an indicative drawing of the geometrical configuration: as shown in figure 4.3 there are in general two hyperbolas for every $\vec{v}_\infty$-$\vec{r}$ pair of vectors, one passing on the "frontside" of the planet and another passing on the "backside" of it.
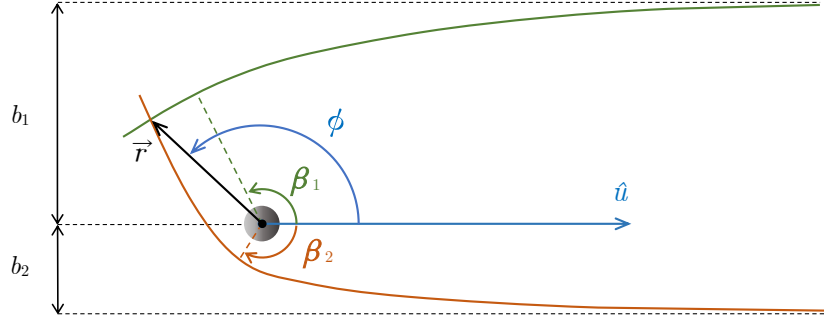

Figure 4.3: Geometric configuration of the problem.

For each hyperbola, the angle β can be defined as the angle lying between $\hat{u}$ and the periapsis position. The frontside angle will be referred to as β_1 while the backside will be called β_2. The value of β can be found as the limit of the true anomaly θ as the radius r goes to infinity in equation 3.2:

$$r(\theta) = \frac{a(1-e^2)}{1+e\cos\theta} \implies \theta(r) = \pm\cos^{-1}\left(\frac{1}{e}\left(\frac{a(1-e^2)}{r}-1\right)\right)$$

$$\beta = \lim_{r\to\infty}\theta(r) = \pm\cos^{-1}\left(-\frac{1}{e}\right)$$

Also, looking at figure 4.3 it can be seen that if $\phi > 0$, then $\beta_1 > 0$ and $\beta_2 < 0$, thus:

$$\beta_1 = +\cos^{-1}\left(-\frac{1}{e_1}\right) \qquad\qquad \beta_2 = -\cos^{-1}\left(-\frac{1}{e_2}\right) \tag{4.7}$$

It is important to note that the difference between β_1 and β_2 is not only the sign, as the eccentricities of the two hyperbolae are not the same ($e_1 \neq e_2$).

The true anomalies θ_1 and θ_2 at the position $\vec{r}$ are the difference between β and ϕ, the sign changing for the departure/arrival and the front/back hyperbola:

$$\theta_1 = \begin{cases} \beta_1 - \phi & \text{at departure} \\ \phi - \beta_1 & \text{at arrival} \end{cases} \qquad \theta_2 = \begin{cases} \phi - \beta_2 & \text{at departure} \\ \beta_2 - \phi & \text{at arrival} \end{cases} \tag{4.8}$$

With this formulation, $\theta < 0$ while the spacecraft is travelling from apoapsis to periapsis, $\theta = 0$ at periapsis and $\theta > 0$ while travelling from periapsis to apoapsis. By using equation 3.4, 3.3 and 3.2, two expressions can be obtained for the parameter $-r/a$:

$$\frac{1}{2}v_\infty^2 = -\frac{\mu}{2a} \implies -\frac{r}{a} = \frac{v_\infty^2 r}{\mu}$$

$$r = \frac{a(1-e^2)}{1+e\cos\theta} \implies -\frac{r}{a} = \frac{e^2-1}{1+e\cos\theta}$$

which can be equated, giving the following relation:

$$\frac{v_\infty^2 r}{\mu} = \frac{e^2 - 1}{1 + e \cos \theta}$$

after this, substituting the expression found before for θ and β, the equation can be rewritten as:

$$\frac{v_\infty^2 r}{\mu} = \frac{e_1^2 - 1}{1 + e_1 \cos \left(\phi - \cos^{-1} \left(-\frac{1}{e_1} \right) \right)} = \frac{e_2^2 - 1}{1 + e_2 \cos \left(\phi + \cos^{-1} \left(-\frac{1}{e_2} \right) \right)} \quad (4.9)$$

This relation is shown in figure 4.4. The equation does not change for arrival and departure, since the cosine of the true anomaly is the same for a negative or positive argument; it does, however, change for the fronside and backside (the signs that follow ϕ are opposite). The only unknowns in the equations are the eccentricities and, despite not being analytically solvable, e_1 and e_2 can be found numerically.
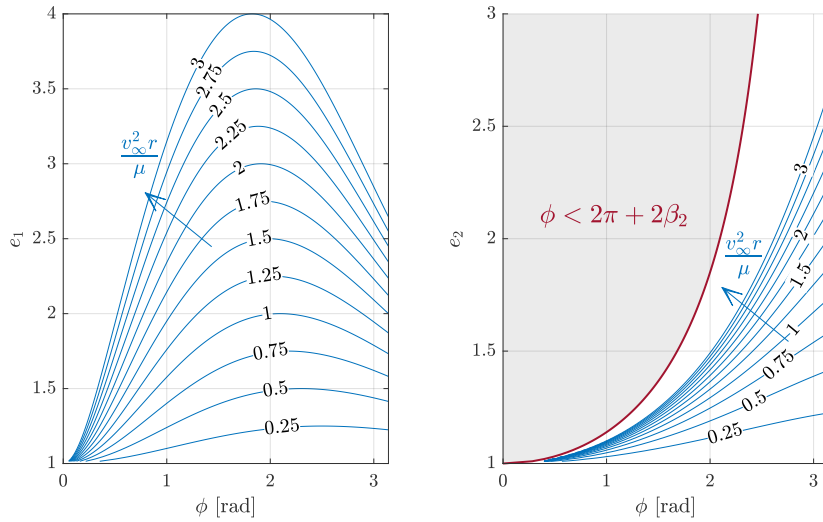
Figure 4.4: Isocurves of $v_\infty^2 r/\mu$ as a function of ϕ and e, as described by equations 4.9. Isocurves are present even where not explicitly shown (except in the grey zone) but have been omitted because the lines would be too dense.

For some values of ϕ and e_2 the denominator in the third member of equation 4.9 becomes negative, but this cannot be possible since the first member is always positive. Thus, to have physical results the following condition must be true

$$1 + e_2 \cos \left(\phi + \cos^{-1} \left(-\frac{1}{e_2} \right) \right) > 0 \implies \phi > 2\pi - 2 \cos^{-1} \left(-\frac{1}{e_2} \right)$$

Which, using the definition of β_2 can be seen to be equivalent to

$$\phi > 2\pi + 2\beta_2 \quad (4.10)$$

When this condition is not satisfied, ϕ is too low to allow any backside hyperbola with eccentricity e_2 to exist for any value of $v_\infty^2 r/\mu$. This condition does not forbid in principle to find an e_2 (thus a backside hyperbola) for any given value of ϕ and $v_\infty^2 r/\mu$ but the

result can be very close to 1, which often corresponds to a periapsis below the surface of the planet. The semiaxis of the orbit can be found from v_∞ with equations 3.3 and 3.4:

$$a = -\frac{\mu}{v_\infty} \tag{4.11}$$

Then, knowing the eccentricity e the impact parameter b is found with:

$$b = -a\sqrt{e^2 - 1} \tag{4.12}$$

The angular momentum unit vector can be calculated as following without knowing explicitly the velocity $\vec{v}$.

$$\hat{h}_1 = \frac{\hat{r} \times \hat{v}_\infty}{|\hat{r} \times \hat{v}_\infty|} \qquad\qquad \hat{h}_2 = \frac{\hat{v}_\infty \times \hat{r}}{|\hat{r} \times \hat{v}_\infty|} \tag{4.13}$$

where $\times$ indicates the cross product. By using $\hat{v}_\infty$ instead of $\hat{u}$, this formulation does not change depending on if the hyperbolic orbit is at arrival or departure, but it changes for the frontside and backside cases. From each one of the two $\hat{h}$ and $\hat{r}$ the angular unit vector $\hat{\theta}$ can be found as:

$$\hat{\theta} = \hat{h} \times \hat{r} \tag{4.14}$$

no normalization is necessary in this case since by construction $\hat{h}$ and $\hat{r}$ are perpendicular. The angle between $\hat{\theta}$ and the velocity is often referred to as *flight path angle* χ and it can be calculated from e and θ:

$$\chi = \arctan\left(\frac{e\sin\theta}{1 + e\cos\theta}\right) \tag{4.15}$$

The *vis viva* equation (3.3) can be used to find the magnitude of the velocity:

$$v = \sqrt{v_\infty^2 + \frac{2\mu}{r}} \tag{4.16}$$

Finally, the velocity vector $\vec{v}$ at the position $\vec{r}$ of an hyperbolic orbit characterized by $\vec{v}_\infty$ can be found with the following expression:

$$\vec{v} = v\left(\sin\chi \ \hat{r} + \cos\chi \ \hat{\theta}\right) \tag{4.17}$$

Both solutions generally valid, altough it can happen that the periapsis of the hyperbola is below the surface of the planet. To check this occurrence the periapsis radius can be calculated from a and e and then required to be above the radius of the planet R_p:

$$r_p = a(1 - e^2) > R_p \tag{4.18}$$

Chapter 5

Cycler optimization

The previous chapter illustrates how to find a parking trajectory and its associated Δv given a number of free parameters:

- **Arrival and departure $\vec{v}_\infty$ and parking time t_p** which are determined by the interplanetary arrival and departure trajectories.

- **Initial state of the parking orbit x_0** which, given the two $\vec{v}_\infty$, corresponds to a certain Δv.

These parameters can be chosen to minimize Δv, with the constrain that the trajectory never goes below the surface of the planet.

5.1 Interplanetary trajectory optimization

Without finding any specific parking orbit, an assumption can be made on the Δv which simplifies the problem:

> *Given an arrival and departure asymptotic velocities $\vec{v}_{\infty a}$, $\vec{v}_{\infty d}$ and parking time t_p, the minimum Δv obtainable by a parking orbit is proportional to the sum of the ideal Δv of $v_{\infty a}$ and $v_{\infty d}$ at the radius of the planet r_p.*

$$\Delta v = \Delta v_{ia} + \Delta v_{id} = \frac{1}{\eta} \left(\Delta v_i(v_{\infty a}, r_p) + \Delta v_i(v_{\infty d}, r_p) \right) \tag{5.1}$$

where Δv_i is the ideal Δv defined in equation 3.11 and r_p is the radius of the planet (plus the atmosphere and and eventual margin). In this way the *parking efficiency η* can be calculated once the specific trajectory is found. The validity of this assumption will be discussed later in section 5.3.

If the only objective was to minimize the Δv across a single Earth $\rightarrow$ Mars $\rightarrow$ Earth mission then the two interplanetary transfer arcs could be simply chosen by looking at the minima of v_∞ at Mars arrival and departure on the corresponding porkchop plot. This would fix the time of arrival t_a and departure t_d at Mars and consequently the parking time $t_p = t_d - t_a$. However, the situation is more complicate if we want to design a *cycler* trajectory where each interplanetary arc determines two v_∞ because now we need to minimize the sum of the Δv_i at the start and at the end of the interplanetary trajectory. To avoid confusion, while the "a" and "d" subscripts will refer to arrival and departure from a parking trajectory, the subscripts "1" and "2" will indicate the beginning and the end of an interplanetary transfer in this context. Since the asymptotic velocities $v_{\infty 1}$ and

$v_{\infty 2}$ can be determined as functions of t_1 and t_2, as shown in sections 3.2 and 3.4, the following quantity can also be computed as a function of t_1 and t_2 for both the Earth $\rightarrow$ Mars and Mars $\rightarrow$ Earth cases:

$$\Delta v_{i1} + \Delta v_{i2} = \sqrt{v_{\infty 1}^2 + \frac{2\mu_\oplus}{r_\oplus}} - \sqrt{\frac{2\mu_\oplus}{r_\oplus}} + \sqrt{v_{\infty 2}^2 + \frac{2\mu_\mars}{r_\mars}} - \sqrt{\frac{2\mu_\mars}{r_\mars}} \qquad (5.2)$$

Such a plot is shown at page 45, for the 2020-2030 year of departure interval. With assumption 5.1, the t_1 and t_2 that give the lowest Δv for parking are the one corresponding to minima in $\Delta v_{i1} + \Delta v_{i2}$. The optimal transfer dates in the 2020-2038 year of departure interval are listed in the tables 5.1 and 5.2 (the meaning of the cell colors will be clarified in the next paragraph):

Table 5.1: optimal **Mars $\rightarrow$ Earth** transfers

t_1 [date]	t_2 [date]	$t_2 - t_1$ [days]	$v_{\infty 1}$ [km/s]	$v_{\infty 2}$ [km/s]	Δv_{i1} [km/s]	Δv_{i2} [km/s]	$\Delta v_{i1} + \Delta v_{i2}$ [km/s]
20/06/2020	24/12/2020	187	3.315	3.009	1.019	0.413	1.431
14/07/2022	12/04/2023	271	3.198	2.912	0.954	0.387	1.341
22/07/2024	07/05/2025	288	2.779	2.656	0.735	0.323	1,058
06/08/2026	11/06/2027	312	2.601	2.913	0.649	0.387	1.036
10/08/2028	12/07/2029	336	2.602	3.528	0.650	0.563	1.213
24/12/2030	04/10/2031	284	3.247	3.429	0.980	0.533	1.513
17/04/2033	01/11/2033	198	2.903	3.215	0.797	0.470	1.267
25/06/2035	09/01/2036	197	3.039	2.535	0.868	0.294	1.162
04/08/2037	07/07/2038	337	4.188	2.535	1.549	0.294	1.844

Table 5.2: optimal **Earth $\rightarrow$ Mars** transfers

t_1 [date]	t_2 [date]	$t_2 - t_1$ [days]	$v_{\infty 1}$ [km/s]	$v_{\infty 2}$ [km/s]	Δv_{i1} [km/s]	Δv_{i2} [km/s]	$\Delta v_{i1} + \Delta v_{i2}$ [km/s]
21/07/2020	05/02/2021	199	3.877	2.779	0.677	0.735	1.412
27/08/2022	05/08/2023	343	4.177	2.707	0.782	0.700	1.482
25/09/2024	26/08/2025	334	3.612	2.550	0.590	0.626	1.215
28/10/2026	26/08/2027	302	3.127	2.681	0.445	0.687	1.132
21/11/2028	15/09/2029	297	3.036	2.973	0.420	0.834	1.253
28/10/2030	02/10/2031	354	2.685	4.184	0.330	1.547	1.877
17/02/2033	15/09/2033	210	2.545	3.370	0.297	1.050	1.346
10/05/2035	17/11/2035	191	3.092	3.277	0.435	0.997	1.432
07/07/2037	30/03/2038	266	3.664	3.395	0.606	1.064	1.670

The Δv_i varies substantially for each transfer, this is due to the fact that Earth and Mars orbits are not circular nor coplanar, so some launch windows are more advantageous than others. Its average value is $\langle \Delta v_{i1} + \Delta v_{i2} \rangle = 1.371$ km/s.

To have the fastest cycler trajectory the spacecraft needs to take the first transfer available after it arrives at a planet; for example a spacecraft departing from Earth on the 20th of June 2020 arrives at Mars on the 24th of December 2020 so the first available transfer back to Earth is on the 27th of August 2021. Since the Earth $\rightarrow$ Mars and the Mars $\rightarrow$ Earth launch windows always overlap it's not possible for a single spacecraft to exploit

all of them but at least two are necessary. This fact also imposes a minimum parkinkg duration t_p at the planet, that is listed in tables 5.4 and 5.3 with the corresponding arrival and departure date t_a and t_p.

Table 5.3: parking duration $t_p = t_d - t_a$ at **Earth**

t_a [date]	t_d [date]	t_p [days]
24/12/2020	27/08/2022	611
12/04/2023	25/09/2024	532
07/05/2025	28/10/2026	539
11/06/2027	21/11/2028	529
12/07/2029	28/12/2030	534
04/10/2031	17/02/2033	502
01/11/2033	10/05/2035	555
09/01/2036	07/07/2037	545

Table 5.4: parking duration $t_p = t_d - t_a$ at **Mars**

t_a [date]	t_d [date]	t_p [days]
05/02/2021	14/07/2022	524
05/08/2023	22/07/2024	352
26/08/2025	06/08/2026	345
26/08/2027	10/08/2028	350
15/09/2029	24/12/2030	465
02/10/2031	17/04/2033	563
15/09/2033	25/06/2035	648
17/11/2035	04/08/2037	626

In tables 5.1, 5.2, 5.4 and 5.3 the rows have been colored with two different colors: all transfers and parking phases with the same color are part of the same cycler trajectory.

Optimal lanunch windows for cycler trajectories

Earth → Mars

Mars → Earth
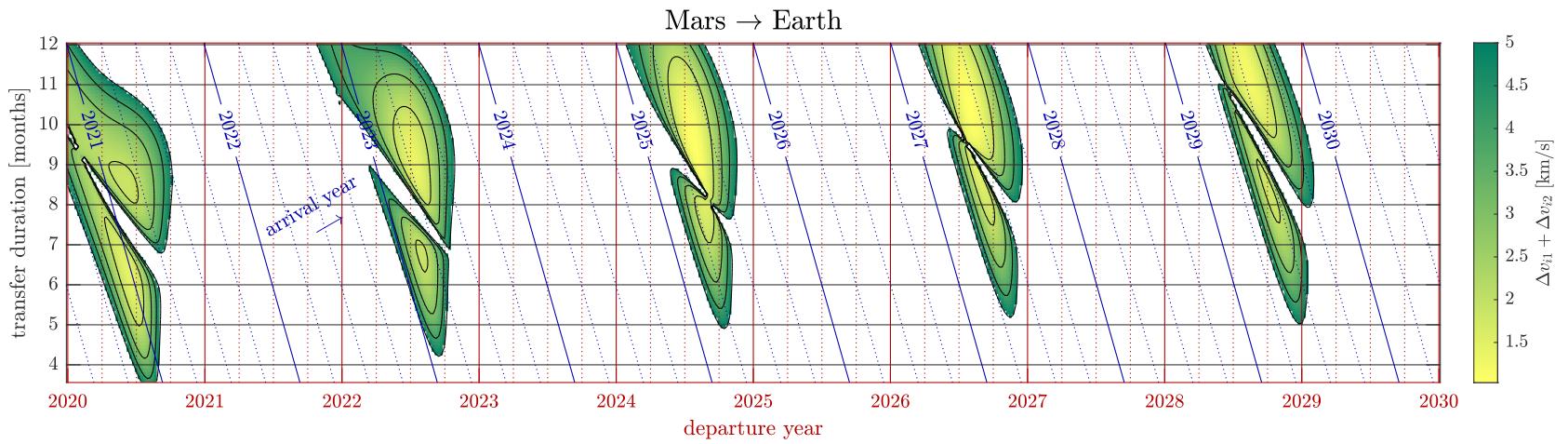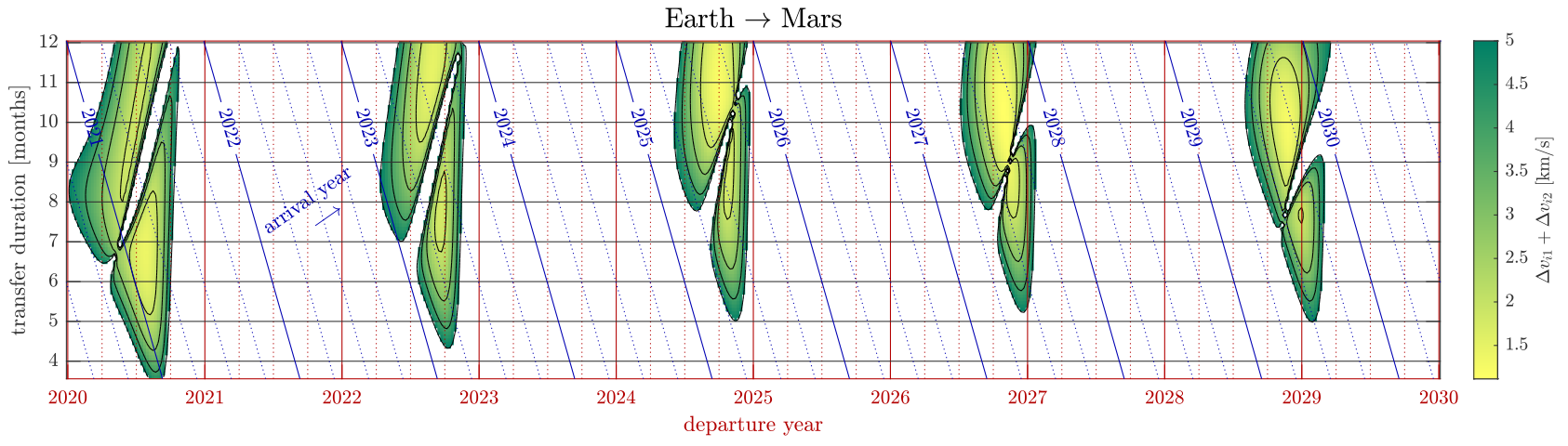
5.2 Coordinate frame conversion

Two different coordinate frames, shown in figure 5.1, are used to compute the interplanetary arc and the parking orbits:

- **Inertial frame -** The Lambert problem is solved in the *J2000 Ecliptic* reference frame, that will be referred in this section as $\{X, Y, Z\}$. This frame is centered in the solar system barycenter (SSB), its XY plane coincides with the ecliptic and the $\hat{X}$ vector points to the Venal point at epoch 2000. Earth does not orbit exactly in the ecliptic since orbital precession has changed slightly its orbital plane since the J2000 reference frame has been defined. Given that the system is centered in the SSB and it doesn't rotate, this frame is inertial.

- **Corotating frame -** The parking orbit is solved in a frame which is defined as follows to approximate the one used in chapter 2 for the study of the CR3BP:

  - The system is centered in the barycenter of the planet (Mars or Earth)
  - The $\hat{x}$ vector is aligned to the vector $\vec{R}$ that connects the SSB to the planet barycenter.
  - The xy plane contains the $\hat{x}$ vector and the velocity vector of the planet in the inertial frame $\vec{V}_p$, the $\hat{y}$ vector is perpendicular to $\hat{x}$ in such a way that it forms an acute angle with $\vec{V}_p$.
  - The $\hat{z}$ vector closes the triplet in such a way that $\hat{x} \times \hat{y} = \hat{z}$.
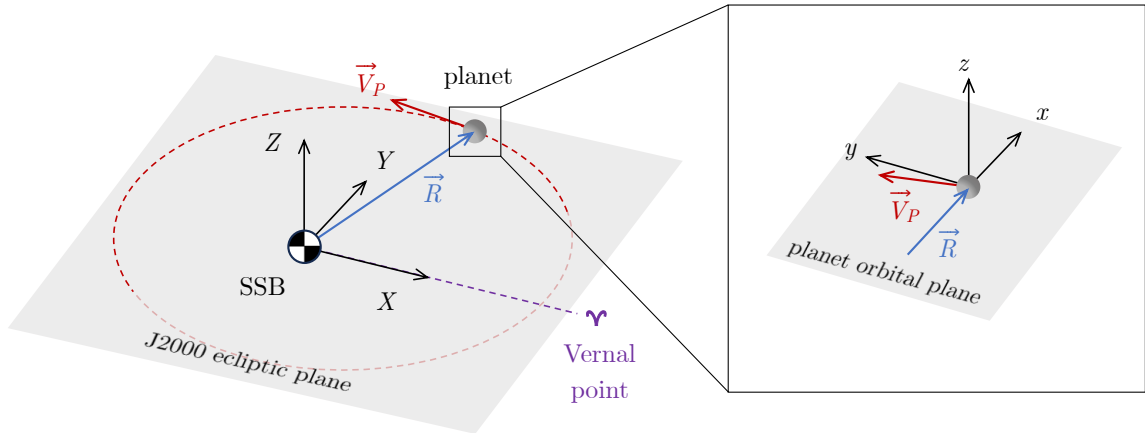
Figure 5.1: Inertial frame (left) and corotating frame (right)

The parking trajectory is modeled in the CR3BP but when the SOI is crossed at high velocity, so before the injection manuever and after the escape one, the two body approximation is valid and the patched conics approach can be used. In this approach the only relevant parameter that "communicates" between various sphere of influences is the $\vec{v}_\infty$, so it's also the only one that needs to be converted between the two frames of reference. Doing that in an exact way would imply a contribution in the corotating frame due to the rotation velocity of the frame itself, but this correction would be of order of magnitude:

$$v_{rot} \sim 2\pi \frac{R_p}{T_{orbit}} \sim \frac{10^4 \text{ km}}{1 \text{ year}} \sim 10^{-4} \text{ km/s} << v_\infty \simeq 3 \text{ km/s}$$

thus, it can be ignored. This makes the conversion from inertial to corotating velocity simply the linear transformation:

$$\begin{bmatrix} v_x \\ v_y \\ v_z \end{bmatrix} = \begin{bmatrix} \hat{R}_X & \hat{R}_Y & \hat{R}_Z \\ \hat{U}_X & \hat{U}_Y & \hat{U}_Z \\ \hat{H}_X & \hat{H}_Y & \hat{H}_Z \end{bmatrix} \begin{bmatrix} v_X \\ v_Y \\ v_Z \end{bmatrix} \quad \text{where} \quad \hat{H} = \frac{\hat{R} \times \vec{V}_p}{V_p} \quad \text{and} \quad \hat{U} = \hat{R} \times \hat{H} \quad (5.3)$$

5.3   Parking trajectory optimization

Having fixed the transfers now $\vec{v}_{\infty a}$, $\vec{v}_{\infty d}$ and t_p are known so a family of parking orbits can be computed as illustrated in chapter 4 and a Δv value assigned for each trajectory; this section shows how to find the one that minimize Δv, taking as an example the parking at Mars between the arrival on the 26th of August 2025 and the departure on the 6th of August 2026, characterized by the following parameters:

$$t_p = 345 \text{ days} \qquad \vec{v}_{\infty a} = \begin{bmatrix} -0.699 \\ -2.353 \\ 0.841 \end{bmatrix} \text{ km/s} \qquad \vec{v}_{\infty d} = \begin{bmatrix} -0.192 \\ -2.430 \\ -0.893 \end{bmatrix} \text{ km/s}$$

As anticipated the x and z components are nonzero due to the fact that Earth and Mars' orbits around the Sun are not circular nor coplanar. The interplanetary transfer arcs that result in these parameters are shown in figure 5.2:
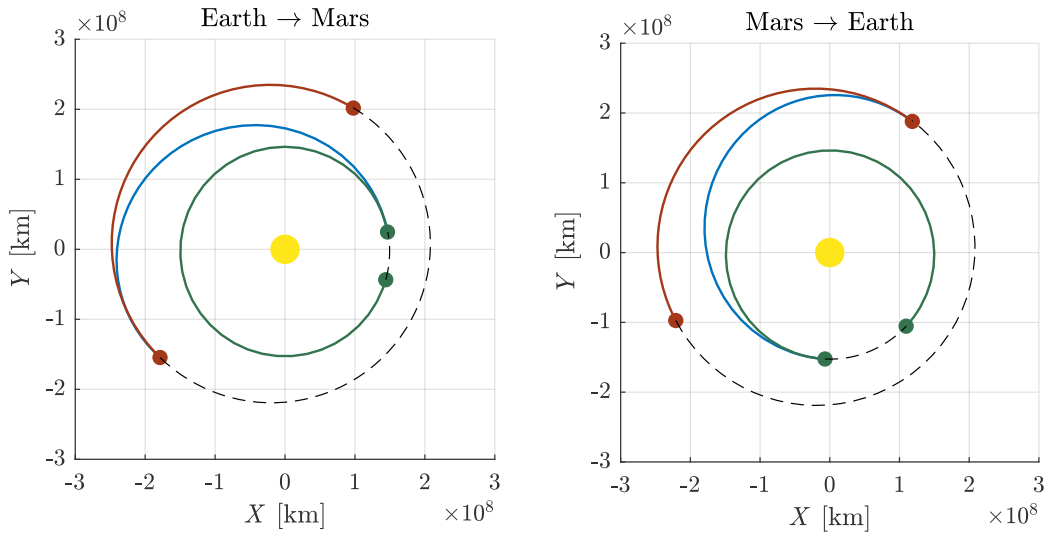
Figure 5.2: Interplanetary transfers for the 2024-2026 launch windows to and from Mars. The spacecraft trajectory is represented by the blue line, the red and green lines are the trajectories of Mars and Earth respectively, while the circles at the end of the curves are the planets' position at the beginning and end of each transfer.

As the duration of the parking orbit is fixed, a trajectory is uniquely identified by the state $\boldsymbol{x}_0$ at its midpoint, which has six degrees of freedom in general, parametrized for example as in equation 4.4: a survey of the phase space would be too computationally expensive but assuming that a 2D symetric parking orbit gives a good initial guess, we can parametrize $\boldsymbol{x}_0$ as in 4.1 and survey the $A_x - \epsilon$ space to find an initial guess to later

optimize. Since the search is in the 2D orbit family, using the 3D $\vec{v}_\infty$ would grossly overestimate the Δv since the out of plane velocity cannot be matched. A much more representative way of conducting this survey that still gives good initial guesses can be done by using a "planified" $\vec{v}_{\infty\text{plan}}$, i.e. projecting it into the $x - y$ plane and rescaling it to match its original magnitude:

$$\vec{v}_\infty = \begin{bmatrix} v_{\infty,x} \\ v_{\infty,y} \\ v_{\infty,z} \end{bmatrix} \qquad \Rightarrow \qquad \vec{v}_{\infty\text{plan}} = \begin{bmatrix} v_{\infty,x} \\ v_{\infty,y} \\ 0 \end{bmatrix} \frac{|\vec{v}_\infty|}{\sqrt{v_{\infty,x}^2 + v_{\infty,y}^2}}$$

In figure 5.4 the result of this survey are shown. It can be seen that there are "branches" of low Δv in the configuration space and looking at the trajectories belonging to these branches it becomes apparent that all of them share the two following properties:

- Low periapses, to maximize the Oberth Effect.

- Small changes of $\hat{v}$ before and after the maneuver, to minimize the Δv "wasted" in rotating the velocity vector without chaning energy.

From this survey the best 2D symmetric trajectory found is in the L_2 $\psi = \pi$ family and is characterized by $A_x = 149\,362$ km $\simeq 0.137\,\gamma$ and $\epsilon|\vec{n}_r| = 79\,804$ km $\simeq 0.074\,\gamma$, shown in figure 5.3. This trajectory, as hinted to in chapter 4, is used as initial guess for the optimal 3D parking orbit.
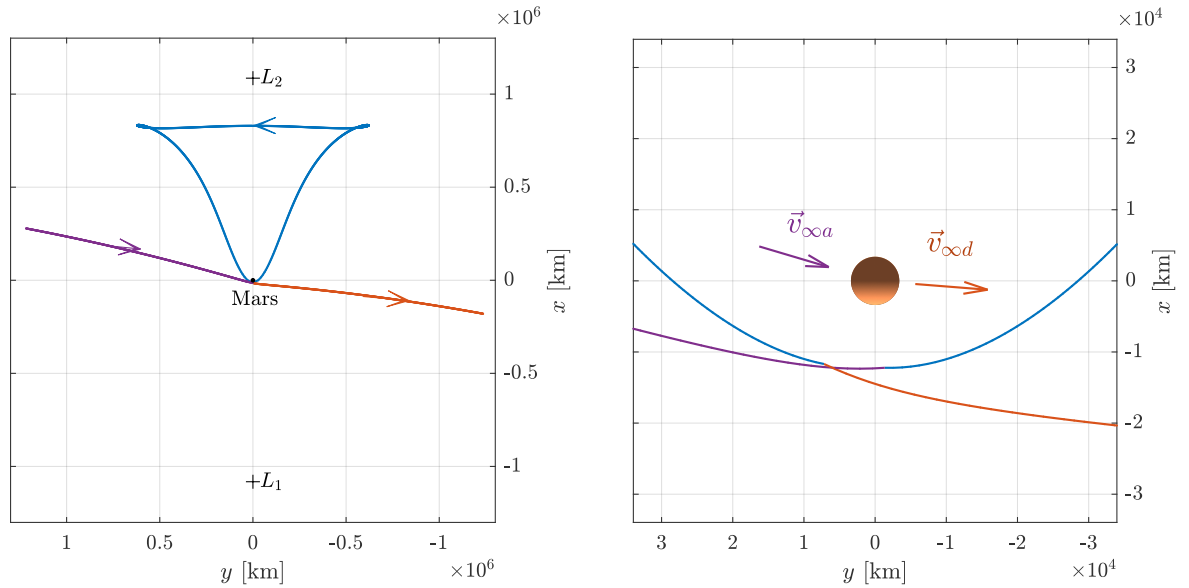
Figure 5.3: Optimal 2D trajectory. Bird's-eye view (left) and detail around Mars with the planet in scale (right). The parking trajectory is in blue while the arrival and departure arcs are shown in purple and orange respectively.
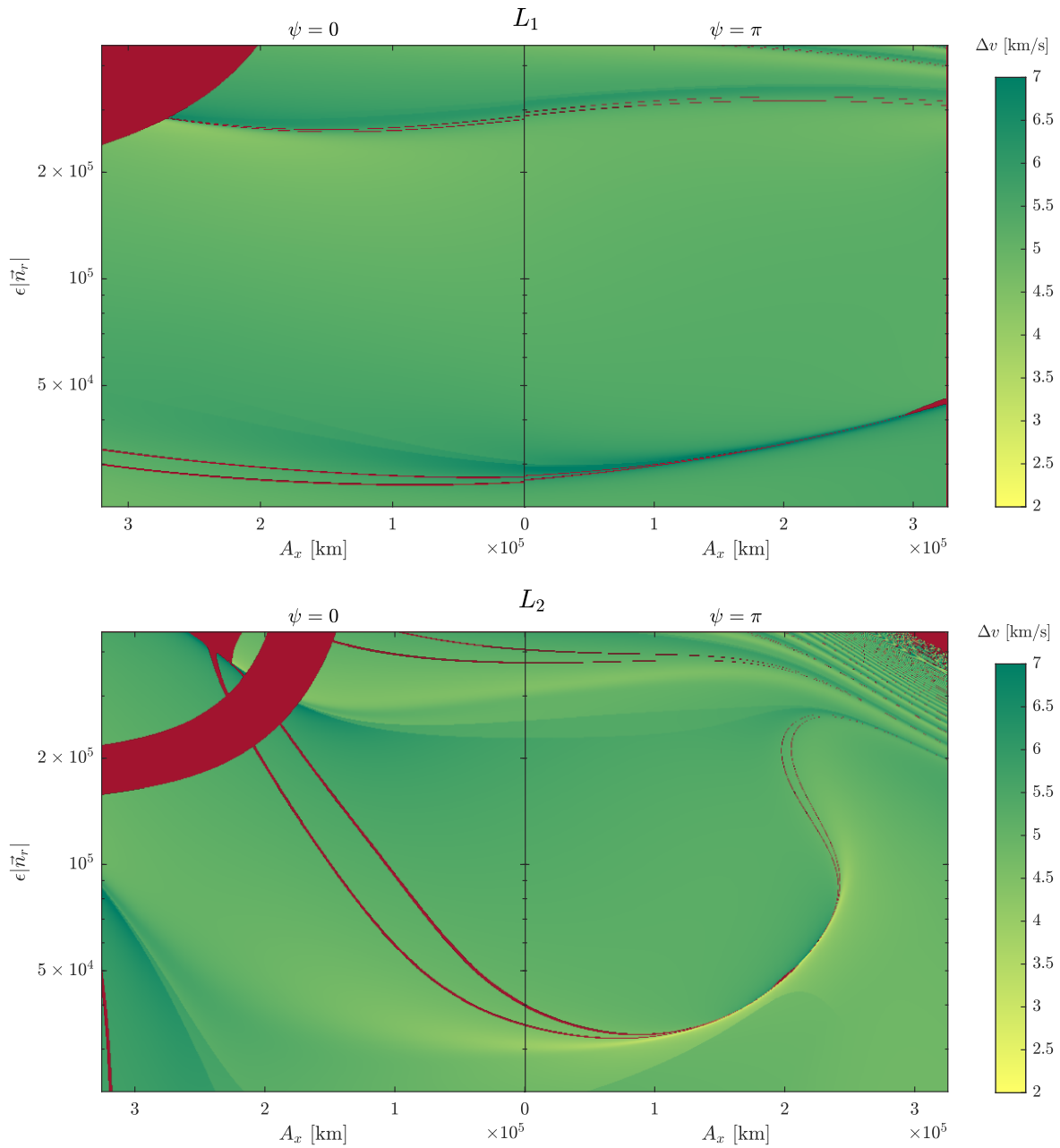
Figure 5.4: Δv survey for symmetric 2D transit orbits around L_1 and L_2. In the abscissa the x-semiamplitude of the Lyapunov orbit is shown, both for the $\psi = 0$ and $\psi = \pi$ cases (they are side by side and reversed because the $\psi = 0$ case can be seen as a $A_x < 0$ and $\psi = \pi$ case). In the ordinate the magnitude of the spatial part $\epsilon \vec{n}_r$ of the phase space vector $\epsilon \boldsymbol{n} = \boldsymbol{x}_0 - \boldsymbol{x}_L$ is shown, which can be thought of as the "distance from equilibrium". Dark red indicates "crashing" trajectories that intersect the planet either in the parking orbit or in the arrival or departure hyperbolas.

The optimization process has been found to be challenging as any algorithm that tried to minimize the Δv varying all 6 free parameters (A_x, c_s, c_u, z_0, v_{z0} and ψ) at the same time would either fail to converge or stop at a non-optimal result. This behaviour has been attributed to two facts:

- The trajectory is much more sensitive to c_s and c_u than to any other parameter.

- Any small change in A_x, z_0, v_{z0} or ψ changes significantly the c_s and c_u for which the lowest Δv is achieved.

To overcome this problem a solution is to use a *layered approach*, by reoptimizing the "sensitive" parameters for each iteration of the "unsensitive" ones. In this way an algorithm can assess the dependence of Δv on the unsensitive parameters independently from the sensitive ones and can converge to an optimum, this however comes at the cost of a big increase in computation time. This approach is illustrated in figure 5.5
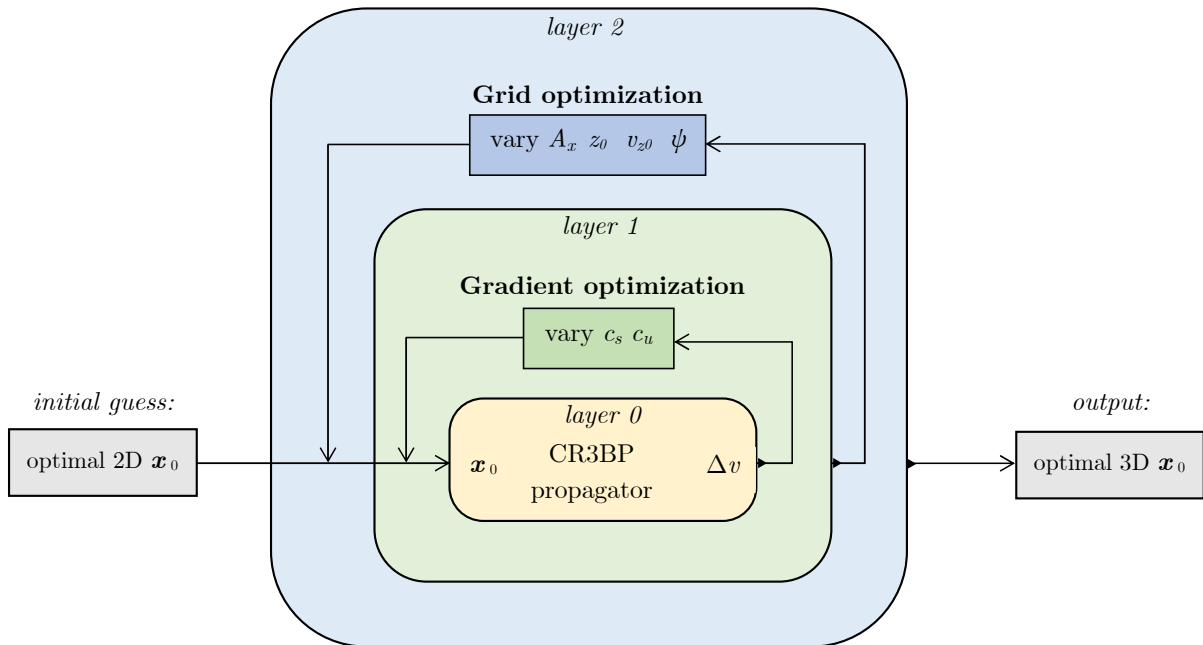
Figure 5.5: Layered optimization method. The second layer uses the grid algorithm and varies the unsensitive variables A_x, z_0, v_{z0} and ψ, while for each iteration the first layer optimizes the sensitive parameters c_s and c_u using the gradient algorithm. A "zero" layer is constituted by the CR3BP integrator and the equations described in chapter 4 for calculating the Δv. Both algorithms are described in detail in appendix C.

Another problem encoutered during the optimization process is constituted by trajectories that pass below the surface of the planet and that due to their low periapsis give a lower Δv despite being obviously unacceptable. To deal with this issue, given a mimimum allowable altitude $r_{\min}$, any positive difference $r_{\min} - r_p$ is added to the Δv "cost" for the optimization: this doesn't change anything if the trajectory stays above $r_{\min}$ but if it does then the cost of that trajectory sharply increases. In other words, the objective

function $f(\boldsymbol{x})$ to minimize by the algorithms is:

$$f(\boldsymbol{x}_0) = \begin{cases} \Delta v(\boldsymbol{x}_0) & \text{if } r_p(\boldsymbol{x}_0) > r_{\min} \\ \Delta v(\boldsymbol{x}_0) + r_{\min} - r_p(\boldsymbol{x}_0) & \text{if } r_p(\boldsymbol{x}_0) < r_{\min} \end{cases} \tag{5.4}$$

Carrying out this procuedure the trajectory shown in figure 5.6 can be found, characterized by the following parameters:

$$A_x = 137\,053 \text{ km} \qquad c_u = 3.675 \cdot 10^{-4} \qquad c_s = 3.906 \cdot 10^{-4}$$
$$z_0 = 117\,855 \text{ km} \qquad v_{z0} = 4.51 \text{ m/s} \qquad \psi = 184.6\,°$$

$$\Delta v = 2.684 \text{ km/s} \qquad r_{pa} = 23\,891 \text{ km} \qquad r_{pd} = 18\,112 \text{ km}$$

The Δv at each layer 2 iteration of the optimization process is shown in figure 5.7. The z extension of the parking trajectory is cleary visible as well as the asymmetry between the arrival and departure trajectories. Interestingly the periapses are not very low and this is not due to the fact that lower periapses aren't possible; however given the specific directions of the $\vec{v}_\infty$ of this transfer window a lower periapsis would increase a lot the angle between the velocity vectors before and after the manuevers, negating the benefit that the Oberth effect would offer. Judging by the criteria outlined in 5.1, the efficiency of this parking orbit is:

$$\eta = \frac{\Delta v_{ia} + \Delta v_{id}}{\Delta v} = \frac{0.626 + 0.649}{2.684} = 47.05\% \tag{5.5}$$

The efficiency is not very high, this is due mainly to the high periapses that are
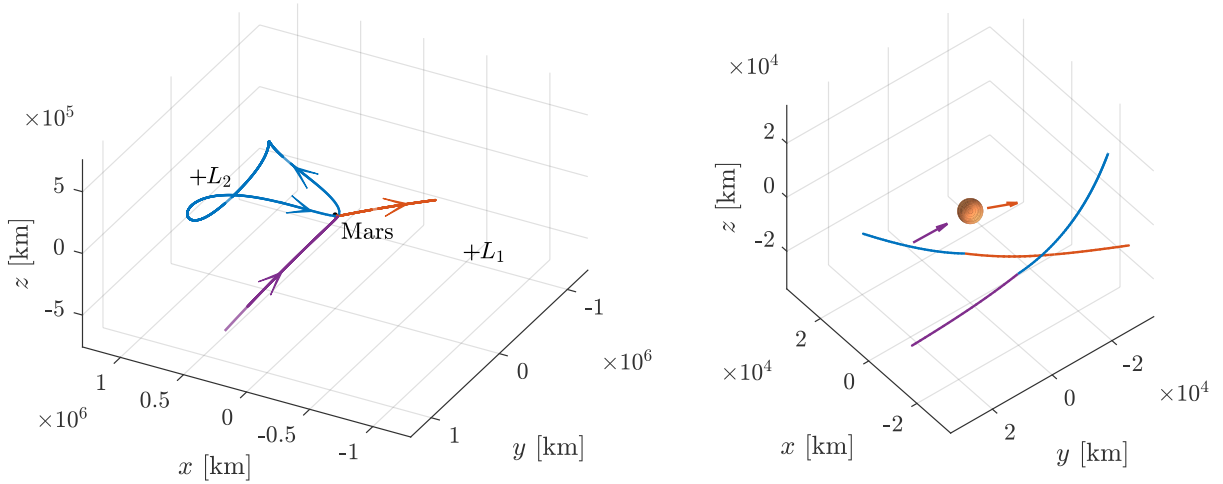
Figure 5.6: Optimal 3D trajectory

unfortunately unavoidable in this specific transfer window. The situation could improve changing the dates of the launch windows, potentially yielding a higher η and an overall lower Δv despite the increase in Δv_i. These findings contradict the hypothesis made at the beginning of section 5.1, or at least they limit its applicability to a "first guess" for finding the actual optimal transfers. This search is not impossible but it's made computationally intensive by the fact that each change of date (both departure and arrival) chages two
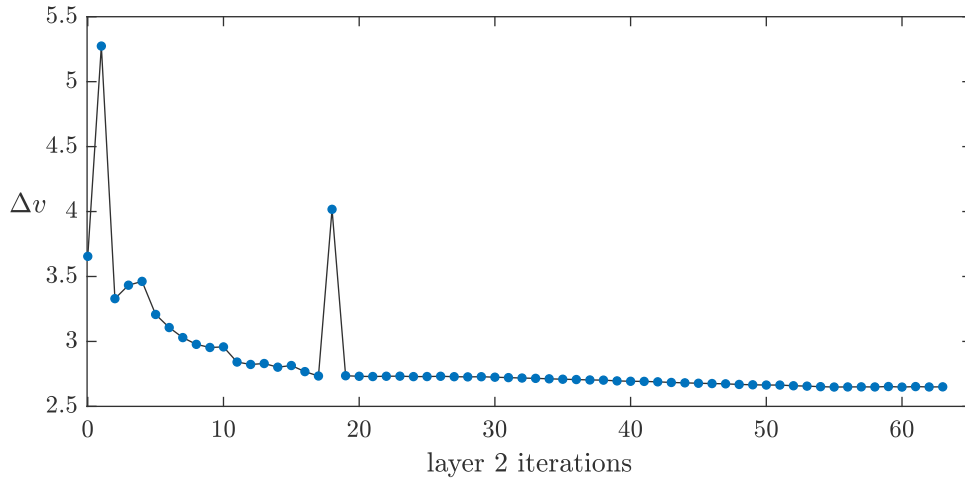
Figure 5.7: Result of layer 2 iterations during the optimization process

$\vec{v}_\infty$ and thus leads to two different parking Δv. Thus, the optimization of the dates for the cycler trajectory cannot be split into separate parking orbits whose Δv gets summed in the end, but has to be done as a whole with all of the N transfers:

$$\Delta v_{\text{cycler}} = f(t_1, t_2, ..., t_{2N}) \tag{5.6}$$

For this reason, the cycler trajectory will be calculated in this thesis with the suboptimal dates shown at page 43. The next cycler phase is the Earth-parking phase whose transfers shown in figure 5.9 are characterized by the following parameters:

$$
\begin{aligned}
t_a &: 26/08/2027 \\
t_d &: 10/08/2028 \\
t_p &= 350 \text{ days}
\end{aligned}
\qquad
\vec{v}_{\infty a} =
\begin{bmatrix}
-0.501 \\
2.8944 \\
0.0867
\end{bmatrix}
\text{ km/s}
\qquad
\vec{v}_{\infty d} =
\begin{bmatrix}
-0.8427 \\
2.5917 \\
1.4521
\end{bmatrix}
\text{ km/s}
$$
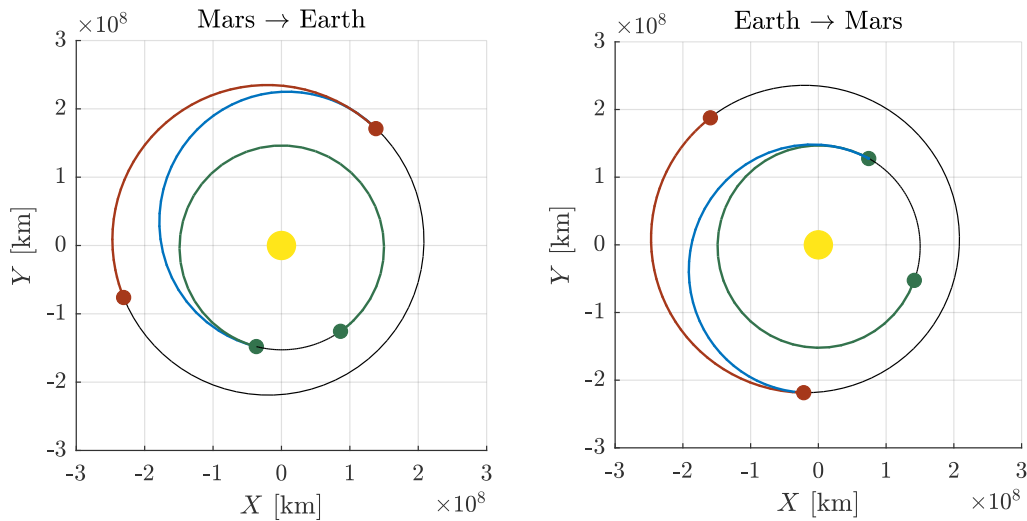
Figure 5.8: Interplanetary transfers for the 2026-2028 launch windows to and from Earth.

The optimal parking orbit, shown in figure 5.9 is much different than the one shown previously around Mars, this is due mainly to the fact that $t_p/T_L T_\star$ ratio and Gm_2 are much higher in this case. It is charachterized by the following parameters:

$$A_x = 91\,174 \text{ km} \qquad c_u = 1.261 \cdot 10^{-4} \qquad c_s = 2.626 \cdot 10^{-4}$$
$$z_0 = -133\,291 \text{ km} \qquad v_{z0} = 86.38 \text{ m/s} \qquad \psi = 159.37\,°$$

$$\Delta v = 3.541 \text{ km/s} \qquad r_{pa} = 99\,308 \text{ km} \qquad r_{pd} = 105\,127 \text{ km}$$

The efficiency of this transfer is even lower than the previous case, at $\eta = 22.79\%$, due to
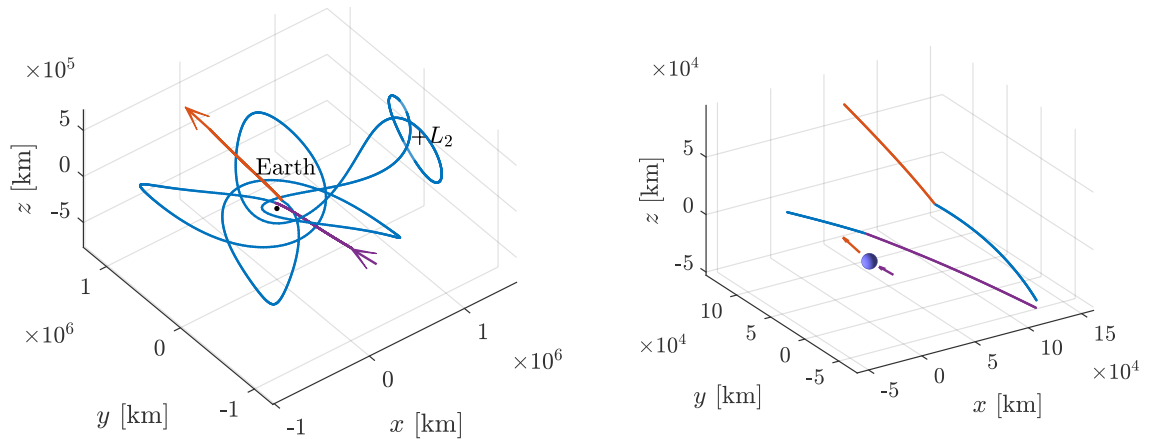
Figure 5.9: Parking orbit around Earth for the 2026-2028 launch windows.

the same reasons. The optimization process takes a similar number of iterations, shown in figure 5.10
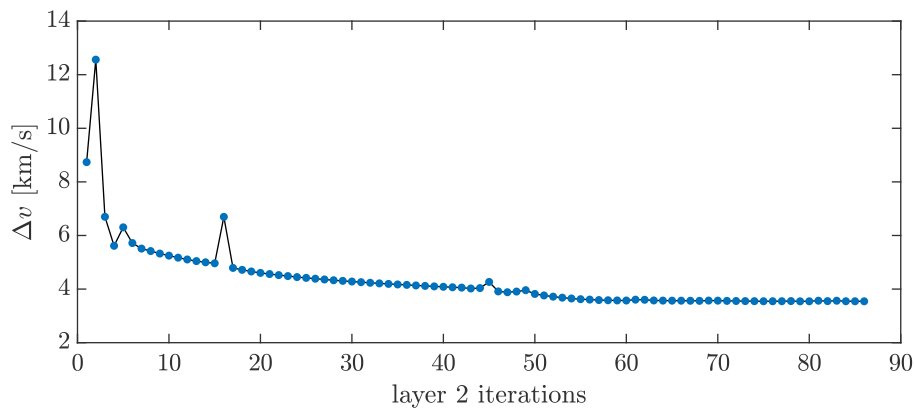
Figure 5.10: Result of layer 2 iterations during the optimization process

5.4   Results

In this section a portion of the two cyclers, schematized in figure 5.11 is shown.
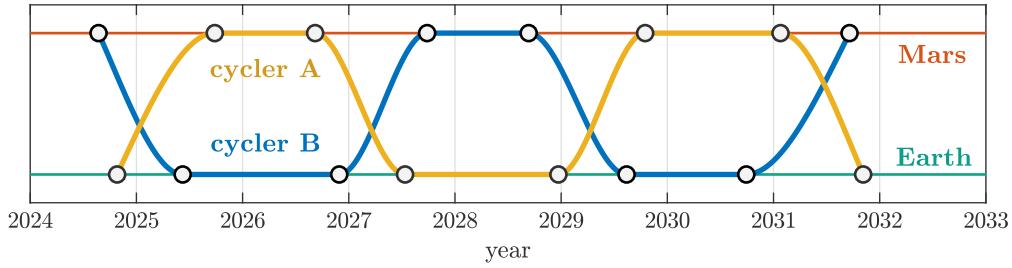
Figure 5.11: The two cycler trajecotries, between years 2024 and 2032
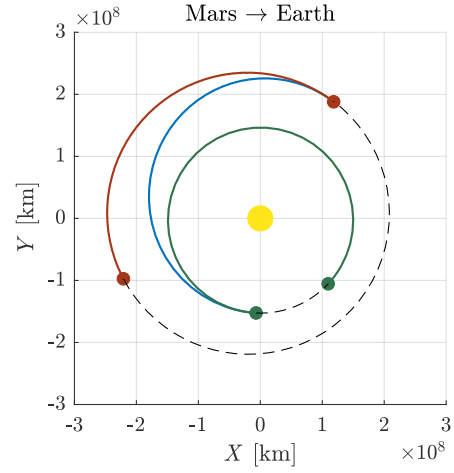
Cycler A

25/09/2024

INTERPLANETARY TRANSFER

$$\vec{v}_\infty = \begin{bmatrix} -0.810 \\ 3.495 \\ -0.484 \end{bmatrix} \text{ km/s (at Earth)}$$

transfer duration: 335 days

$$\vec{v}_\infty = \begin{bmatrix} -0.699 \\ -2.353 \\ 0.841 \end{bmatrix} \text{ km/s (at Mars)}$$
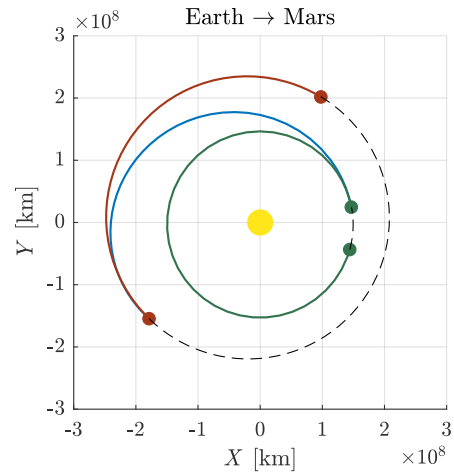
26/08/2025

MARS PARKING ORBIT
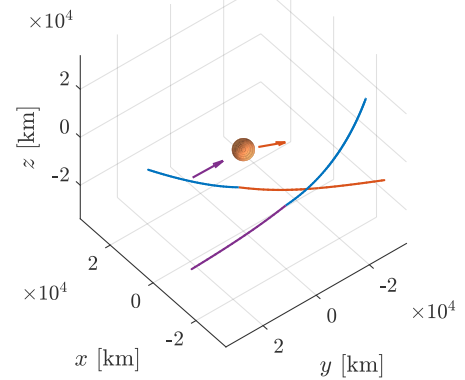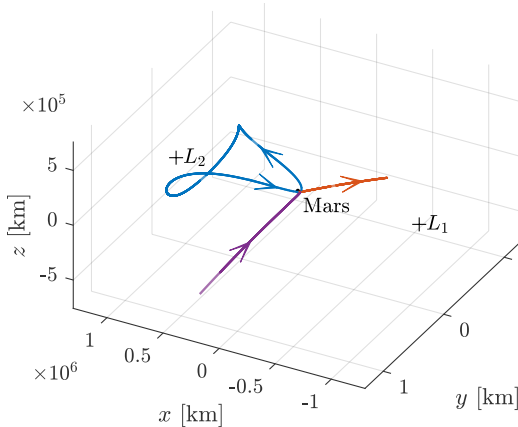
$$A_x = 137\,053 \text{ km} \quad c_u = 3.675 \cdot 10^{-4} \quad c_s = 3.906 \cdot 10^{-4}$$
$$z_0 = 117\,855 \text{ km} \quad v_{z0} = 4.51 \text{ m/s} \quad \psi = 184.6°$$

$$\Delta v = 2.684 \text{ km/s} \quad r_{pa} = 23\,891 \text{ km} \quad r_{pd} = 18\,112 \text{ km}$$
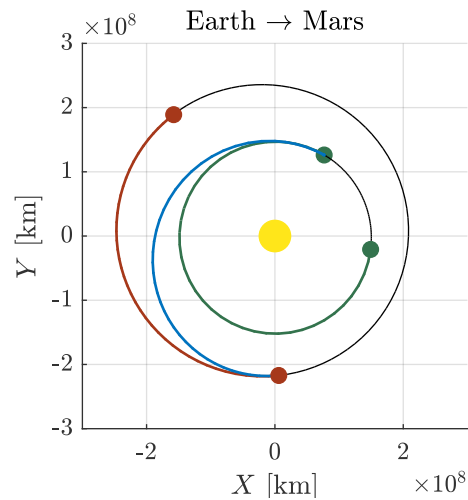
06/08/2026

06/08/2026

INTERPLANETARY TRANSFER

$$\vec{v}_\infty = \begin{bmatrix} -0.192 \\ -2.430 \\ -0.893 \end{bmatrix} \text{ km/s (at Mars)}$$

transfer duration: 309 days

$$\vec{v}_\infty = \begin{bmatrix} -0.843 \\ 2.592 \\ 1.452 \end{bmatrix} \text{ km/s (at Earth)}$$

Mars → Earth

11/06/2027

EARTH PARKING ORBIT
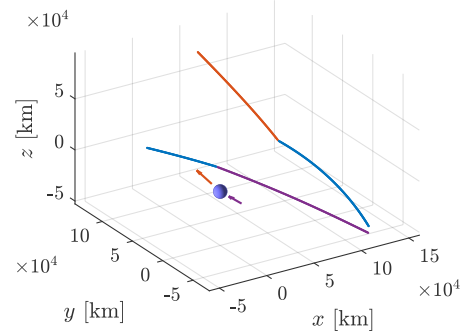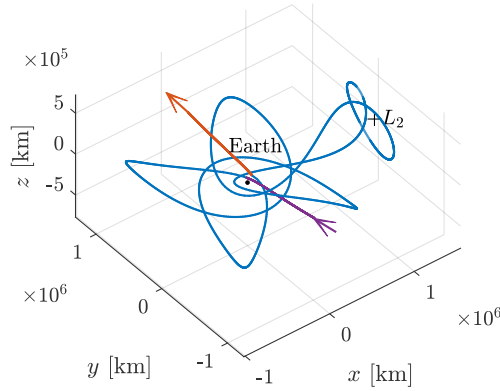
$A_x = 91\,174$ km $c_u = 1.261 \cdot 10^{-4}$ $c_s = 2.626 \cdot 10^{-4}$

$z_0 = -133\,291$ km $v_{z0} = 86.38$ m/s $\psi = 159.37\,^\circ$

$\Delta v = 3.541$ km/s $r_{pa} = 99\,308$ km $r_{pd} = 105\,127$ km

10/08/2028

INTERPLANETARY TRANSFER

$$\vec{v}_\infty = \begin{bmatrix} -0.843 \\ 2.592 \\ 1.452 \end{bmatrix} \text{ km/s (at Earth)}$$
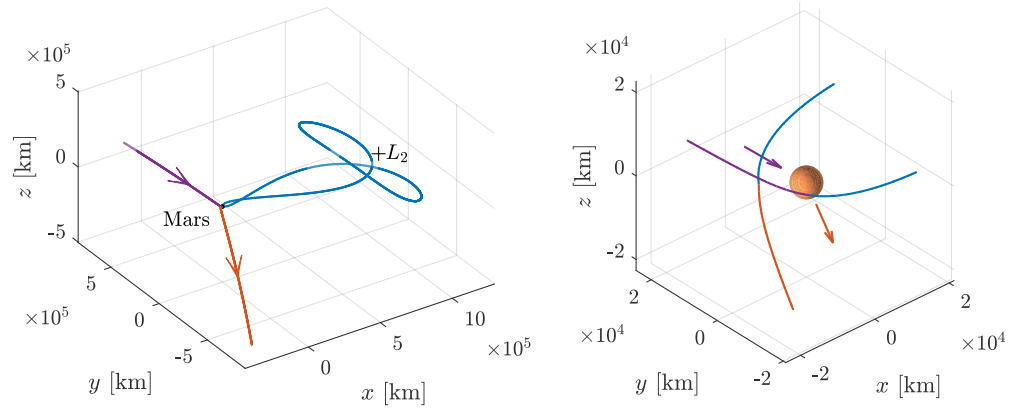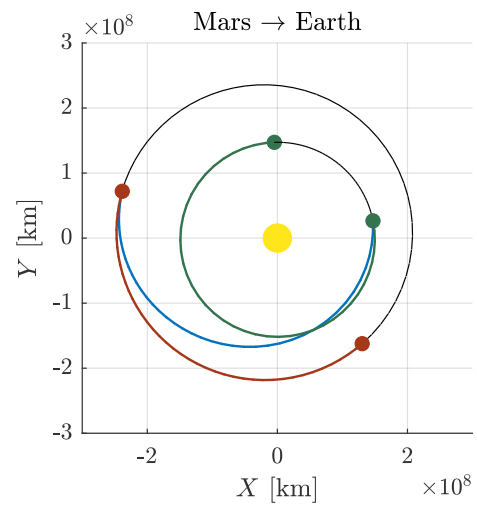
transfer duration: 298 days

$$\vec{v}_\infty = \begin{bmatrix} -0.316 \\ -2.949 \\ -0.211 \end{bmatrix} \text{ km/s (at Mars)}$$

Earth → Mars

26/08/2029

26/08/2029

EARTH PARKING ORBIT

$$A_x = 149\,142 \text{ km} \quad c_u = 7.535 \cdot 10^{-5} \quad c_s = 8.099 \cdot 10^{-5}$$

$$z_0 = 25\,986 \text{ km} \quad v_{z0} = 7.48 \text{ m/s} \quad \psi = 185.79\,^\circ$$

$$\Delta v = 2.06 \text{ km/s} \quad r_{pa} = 4\,772 \text{ km} \quad r_{pd} = 9\,658 \text{ km}$$

24/12/2030

INTERPLANETARY TRANSFER

$$\vec{v}_\infty = \begin{bmatrix} -0.852 \\ -2.275 \\ -0.887 \end{bmatrix} \text{ km/s (at Mars)}$$

transfer duration: 284 days

$$\vec{v}_\infty = \begin{bmatrix} 1.814 \\ 2.843 \\ 1.036 \end{bmatrix} \text{ km/s (at Earth)}$$
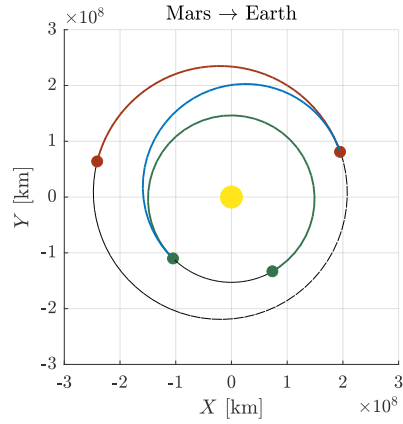

Mars → Earth

04/10/2031

Cycler B

22/07/2024

INTERPLANETARY TRANSFER

$$\vec{v}_\infty = \begin{bmatrix} 0.014 \\ -2.780 \\ 0.084 \end{bmatrix} \text{ km/s (at Mars)}$$
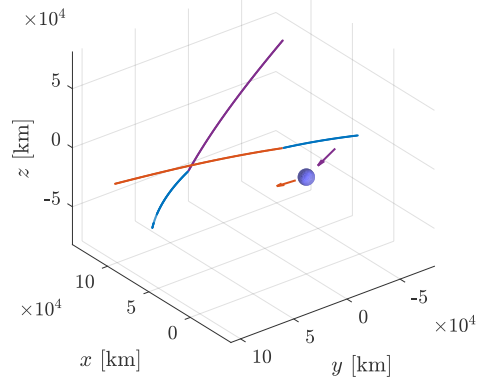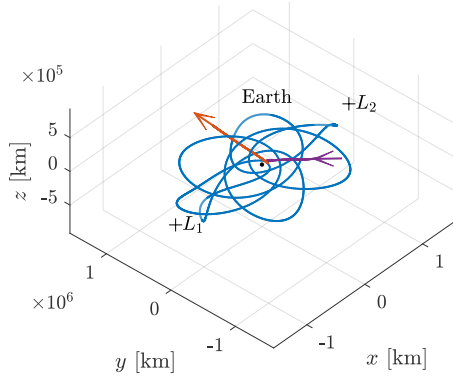
transfer duration: 289 days

$$\vec{v}_\infty = \begin{bmatrix} -0.168 \\ 2.399 \\ -1.136 \end{bmatrix} \text{ km/s (at Earth)}$$

07/05/2025

EARTH PARKING ORBIT

$$A_x = 52\,208 \text{ km} \quad c_u = 1.837 \cdot 10^{-3} \quad c_s = 2.444 \cdot 10^{-3}$$
$$z_0 = -107\,711 \text{ km} \quad v_{z0} = -21.45 \text{ m/s} \quad \psi = -22.92\,^\circ$$

$$\Delta v = 3.054 \text{ km/s} \quad r_{pa} = 99\,308 \text{ km} \quad r_{pd} = 105\,127 \text{ km}$$
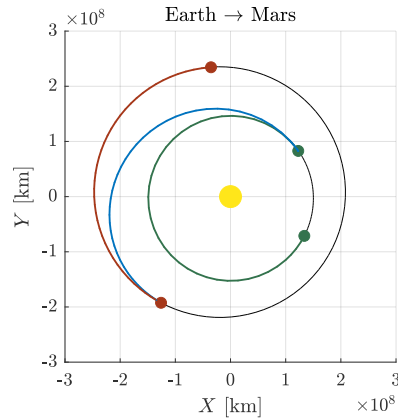
28/10/2026

INTERPLANETARY TRANSFER

$$\vec{v}_\infty = \begin{bmatrix} 0.014 \\ -2.780 \\ 0.084 \end{bmatrix} \text{ km/s (at Earth)}$$
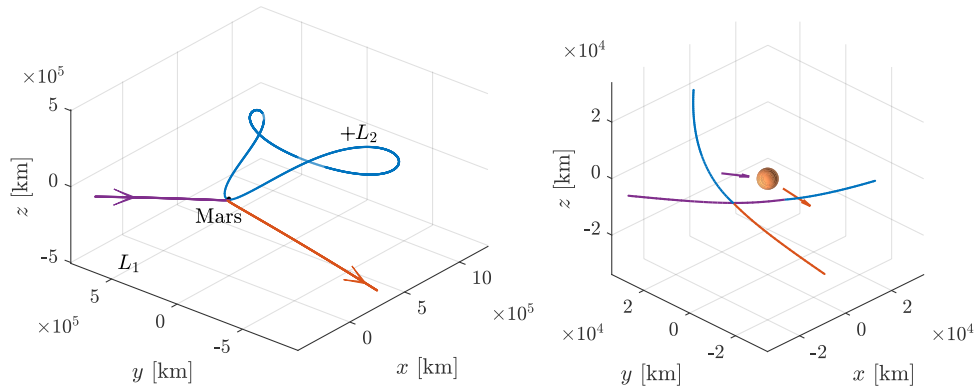
transfer duration: 302 days

$$\vec{v}_\infty = \begin{bmatrix} 0.653 \\ -2.575 \\ 0.481 \end{bmatrix} \text{ km/s (at Mars)}$$

26/08/2027

26/08/2027

MARS PARKING ORBIT

$$A_x = 52\,208 \text{ km} \quad c_u = 1.837 \cdot 10^{-3} \quad c_s = 2.444 \cdot 10^{-3}$$

$$z_0 = -107\,711 \text{ km} \quad v_{z0} = -21.45 \text{ m/s} \quad \psi = -22.92\,^\circ$$

$$\Delta v = 3.054 \text{ km/s} \quad r_{pa} = 99\,308 \text{ km} \quad r_{pd} = 105\,127 \text{ km}$$
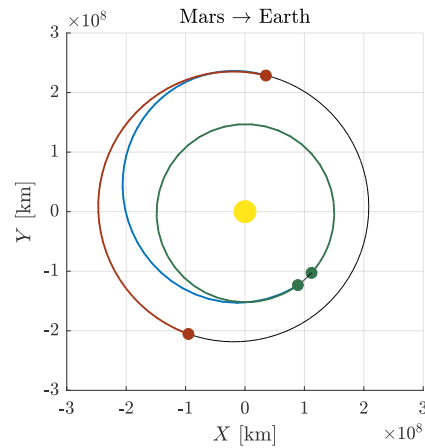
10/08/2028

INTERPLANETARY TRANSFER

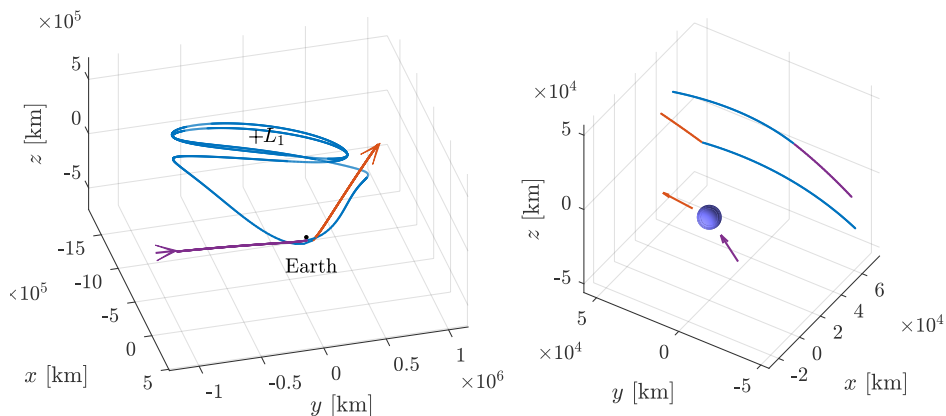$$\vec{v}_\infty = \begin{bmatrix} 0.754 \\ -2.231 \\ -0.961 \end{bmatrix} \text{ km/s (at Mars)}$$

transfer duration: 336 days

$$\vec{v}_\infty = \begin{bmatrix} ???? \\ -2.231 \\ -0.961 \end{bmatrix} \text{ km/s (at Earth)}$$

12/07/2029

EARTH PARKING ORBIT

$$A_x = 251\,282 \text{ km} \quad c_u = 1.114 \cdot 10^{-3} \quad c_s = 9.141 \cdot 10^{-4}$$

$$z_0 = 1\,149 \text{ km} \quad v_{z0} = -89.42 \text{ m/s} \quad \psi = 0.57\,^\circ$$

$$\Delta v = 3.836 \text{ km/s} \quad r_{pa} = 63\,912 \text{ km} \quad r_{pd} = 61\,494 \text{ km}$$
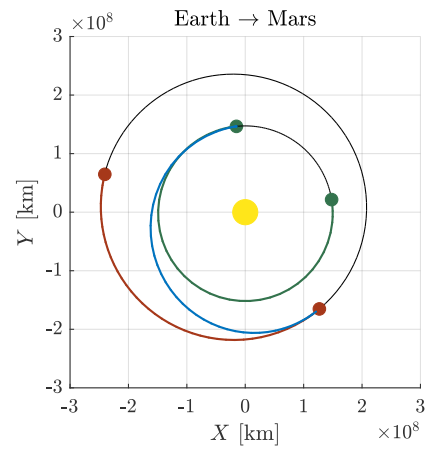
28/12/2030

28/12/2030

INTERPLANETARY TRANSFER

$$\vec{v}_\infty = \begin{bmatrix} -1.5397 \\ 2.104 \\ 1.947 \end{bmatrix} \text{ km/s (at Earth)}$$

transfer duration: 278 days

$$\vec{v}_\infty = \begin{bmatrix} 0.021 \\ -3.301 \\ 1.643 \end{bmatrix} \text{ km/s (at Mars)}$$

02/10/2031

Conclusions and future work

The use of three-body parking orbits for an Earth-Mars cycler that transfers between the planets during the low v_∞ transfer windows appears to be feasible, however the Δv requirement found with the optimization methods outlined in this thesis is $2 \sim 3$ times larger than the theoretical minimum that this cycler strategy can yield. Better result could be found, as the method can be improved in a number of ways:

- The dates of the transfers have been chosen based on the lowest Δv_i criteria, assuming that it was the main driver in determining the Δv of the cycler. However, it has been found that the Δv of a parking orbit is highly dependent on the direction of the $\vec{v}_\infty$ vectors: changing slightly the date of the transfers could change the direction of $\vec{v}_\infty$ without having a big effect on Δv_i, with the possibility of lowering the periapses of the optimal parking orbits and thus the overall Δv. This would probably require either more computational power, time or a much faster optimization scheme.

- The Earth parking trajectories are the most Δv demanding between the two planets. Improvements can be made by exploiting the presence of the Moon trough gravity assists (potentially also with maneuvers at periselene that use the Oberth effect), which has been neglected for simplicity in this thesis.

- Only two maneuvers have been assumed, one for injection and one for escape, while keeping the parking trajectory entirely ballistic. Additional mid-parking maneuvers can be added in order to change the direction of $\vec{v}$ at periapsis and improve η. If these maneuvers are made near the Lyapunov orbit they can change the trajectory drastically with small amounts Δv.

- The parking trajectories have been found in the circular three-body problem but Earth and Mars' orbits around the sun are not circular (especially the latter). A more correct model is the *elliptical* restricted three body problem, or even better the usage of a full-ephemeris model. This would not necessarily yield a lower Δv but would be necessary to compute "real" trajectories.

Finally, the methodologies outlined in this thesis can be applied to a more general set of problems than the design of a cycler, for example single return Mars missions or ESA's upcoming Comet Interceptor mission.

Appendix A

Derivatives of the effective potential

The effective potential has the following expression:

$$U(x, y, z) = \frac{1}{2}\left((x + 1 - \nu)^2 + y^2\right) + \frac{1 - \nu}{r_1} + \frac{\nu}{r_2}$$

where r_1 and r_2 have expression:

$$r_1 = \sqrt{(x + 1)^2 + y^2 + z^2} \qquad\qquad r_2 = \sqrt{x^2 + y^2 + z^2}$$

Its derivatives are the following, using the notation $\frac{\partial}{\partial q_j} = \partial_{q_j}$

$$\partial_x U = (x + 1 - \nu) - \frac{1 - \nu}{r_1^3}(x + 1) - \frac{\nu}{r_2^3}x \tag{A.1}$$

$$\partial_y U = y - \left(\frac{1 - \nu}{r_1^3} + \frac{\nu}{r_2^3}\right)y \tag{A.2}$$

$$\partial_z U = -\left(\frac{1 - \nu}{r_1^3} + \frac{\nu}{r_2^3}\right)z \tag{A.3}$$

$$\partial_{xx} U = 1 - \frac{1 - \nu}{r_1^3} - \frac{\nu}{r_2^3} + 3\left(\frac{1 - \nu}{r_1^5}(x + 1)^2 + \frac{\nu}{r_2^5}x^2\right) \tag{A.4}$$

$$\partial_{yy} U = 1 - \frac{1 - \nu}{r_1^3} - \frac{\nu}{r_2^3} + 3\left(\frac{1 - \nu}{r_1^5} + \frac{\nu}{r_2^5}\right)y^2 \tag{A.5}$$

$$\partial_{zz} U = -\frac{1 - \nu}{r_1^3} - \frac{\nu}{r_2^3} + 3\left(\frac{1 - \nu}{r_1^5} + \frac{\nu}{r_2^5}\right)z^2 \tag{A.6}$$

$$\partial_{xy} U = 3\left(\frac{1 - \nu}{r_1^5}(x + 1) + \frac{\nu}{r_2^5}x\right)y \tag{A.7}$$

$$\partial_{xz} U = 3\left(\frac{1 - \nu}{r_1^5}(x + 1) + \frac{\nu}{r_2^5}x\right)z \tag{A.8}$$

$$\partial_{zy} U = 3\left(\frac{1 - \nu}{r_1^5} + \frac{\nu}{r_2^5}\right)zy \tag{A.9}$$

Appendix B

Sign of the second y-derivative of the effective potential

Recalling from appendix A that the first x-derivative of the potential is:

$$\partial_x U = (x + 1 - \nu) - \frac{1 - \nu}{r_1^3}(x + 1) - \frac{\nu}{r_2^3}x$$

it can be evaluated at L_1 or L_2 by substituting $y = z = 0$, $x = \gamma$, $r_1 = 1 + \gamma$, $r_2 = |\gamma|$. Doing that and recalling that the first derivative of the potential is zero at equilibrium points gives:

$$\partial_x U_\gamma = \gamma + 1 - \nu - \frac{1 - \nu}{(\gamma + 1)^2} - \frac{\nu}{|\gamma|^3}\gamma = 0 \tag{B.1}$$

which rearranging the terms becomes:

$$\frac{1 - \nu}{(\gamma + 1)^2} = \gamma + 1 - \nu - \frac{\nu}{|\gamma|^3}\gamma \tag{B.2}$$

Recalling equation 2.21, the second-y derivative of U at the collinear points is:

$$\partial_{yy} U_\gamma = 1 - \frac{1 - \nu}{(\gamma + 1)^3} - \frac{\nu}{|\gamma|^3}$$

Using equation B.2 to rewrite the first fraction the following steps can be made:

$$\partial_{yy} U_\gamma = 1 - \left(\gamma + 1 - \nu - \frac{\nu}{|\gamma|^3}\gamma\right)\frac{1}{\gamma + 1} - \frac{\nu}{|\gamma|^3}$$

$$= \cancel{1} - \frac{\gamma + \cancel{1}}{\cancel{\gamma + 1}} + \frac{\nu}{\gamma + 1} + \frac{1}{\gamma + 1}\frac{\nu}{|\gamma|^3} - \frac{\nu}{|\gamma|^3}$$

$$= \frac{\nu}{\gamma + 1} + \frac{\nu}{|\gamma|^3}\left(\frac{\cancel{\gamma} - \cancel{\gamma} - 1}{\gamma + 1}\right)$$

$$= \frac{\nu}{\gamma + 1}\left(1 - \frac{1}{|\gamma|^3}\right)$$

Since $\frac{\nu}{\gamma + 1}$ is positive the sign of $\partial_{yy} U_\gamma$ is decided by $1 - \frac{1}{|\gamma|^3}$: γ is the adimensional distance of L_1 or L_2 from m_2 so it is necessary less than the distance between m_1 and m_2: this means that $\gamma < 1$ wich in turn implies $1 - \frac{1}{|\gamma|^3} < 0$. Thus

$$\partial_{yy} U_\gamma < 0 \tag{B.3}$$

Appendix C

Optimization algorithms

Consider the function $f(\boldsymbol{x})$ where $\boldsymbol{x} = [x_1 \ ... \ x_n]^{\mathrm{T}}$, whith a minimum $\min_{\boldsymbol{x}} f = f(\boldsymbol{x}_{\mathrm{opt}})$; there are many algorithms that from an initial guess $\boldsymbol{x}^{(0)}$, here are illustrated the two used in this thesis.

C.1 Gradient method

This algorithm relies on the fact that ∇f is a vector oriented in the direction where f grows in the $\boldsymbol{x}$ space. The algorithm is outlined below and illustrated in figure C.1a

> **input** $\boldsymbol{x}^{(0)}$, s_0 ▷ choose initial $\boldsymbol{x}$ and step size
> $f_0 = f(\boldsymbol{x}_0)$, $\nabla f_0 = [\partial_1 f \ ... \ \partial_n f]_{\boldsymbol{x}_0}$ ▷ calculate initial f and gradient
> $m, l \leftarrow 0$
> **while** $s_l < s_{\min}$ **do**   ▷ iterate until step size is below a treshold $s_{\min}$
> $\boldsymbol{x}^{(m+1)} = \boldsymbol{x}^{(m)} - s_l \frac{\nabla f_m}{|\nabla f_m|}$ ▷ calculate next $\boldsymbol{x}$ making a step opposite to gradient
>   **if** $f_{m+1} < f_m$ **then**
> $m \leftarrow m + 1$ ▷ if f decreases, make another step
>   **else**
> $s_{l+1} = s_l/k$ ▷ if f increase, reduce step size by a factor $k > 1$
> $l \leftarrow l + 1$
>   **end if**
> **end while**
> **output** $\boldsymbol{x}^{(m)}$ ▷ the last value of $\boldsymbol{x}$ is approximately $\boldsymbol{x}_{\mathrm{opt}}$

The factor k, as well as the minimum step size $s_{\min}$, can be set to different values and in the optimization process describe at page 50: the following have been found to work:

$$s_{\min} = 10^{-12} \qquad\qquad s_0 = 10^{-5} \qquad\qquad k = \sqrt{10}$$

This method requires the gradient to be computed at each step: when f has no closed form therefore no expression for its derivative (such is the case for the Δv calculation), it can be approximated by finite differences of f evluated at two positions $s_{\min}$ apart:

$$\partial_j f|_{\boldsymbol{x}} \simeq \frac{f(\boldsymbol{x} + s_{\min}\hat{\boldsymbol{x}}_j) - f(\boldsymbol{x})}{s_{\min}}$$

C.2 Grid method

This algorithm, shown in figure C.1b, is simpler and more robust but less efficient, it makes steps in the $\boldsymbol{x}$ space one dimension at a time instead of finding the best direction.

> **input** $\boldsymbol{x}^{(0)}$, $s_{0,1}$, ... , $s_{0,n}$ ▷ choose initial $\boldsymbol{x}$ and step sizes
> $f_0 = f(\boldsymbol{x}_0)$ ▷ calculate initial f
> $m \leftarrow 0$
> **while** $m < m_{\max}$ **do**   ▷ iterate until desired level $m_{\max}$ is reached
>   **for** $j \in \{1, ..., n\}$ **do** for each dimension
>   **if** $f(\boldsymbol{x}^{(m)} + s_{m,j}\hat{\boldsymbol{x}}_j) < f_m$ **then**   ▷ if f decreases in $+s$ direction
> $D \leftarrow +1$ ▷ set direction to $+s$
>   **else if** $f(\boldsymbol{x}^{(m)} - s_{m,j}\hat{\boldsymbol{x}}_j) < f_m$ **then**   ▷ if f decreases in $-s$ direction
> $D \leftarrow -1$ ▷ set direction to $-s$
>   **else**
> $D \leftarrow 0$ ▷ else no decrease of f in either direction
>   **end if**
>   **while** $D \neq 0$ **do**   ▷ while f decreases in some direction
>   **if** $f(\boldsymbol{x}^{(m)} + Ds_{m,j}\hat{\boldsymbol{x}}_j) < f_m$ **then**   ▷ if f decreases in next step
> $\boldsymbol{x}^{(m)} \leftarrow \boldsymbol{x}^{(m)} + Ds_{m,j}\hat{\boldsymbol{x}}_j$ ▷ step along current dimension
>   **else**
> $D \leftarrow 0$ ▷ else no decrease of f in either direction
>   **end if**
>   **end while**
> $j \leftarrow j + 1$ ▷ next variable
> $s_{m+1,j} = s_{m,j}/k$ ▷ reduce step size
>   **end for**
> $m \leftarrow m + 1$ ▷ next level
> **end while**
> **output** $\boldsymbol{x}^{(m)}$ ▷ the last value of $\boldsymbol{x}$ is approximately $\boldsymbol{x}_{\mathrm{opt}}$
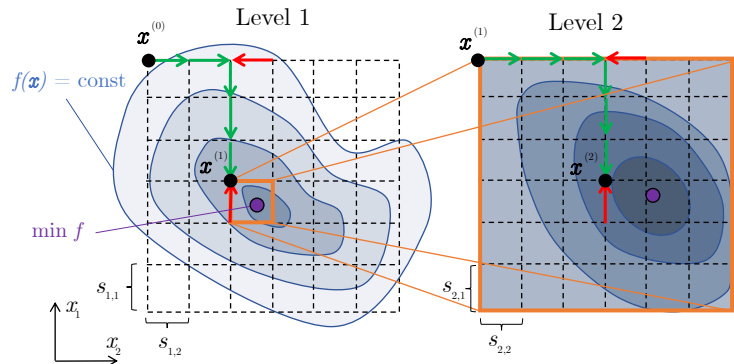
As previously, the factor k and the maximum level $m_{\max}$, can be set to different values. Those used in the process described at page 50 are:

$$m_{\max} = 3 \qquad\qquad k = 10$$
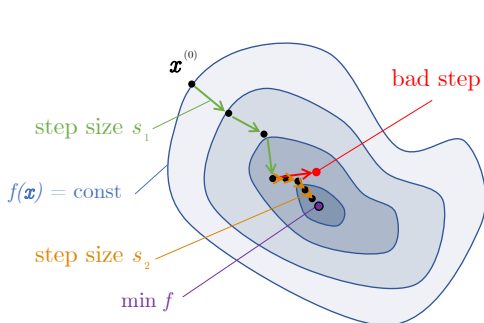
(a) Gradient method

(b) Grid method

Figure C.1: Visualizations of the optimization algrithms

References

1. Byrnes, D. V., Longuski, J. M. & Aldrin, B. Cycler orbit between Earth and Mars. *Journal of Spacecraft and Rockets* **30,** 334–336 (1993).

2. Friedlander, A, Niehoff, J, Byrnes, D & Longuski, J. *Circulating transportation orbits between Earth and Mars* in *Astrodynamics Conference* (1986), 2009.

3. Koon, W. S., Lo, M. W., Marsden, J. E. & Ross, S. D. *Dynamical systems, the three-body problem and space mission design* (World Scientific, 2000).

4. Lancaster, E. *A unified form of Lambert's theorem* (National Aeronautics and Space Administration, 1969).

5. Curtis, H. *Orbital mechanics for engineering students* (Butterworth-Heinemann, 2013).

6. Jet Propulsion Laboratory. *Horizons System* `https://ssd.jpl.nasa.gov/horizons/app.html#/`.

7. Oberth, H. Ways to spaceflight. *Translation into english of the book "Wege zur Raumschiffahrt" Munich-Berlin, 1929.* page 194-217 (1972).